Development of anion-exchange resin incorporating single metal particles for rapid removal and catalytic decomposition of nitrate in water toward groundwater purification

(地下水浄化に向けた水中硝酸イオンの迅速除去と触媒分解のための単一金属粒子を取り込んだ陰イオン交換樹脂の開発)

Bobo Yan

Division of Environmental Materials Science

Graduate School of Environmental Science

Hokkaido University

Table of contents

Chapter 1

General introduction

1-1 Clean freshwater and water crisis

It is well known that many countries around the world are facing a problem of water crisis. The main causes of the water crisis are the shortage of available water and water pollution. Fresh water accounts for only 3 % of the world's water resources, and 70 % of the fresh water are glaciers, which means that the water available for consumption is around 1 % of the world's water resources [1]. Moreover, as population grows, urbanization and industrial activity increase, freshwater demand is also increasing [2, 3], and the United Nations World Water Development Report (2020) highlighted that global water consumption has increased six times over the past 100 years and continued to grow at approximately 1 %/year [4]. The mismatch between demands by people and natural freshwater supplies is leading to water shortages, affecting industrial and agricultural production [5].

On the other hand, the quality and stability of fresh water are critical for human health and for economies and ecosystem stability. World Health Organization (WHO) experts have found that 80 % of all diseases and 50 % of child deaths worldwide are related to unsatisfactory quality of drinking water [6, 7]. Contamination of surface water and groundwater is another cause of the current water crisis [3, 4]. Water pollution is caused mainly by natural and anthropogenic causes [8, 9]. Natural sources of water pollution include soil erosion, leaching of minerals from rocks and decaying of organic matter, whereas anthropogenic sources of water pollution include discharge of waste into water bodies from agriculture, households and industrial units [9]. Agro-chemical wastes include fertilizers and pesticides widely used in crop fields to enhance productivity, which is a serious cause for water contamination. Increased urban surface runoff and increased municipal and industrial discharges all result in increased loadings of nutrients to urban streams. Moreover, chemicals containing acids, alkalis and dyes from industries, metallurgical units, food processing units, paper mills and textiles are dumped and poured down into rivers as effluents. The disposal of polluted water into water bodies without

proper treatment must cause outbreak of serious diseases, which further decreases available freshwater resources and exacerbates the water crisis [9].

1-2 Current status of nitrate pollution in groundwater

Nitrate pollution in groundwater is becoming more and more serious, and there are many causes for that (Fig. 1-1). The excessive use of nitrogen fertilizers in agricultural development was the main cause of nitrate pollution in groundwater. Crop yields increased after 1940 because of the mechanization of agriculture in industrialized countries in North America and Western and Central Europe, but it had caused soil erosion and pollution of surface water and groundwaters, which was a direct consequence of applying large quantities of fertilizers in these countries [10, 11] . In addition, domestic and industrial wastewater are among the fastest-growing sources of nitrate for groundwater [12, 13]. Moreover, the use of manure to farmland also caused the nitrate pollution in groundwater [14, 15]. While agricultural activities were the major cause of nitrate pollution, non-agricultural activities, including leakage from septic tanks, sewage systems, landfills, and the discharge of improperly treated industrial and domestic wastewater also caused serious nitrate pollution [16].

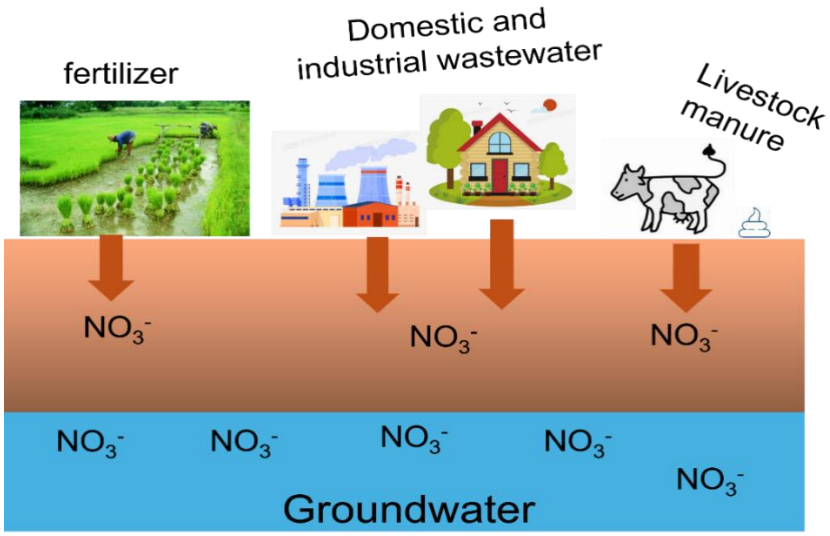

Fig. 1-1 Nitrate resources polluting groundwater.

Groundwater is one of the significant sources of freshwater, and most of which was used for agriculture and drinking purposes [12, 17, 18, 19]. Nitrate in groundwater and drinking water has long been studied for detrimental effects on human health. In 1945, it was found that nitrate in drinking water can cause methemoglobinemia (blue baby syndrome), particularly to infants and fetuses [20, 21, 22, 23, 24, 25] , which promoted the U.S. EPA to establish a drinking water standard of 10 ppm NO_3-N. Similarly, the World Health Organization (WHO) had set a Maximum Contaminant Level (MCL) as 11.3 ppm NO_3-N, which is based on no blue baby syndrome under such levels [26, 27, 28, 29]. In addition, research has emerged on the link between nitrates and thyroid cancer, which is the 9th most common cancer and represents 5.1 % of the female cancer [26, 28]. Nitrate-contaminated drinking water during pregnancy is also associated with a higher risk of congenital disabilities such as neural tube congenital disabilities and preterm birth, as well as meagre birth weight [16, 29]. Moreover, it was proved that exposure to nitrate-contaminated water caused colorectal cancer, thyroid issues, and congenital disabilities [16, 29]. In view of this, the removal of nitrate in groundwater is necessary and urgent.

1-3 Common methods for nitrate removal from groundwater

Groundwater polluted with nitrate is a worldwide problem, and there are so many researchers paying attention to this area all over the world. Accordingly, various methods were used to treat it, including biological denitrification [30, 31], reverse osmosis [32], ion exchange [33, 34, 35] and catalytic reduction [36, 37, 38, 39] and so on.

Among these methods, ion-exchange method has been intensively investigated for the removal of NO_3^- in water because of facile operation and rapid treatment [23, 40, 41, 42]. Anion-exchange resins are among the most useful and common anion-exchangers [43, 44, 45, 46]. However, anion-exchange resins must be regenerated using brine (a concentrated salt solution) when their ion-exchange capacity is saturated [47, 48, 49]. Consequently, the regeneration of spent resin produces waste brine containing concentrated NO_3^-, which requires cumbersome post-treatment [49].

In contrast to ion exchange, the catalytic reduction of NO_3^- in water has attracted

considerable attention because NO_3^- can be ideally decomposed to harmless N_2 (eq. 1-1) [50, 51, 52, 53, 54].

$$NO_3^- + 5/2H_2 \rightarrow 1/2N_2 + 2H_2O + OH^- \quad \text{(eq. 1-1)}$$

Bimetals consisting of precious metals such as Pd and Pt and base metals such as Cu, Sn, and In, which typically require supports, have been used as catalysts for this reaction [36, 50, 55, 56, 57]. The reaction mechanism for NO_3^- reduction over bimetallic catalysts has been widely studied [58]. As shown in Scheme 1-1, NO_3^- is reduced to NO_2^- on the surface of the base metal (Cu, Sn, and In), while noble metal has no activity in this process. But NO_2^- is further decomposed to N_2 or NH_4^+ completely on the surface of noble metal (Pd, Pt, and Rh). The oxidized base metal formed by the reduction of NO_3^- is reduced to regenerate low valent state of the metal by the reaction with hydrogen activated on the noble metal surface.

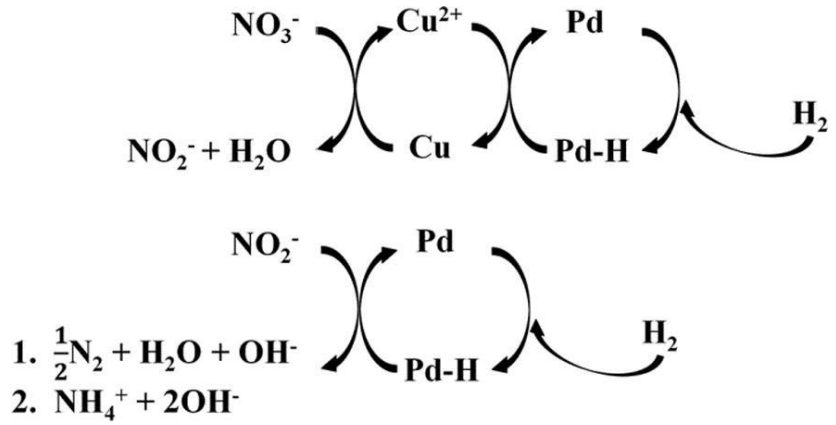

Scheme 1-1. Reaction pathway of nitrate reduction with a bimetallic catalyst [58].

However, a major limitation of this method is the formation of undesirable nitrite and ammonia (eqs. 1-2 and 1-3, respectively) [36, 37, 56]. In addition, a slow reaction rate is another problem on the catalytic reduction which necessitates a long treatment time and a large reactor [25].

$$NO_3^- + H_2 \rightarrow NO_2^- + H_2O \quad \text{(eq. 1-2)}$$

$$NO_3^- + 4H_2 \rightarrow NH_3 + 2H_2O + OH^- \quad \text{(eq. 1-3)}$$

1-4 Two-step process for nitrate removal and decomposition

To address the problems of ion exchange and catalytic methods simultaneously, Choi et al [58]. proposed the integration of catalytic reduction with anion-exchange removal using a metal-loaded anion-exchange resin (Fig. 1-2). They developed a bimetallic PdCu-nanoparticle-containing anion-exchange resin (PdCu@resin). In this process, PdCu@resin initially captured NO_3^- in water through an anion-exchange reaction. Subsequently, the PdCu@resin was removed from water and treated with a H_2/CO_2 mixture at 6 bar for the catalytic reduction of NO_3^- in the resin. Herein, this is referred to as a two-step process. An advantage of the two-step process is that it enables the rapid treatment of polluted water based on an ion-exchange reaction. Another advantage of this process is that the decomposition of NO_3^- and regeneration of the spent resin occur simultaneously, because NO_3^- on the anion-exchange sites in the spent resin is replaced with OH^- formed by the reduction of NO_3^- (eq. 1-1). Therefore, brine is unnecessary for regenerating the spent resin. Furthermore, the formation of undesirable byproducts (nitrite and ammonia) does not need to be considered so much, because these byproducts do not contaminate the treated water.

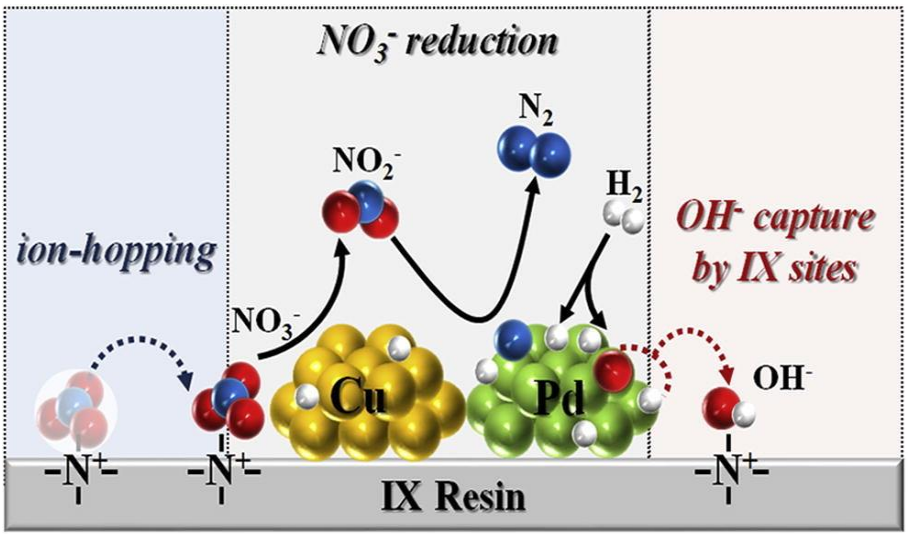

Fig. 1-2 Two-step process for NO_3^- reduction [58].

1-5 Purpose of this study

As mentioned in Chapter 1-3, bimetallic Pd particles, including PdCu and PdSn, are necessary as catalytically active species to decompose NO_3^-. Moreover, studies on the catalytic reduction of NO_3^- in water indicate that bimetallic Pd particles are essential because the bimetallic sites promote the first step of the reaction ($NO_3^- \rightarrow NO_2^-$) [59, 60, 61, 62], which is a rate-determining step in the catalytic reduction of NO_3^- in water [59, 60, 63, 64, 65]. However, the preparation method of bimetallic Pd catalysts was complicated compared with single metal catalysts. Furthermore, bimetals involve a considerably larger number of parameters in the catalyst preparation to determine the performance [66, 67, 68], making it difficult to optimally design and understand the catalysis for the reaction.

According to previous studies, single metals in supported catalysts have low activity (even no activity) for NO_3^- reduction in water. However, this author thought that the catalytic performance of single metal catalyst for NO_3^- decomposition would be affected by the preparation method, type of supports and reaction conditions, and such single metal catalysts should show catalytic activity for NO_3^- reduction if the appropriate metal is selected, properly prepared, and reacted under the appropriate reaction conditions. Especially, because the reaction conditions (temperature, hydrogen pressure, and presence/absence of water) for NO_3^- decomposition in the two-step process are markedly different from those of the conventional catalytic reduction of NO_3^- in water, and this author expected that the NO_3^- decomposition to regenerate spent resin proceeded even with a single-metal catalyst if the appropriate metal and reaction conditions were used. Therefore, the purpose of this study is to develop a single-metal catalyst that is highly active in the decomposition of NO_3^- in anion-exchange resin for the two-step process.

1-6 Structure of this thesis

This thesis consists of five chapters.

In the first chapter, the current freshwater use and problem, situation of nitrate contamination in groundwater and the harm of nitrate pollution to humans are described. And after comprehensively considering the advantages and disadvantages of various methods usable for nitrate removal, especially ion exchange and catalytic methods. Finally, the purpose of this study which is to develop an anion exchange resin containing single metal catalyst that is highly active in the decomposition of NO_3^- in the two-step process is clearly stated.

In the second chapter, anion-exchange resin (Amberlite^{TM} IRA410(OH), Organo Co.) containing metal particles (M@AER) was prepared and the ion-exchange and catalytic performance of M@AER for NO_3^- decomposition was investigated using a two-step process. Among the tested metals, Au was chosen as an active single metal introduced into the resin because $AuCl_4^-$ in resin did not need to be reduced by additional reducing agents. The preparation conditions of anion-exchange resin containing Au particles (Au@AER) and the reaction conditions for NO_3^- decomposition was intensively investigated to improve the catalytic performance for NO_3^- decomposition. Finally, the reusability of Au@AER was also tested.

In the third chapter, the decomposition mechanism of the NO_3^- in Au@AER was investigated especially focusing on the role of water on the reaction, and it was proved that water in Au@AER played an important role in NO_3^- decomposition.

In the fourth chapter, the catalytic performance of Ru@AER, which showed the highest activity for NO_3^- decomposition in Chapter 2, was investigated. The influence of the reduction conditions of $RuCl_4^-$ in Ru@AER and the reaction conditions for NO_3^- decomposition was investigated. Finally, the reusability of Ru@AER was also tested.

In the fifth chapter, the conclusions and future perspective of the study are stated.

1-7 References

[1] A. Czajkowski, L. Remiorz, S. Pawlak, E. Remiorz, J. Szyguła, D. Marek, M. Paszkuta, G. Drabik, G. Baron, J. Paduch and O. Antemijczuk. Global water crisis: Concept of a new interactive shower panel based on IoT and cloud computing for rational water consumption, Applied Scienes. 11 (2021) 4081, https://doi.org/10.3390/app11094081

[2] M. M. I. Sourav, M. N. Islam and A. A. Abeer. Identifying the key attributes of fresh water crisis in Dhaka city: a structural equation modeling approach, Water Practice & Technology. 17 (2022) 2113-2124, https://doi.org/10.2166/wpt.2022.126

[3] A. Roshan and M. Kumar. Water end-use estimation can support the urban water crisis management: A critical review, Journal of Environmental Management. 268 (2020) 110663, https://doi.org/10.1016/j.jenvman.2020.110663

[4] X. Wang, Y. Chen, G. Fang, Z. Li and Y. Liu. The growing water crisis in Central Asia and the driving forces behind it, Journal of Cleaner Production. 378 (2022) 134574, https://doi.org/10.1016/j.jclepro.2022.134574

[5] P. H. Gleick and H. Cooley. Freshwater scarcity, Annual Review of Environment and Resources. 46 (2021) 319-348, https://doi.org/10.1146/annurev-environ-012220-101319

[6] T. M. Joseph, H. E. Al-Hazmi, B. Śniatała, A. Esmaeili and S. Habibzadeh. Nanoparticles and nanofiltration for wastewater treatment: From polluted to fresh water, Environmental Research. (2023) 117114, https://doi.org/10.1016/j.envres.2023.117114

[7] O. Machate, D. S. Schmeller, T. Schulze and W. Brack. Mountain lakes as freshwater resources at risk from chemical pollution, Environmental Sciences Europe. 35 (2023) 3.

[8] E. J. Isukuru, J. O. Opha, O. W. Isaiah, B. Orovwighose and S. S. Emmanuel. Nigeria's water crisis: Abundant water, polluted reality, Cleaner Water. (2024) 100026, https://doi.org/10.1016/j.clwat.2024.100026

[9] A. Bala, P. Mehta and U. K. Singh. Water pollution and water crisis, Facets of Environmental Sciences. 30,

[10] N. J. Howden, T. P. Burt, F. Worrall, S. Mathias and M. J. Whelan. Nitrate pollution

in intensively farmed regions: What are the prospects for sustaining high-quality groundwater?, Water Resources Research. 47 (2011), https://doi.org/10.1029/2011WR010843

[11] E. Craswell. Fertilizers and nitrate pollution of surface and ground water: an increasingly pervasive global problem, SN Applied Sciences. 3 (2021) 518, https://doi.org/10.1007/s42452-021-04521-8

[12] X. Kou, J. Ding, Y. Li, Q. Li, L. Mao, C. Xu, Q. Zheng and S. Zhuang. Tracing nitrate sources in the groundwater of an intensive agricultural region, Agricultural Water Management. 250 (2021) 106826, https://doi.org/10.1016/j.agwat.2021.106826

[13] R. Das, N. S. Rao, H. Sahoo and G. Sakram. Nitrate contamination in groundwater and its health implications in a semi-urban region of Titrol block, Jagatsinghpur district, Odisha, India, Physics and Chemistry of the Earth, Parts A/B/C. 132 (2023) 103424, https://doi.org/10.1016/j.pce.2023.103424

[14] J. A. Torres-Martínez, A. Mora, J. Mahlknecht, L. W. Daesslé, P. A. Cervantes-Avilés and R. Ledesma-Ruiz. Estimation of nitrate pollution sources and transformations in groundwater of an intensive livestock-agricultural area (Comarca Lagunera), combining major ions, stable isotopes and mixsiar model, Environmental Pollution. 269 (2021) 115445, https://doi.org/10.1016/j.envpol.2020.115445

[15] X. Zhu, P. Miao, J. Qin, W. Li, L. Wang, Z. Chen and J. Zhou. Spatio-temporal variations of nitrate pollution of groundwater in the intensive agricultural region: Hotspots and driving forces, Journal of Hydrology. 623 (2023) 129864, https://doi.org/10.1016/j.jhydrol.2023.129864

[16] A. Verma, A. Sharma, R. Kumar and P. Sharma. Nitrate contamination in groundwater and associated health risk assessment for Indo-Gangetic Plain, India, Groundwater for Sustainable Development. 23 (2023) 100978, https://doi.org/10.1016/j.gsd.2023.100978

[17] B. Panneerselvam, K. Muniraj, K. Duraisamy, C. Pande, S. Karuppannan and M. Thomas. An integrated approach to explore the suitability of nitrate-contaminated

groundwater for drinking purposes in a semiarid region of India, Environmental Geochemistry and Health. 45 (2023) 647-663, https://doi.org/10.1007/s10653-022-01237-5

[18] G. Yu, J. Wang, L. Liu, Y. Li, Y. Zhang and S. Wang. The analysis of groundwater nitrate pollution and health risk assessment in rural areas of Yantai, China, BMC Public Health. 20 (2020) 1-6, https://doi.org/10.1186/s12889-020-08583-y

[19] K. M. Ransom, B. T. Nolan, P. Stackelberg, K. Belitz and M. S. Fram. Machine learning predictions of nitrate in groundwater used for drinking supply in the conterminous United States, Science of The Total Environment. 807 (2022) 151065, https://doi.org/10.1016/j.scitotenv.2021.151065

[20] H. Yousefi and B. K. Douna. Risk of nitrate residues in food products and drinking water, Asian Pacific Journal of Environment and Cancer. 6 (2023) 69-79, https://doi.org/10.31557/APJEC.2023.6.1.69-79.

[21] Z. A. Mohtfer and A. Y. Al-Saffawi. Probabilistic risk of nitrates to human health via drinking water: A case study of water supply for Dandan station and its quarters in Mosul, Iraq, Journal of Advances in Environmental Health Research. 11 (2023) 246-252, https://doi.org/10.34172/JAEHR.1310.

[22] Y. Sailaukhanuly, S. Azat, M. Kunarbekova, A. Tovassarov, K. Toshtay, Z. Tauanov, L. Carlsen and R. Berndtsson. Health risk assessment of nitrate in drinking water with potential source identification: A case study in Almaty, Kazakhstan, International Journal of Environmental Research and Public Health. 21 (2023) 55, https://doi.org/10.3390/ijerph21010055.

[23] S. Patra, A. Pranudta, N. Chanlek, T. T. Nguyen, N. H. Nhat, M. M. El-Moselhy and S. Padungthon. Denitrification of nitrate in regeneration waste brine using hybrid cation exchanger supported nanoscale zero-valent iron with/without palladium nanoparticles, Chemosphere. 310 (2023) 136851, https://doi.org/10.1016/j.chemosphere.2022.136851

[24] L. Zhang, S. Jiang, Y. Jia, M. Zhang and J. Guo. Effects of Na^+/H_2O_2 on nitrogen removal and sludge activity: Performance and mechanism, Journal of Environmental

Chemical Engineering. (2024) 113194, https://doi.org/10.1016/j.jece.2024.113194

[25] W. Xie, T. Zhu, B. Yuan, S. Fu, Z. Mao, Z. Ye, Z. Zhu and X. Zhang. Plasma-catalyzed combined dynamic wave scrubbing: A novel method for highly efficient removal of multiple pollutants from flue gas at low temperatures, Journal of Hazardous Materials. 461 (2024) 132518, https://doi.org/10.1016/j.jhazmat.2023.132518

[26] A. Q. Tariqi and C. C. Naughton. Water, health, and environmental justice in California: Geospatial analysis of nitrate contamination and thyroid cancer, Environmental engineering science. 38 (2021) 377-388, https://doi.org/10.1089/ees.2020.0315

[27] R. Nieder and D. K. Benbi. Reactive nitrogen compounds and their influence on human health: An overview, Reviews on Environmental Health. 37 (2022) 229-246, https://doi.org/10.1515/reveh-2021-0021

[28] W. Feng, C. Wang, X. Lei, H. Wang and X. Zhang. Distribution of nitrate content in groundwater and evaluation of potential health risks: A case study of rural areas in Northern China, International journal of environmental research and public health. 17 (2020) 9390, https://doi.org/10.3390/ijerph17249390

[29] L. Lin, S. St Clair, G. D. Gamble, C. A. Crowther, L. Dixon, F. H. Bloomfield and J. E. Harding. Nitrate contamination in drinking water and adverse reproductive and birth outcomes: A systematic review and meta-analysis, Scientific Reports. 13 (2023) 563, https://doi.org/10.1038/s41598-022-27345-x

[30] D. Koren, W. D. Gould and P. Bedard. Biological removal of ammonia and nitrate from simulated mine and mill effluents, Hydrometallurgy. 56 (2000) 127-144, https://doi.org/10.1016/S0304-386X(99)00088-2

[31] E. Wąsik, J. Bohdziewicz and M. Błaszczyk. Removal of nitrates from ground water by a hybrid process of biological denitrification and microfiltration membrane, Process Biochemistry. 37 (2001) 57-64, https://doi.org/10.1016/S0032-9592(01)00177-7

[32] J. Schoeman and A. Steyn. Nitrate removal with reverse osmosis in a rural area in South Africa, Desalination. 155 (2003) 15-26, https://doi.org/10.1016/S0011-

9164(03)00235-2

[33] A. A. Hekmatzadeh, A. Karimi-Jashni, N. Talebbeydokhti and B. Kløve. Adsorption kinetics of nitrate ions on ion exchange resin, Desalination. 326 (2013) 125-134, https://doi.org/10.1016/j.desal.2013.07.017

[34] M. Chabani, A. Amrane and A. Bensmaili. Kinetic modelling of the adsorption of nitrates by ion exchange resin, Chemical Engineering Journal. 125 (2006) 111-117, https://doi.org/10.1016/j.cej.2006.08.014

[35] Y. Sun, W. Zheng, X. Ding and R. P. Singh. Selective removal of nitrate using a novel asymmetric amine based strongly basic anion exchange resin, Adsorption Science & Technology. 38 (2020) 271-285, https://doi.org/10.1177/0263617420945839

[36] I. Sanchis, E. Diaz, A. Pizarro, J. Rodriguez and A. Mohedano. Nitrate reduction with bimetallic catalysts. A stability-addressed overview, Separation and Purification Technology. 290 (2022) 120750, https://doi.org/10.1016/j.seppur.2022.120750

[37] I. Sanchis, J. J. Rodriguez, A. F. Mohedano and E. Diaz. Activity and stability of Pd bimetallic catalysts for catalytic nitrate reduction, Catalysts. 12 (2022) 729, https://doi.org/10.3390/catal12070729

[38] M. Rachini, M. Jaafar, N. Tabaja, S. Tlais, R. Hamdan, F. Al Ali, O. Haidar, C. Lancelot, M. Kassem and E. Bychkov. Comparative study between supported bimetallic catalysts for nitrate remediation in water, Open Chemistry. 21 (2023) 20220303, https://doi.org/10.1515/chem-2022-0303

[39] K. Hong, D. J. Rivera, J. Donoso, B. Shin, H. P. Jacobs, B. J. Cha, K. N. Heck, W. C. Elias, P. Westerhoff and Y. Han. Nickel enhances InPd-catalyzed nitrate reduction activity and N_2 selectivity, ACS ES&T Engineering. (2024), https://doi.org/10.1021/acsestengg.4c00552

[40] S. O. Abayie and T. Leiviskä. Removal of nitrate from underground mine waters using selective ion exchange resins, Journal of Environmental Chemical Engineering. 10 (2022) 108642, https://doi.org/10.1016/j.jece.2022.108642

[41] T. T. Nguyen, V. A. K. Tran, L. B. Tran, P. T. Phan, M. T. Nguyen, L. G. Bach, S.

Padungthon, C. K. Ta and N. H. Nguyen. Synthesis of cation exchange resin-supported iron and magnesium oxides/hydroxides composite for nitrate removal in water, Chinese Journal of Chemical Engineering. 32 (2021) 378-384, https://doi.org/10.1016/j.cjche.2020.11.032

[42] H. Dong, H. Chen, C. Shepsko and A. SenGupta. Resilient nitrate removal by a biological nitrate-selective ion exchange (BIO-NIX) process, ACS ES&T Water. 3 (2023) 2989-2995, https://doi.org/10.1021/acsestwater.3c00220

[43] R. Xiao, A. Wang, J. Hu, J. Long, M. Chu, B. Ma, C. Yan and L. Feng. Synthesis of a novel porous self-settling magnetic anion exchange resin and its removal mechanism for tannic acid, ChemistrySelect. 8 (2023) e202302602, https://doi.org/10.1002/slct.202302602

[44] D. Beery, M. A. Mottaleb, M. J. Meziani, J. Campbell, I. P. Miranda and M. Bellamy. Efficient route for the preparation of composite resin incorporating silver nanoparticles with enhanced antibacterial properties, Nanomaterials-Basel. 12 (2022) 471, https://doi.org/10.3390/nano12030471

[45] Z. Shen, M. Fang, L. Tang, J. Shi and W. Wang. Pd/Cu bimetallic nano-catalyst supported on anion exchange resin (A520E) for nitrate removal from water: High property and stability, Environmental Research. 241 (2024) 117616, https://doi.org/10.1016/j.envres.2023.117616

[46] L. S. Muhammed and H. T. Sadeq. Using modified resins in chromium ion removal from aqueous solutions, (2023)

[47] Z. Pan, Z. Li, B. Zeng, L. Shen and H. Lin. Enhanced denitrification performance of granular sludge for the treatment of waste brine from ion exchange resin process, Journal of Environmental Management. 344 (2023) 118473, https://doi.org/10.1016/j.jenvman.2023.118473

[48] Z. Liu, M. Haddad, S. Sauvé and B. Barbeau. Alleviating the burden of ion exchange brine in water treatment: From operational strategies to brine management, Water Research. 205 (2021) 117728, https://doi.org/10.1016/j.watres.2021.117728

[49] J. A. Korak, A. L. Mungan and L. T. Watts. Critical review of waste brine management strategies for drinking water treatment using strong base ion exchange, Journal of Hazardous Materials. 441 (2023) 129473, https://doi.org/10.1016/j.jhazmat.2022.129473

[50] C. A. Boasiako, Z. Zhou, X. Huo and T. Ye. Development of Pd-based catalysts for hydrogenation of nitrite and nitrate in water: A review, Journal of Hazardous Materials. 446 (2023) 130661, https://doi.org/10.1016/j.jhazmat.2022.130661

[51] G. Tokazhanov, E. Ramazanova, S. Hamid, S. Bae and W. Lee. Advances in the catalytic reduction of nitrate by metallic catalysts for high efficiency and N_2 selectivity: A review, Chemical Engineering Journal. 384 (2020) 123252, https://doi.org/10.1016/j.cej.2019.123252

[52] I. Sanchis, J. Rodriguez, A. Mohedano and E. Diaz. N-doped activated carbon as support of Pd-Sn bimetallic catalysts for nitrate catalytic reduction, Catalysis Today. 423 (2023) 114011, https://doi.org/10.1016/j.cattod.2023.01.018

[53] S. Xie, Y. Li, C. Wang, K.-B. Low, K. Ye, D. Kim, X. Zhang, Y. Li, Y. Zhang and F. Shi. Silica modulated palladium catalyst with superior activity for the selective catalytic reduction of nitrogen oxides with hydrogen, Applied Catalysis B: Environmental. 327 (2023) 122437, https://doi.org/10.1016/j.apcatb.2023.122437

[54] K. Chen, J. Wan, T. Wang, Q. Sun and R. Zhou. Construction of bimetallic Pt–Pd/CeO_2–ZrO_2–La_2O_3 catalysts with different Pt/Pd ratios and its structure–activity correlations for three-way catalytic performance, Journal of Rare Earths. 41 (2023) 896-904, https://doi.org/10.1016/j.jre.2022.10.014

[55] L. Wei, D.-J. Liu, B. A. Rosales, J. W. Evans and J. Vela. Mild and selective hydrogenation of nitrate to ammonia in the absence of noble metals, ACS Catalysis. 10 (2020) 3618-3628, https://doi.org/10.1021/acscatal.9b05338

[56] A. S. G. Santos, J. Restivo, C. A. Orge, M. F. R. Pereira and O. S. G. Soares. Nitrate catalytic reduction over bimetallic catalysts: Catalyst optimization, C. 6 (2020) 78, https://doi.org/10.3390/c6040078

[57] S. Hamid, Y. Niaz, S. Bae and W. Lee. Support induced influence on the reactivity and selectivity of nitrate reduction by Sn-Pd bimetallic catalysts, Journal of Environmental Chemical Engineering. 8 (2020) 103754, https://doi.org/10.1016/j.jece.2020.103754

[58] Y.-N. Kim, M. Y. Kim and M. Choi. Synergistic integration of catalysis and ion-exchange for highly selective reduction of nitrate into N_2, Chemical Engineering Journal. 289 (2016) 423-432, https://doi.org/10.1016/j.cej.2016.01.002

[59] F. Cai, L. Yang, S. Shan, D. Mott, B. H. Chen, J. Luo and C.-J. Zhong. Preparation of PdCu alloy nanocatalysts for nitrate hydrogenation and carbon monoxide oxidation, Catalysts. 6 (2016) 96, https://doi.org/10.3390/catal6070096

[60] H. Berndt, I. Mönnich, B. Lücke and M. Menzel. Tin promoted palladium catalysts for nitrate removal from drinking water, Applied catalysis B: environmental. 30 (2001) 111-122, https://doi.org/10.1016/S0926-3373(00)00225-3

[61] N. Barrabes, A. Frare, K. Föttinger, A. Urakawa, J. Llorca, G. Rupprechter and D. Tichit. Pt-Cu bimetallic catalysts obtained from layered double hydroxides by an anion-exchange route, Applied Clay Science. 69 (2012) 1-10, https://doi.org/10.1016/j.clay.2012.07.011

[62] U. Prüsse, M. Hähnlein, J. Daum and K.-D. Vorlop. Improving the catalytic nitrate reduction, Catalysis today. 55 (2000) 79-90, https://doi.org/10.1016/S0920-5861(99)00228-X

[63] L. Calvo, M. A. Gilarranz, J. A. Casas, A. F. Mohedano and J. J. Rodriguez. Denitrification of water with activated carbon-supported metallic catalysts, Industrial & engineering chemistry research. 49 (2010) 5603-5609, https://doi.org/10.1021/ie100838r

[64] A. Pizarro, C. Molina, J. Rodriguez and F. Epron. Catalytic reduction of nitrate and nitrite with mono-and bimetallic catalysts supported on pillared clays, Journal of Environmental Chemical Engineering. 3 (2015) 2777-2785, https://doi.org/10.1016/j.jece.2015.09.026

[65] M. Gholinejad, F. Khosravi, M. Afrasi, J. M. Sansano and C. Nájera. Applications of

bimetallic PdCu catalysts, Catalysis Science & Technology. 11 (2021) 2652-2702, DOI: 10.1039/D0CY02339F

[66] U. Prüsse and K.-D. Vorlop. Supported bimetallic palladium catalysts for water-phase nitrate reduction, Journal of Molecular Catalysis A: Chemical. 173 (2001) 313-328, https://doi.org/10.1016/S1381-1169(01)00156-X

[67] G. Strukul, R. Gavagnin, F. Pinna, E. Modaferri, S. Perathoner, G. Centi, M. Marella and M. Tomaselli. Use of palladium based catalysts in the hydrogenation of nitrates in drinking water: From powders to membranes, Catalysis today. 55 (2000) 139-149, https://doi.org/10.1016/S0920-5861(99)00233-3

[68] F. Gauthard, F. Epron and J. Barbier. Palladium and platinum-based catalysts in the catalytic reduction of nitrate in water: Effect of copper, silver, or gold addition, Journal of Catalysis. 220 (2003) 182-191, https://doi.org/10.1016/S0021-9517(03)00252-5

Chapter 2

Rapid removal and catalytic decomposition of nitrate in anion-exchange resin containing gold nanoparticles

2-1 Introduction

As mentioned in Chapter 1, anion exchange resin is a commonly used anion-exchanger for NO_3^- removal, and Choi et al. [1] developed a bimetallic PdCu-nanoparticle-containing anion-exchange resin (PdCu@resin) for a two-step process. Mendow et al. also reported the removal and decomposition of NO_3^- in a two-step process using a catalyst similar to that used by Choi et al. (PdCu@resin), while they used H_2 at 1 bar instead of the H_2/CO_2 mixture at 6 bar [2]. Mendow et al. further investigated bimetallic PdSn particles in resin and found that PdSn@resin was regenerated in a shorter reaction time than PdCu@resin [3].

Although bimetallic catalysts are active for NO_3^- reduction, the preparation process is complicated, and the performance can be affected by a lot of parameters. Therefore, it is worth considering whether anion exchange resin containing single metals are active for NO_3^- reduction in the two-step process.

In this chapter, the performance of anion exchange resin containing most of precious metals, including Ru, Rh, Pd, Ir, Pt and Au, for NO_3^- decomposition in the resin was investigated, and it was found that all of them exhibited catalytic activity for NO_3^- decomposition in 1 bar H_2 at 80 °C. However, among the precious metals examined, only Au did not require a reduction treatment with additional reducing reagent to form metal particles in the resin, because $AuCl_4^-$ was spontaneously reduced in the resin. The spontaneous reduction mechanism of $AuCl_4^-$ in the resin was also explored. Because the spontaneous reduction of $AuCl_4^-$ could be advantageous for large-scale applications, Au-introduced resin was further investigated in the preparation conditions to improve the catalytic performance for NO_3^- decomposition. The optimal reaction conditions for NO_3^- decomposition and the products of NO_3^- decomposition were also investigated. Finally, the reusability of the catalyst was tested to demonstrate the feasibility of the two-step process with this catalyst.

2-2 Experimental

2-2-1 Material preparation

Ten grams of anion-exchange resin (Amberlite^{TM} IRA410(OH), Organo Co.), which have quaternary ammonium groups (–[$(CH_3)_2N(C_2H_4OH)]^+OH^-$) as anion-exchange sites, were treated in 100 mL of 5 % NaCl solution at room temperature for 1 h to exchange OH^- in the resin with Cl^-. Subsequently, the resin was further treated in 100 mL of ultrapure water at room temperature for 15 min and collected via filtration. This process was repeated five times. The obtained resin is referred to as AER.

Gold nanoparticles-incorporated AER was prepared as follows. An aqueous solution of $HAuCl_4$ was prepared by dissolving a certain amount of $HAuCl_4 \cdot 4H_2O$ (FUJIFILM Wako Pure Chemical Co.) in 10 mL of ultrapure water. AER (0.5 g) was added to the solution, and the suspension was stirred at 38 °C for 12 h. The resin was collected via filtration and washed with ultrapure water. The obtained material is subsequently referred to as Au@AER. Au@AER samples with different Au loadings were prepared by changing the amount of $HAuCl_4 \cdot 4H_2O$ in the solution.

The hydrogen treatment of Au@AER was performed as follows: 0.5 g of Au@AER was placed in a glass tube reactor, and N_2 (10 mL min^{-1}) was allowed to flow into the reactor at room temperature for 30 min. After that, the gas was changed to H_2 (10 mL min^{-1}), and the temperature was increased to 80 °C and the reactor was maintained at this temperature for 1 h. The material obtained after this treatment is referred to as Au@AER(H_2).

M@AER(H_2) (M=Pd, Pt, Rh, and Ir) samples were prepared using the same procedure as that for Au@AER(H_2) but K_2PdCl_4 (FUJIFILM Wako Pure Chemical Co.), $H_2PtCl_6 \cdot 6H_2O$ (FUJIFILM Wako Pure Chemical Co.), Na_3RhCl_6(FUJIFILM Wako Pure Chemical Co.), and $Na_2IrCl_6 \cdot 6H_2O$ (Sigma-Aldrich) were used instead of $HAuCl_4 \cdot 4H_2O$. Only for Ru@AER(H_2), $RuCl_3 \cdot nH_2O$ (FUJIFILM Wako Pure Chemical Co.) was dissolved in 6 mL of hydrochloric acid (0.1 mol L^{-1}, FUJIFILM Wako Pure Chemical Co.) instead of ultrapure water, because it was not dissolved in ultrapure water, and

anionic $RuClx^{n-}$ complex was formed in the solution.

Furthermore, Au@AER was treated with $NaBH_4$. Au@AER was added to 100 mL of $NaBH_4$ (Kanto Chemical Co.) solution (molar ratio of $NaBH_4$ to Au was 10), and the mixture was stirred at room temperature for 1 h. After that, the resin was collected via filtration and washed with ultrapure water. The resulting material is referred to as Au@AER($NaBH_4$). In addition, Au@AER was treated with $NaBH_4$ after grinding in a mortar for 5 min. The resulting material is referred to as Au@AER (ground-$NaBH_4$).

2-2-2 Characterization

Powder X-ray diffraction (XRD) patterns were collected using an X-ray diffractometer (Bruker, D2 PHASER 2nd Generation) with Cu Kα radiation at a scan step of 0.02º in the 2θ range of 10 - 80º. The average size of gold particle was calculated by Scherrer's equation.

Gold particles in the materials were observed using a transmission electron microscope (JEOL JEM-2010) and particle size distributions of Au particles were estimated from TEM images.

The oxidation state of the surface of the Au particles was investigated using X-ray photoelectron spectroscopy (XPS; JPS-9010MC, JEOL) with Al Kα radiation.

Temperature-programmed reduction (H_2-TPR) profile was obtained using a catalyst analyzer (BEL-CAT, MicrotracBEL Co.) under 1 % H_2 flow. After the sample was pretreated in He flow (25 mL min^{-1}) at room temperature for 1 h, the sample temperature was increased in a flow of 1% H_2 (Ar balance) at 5 °C min^{-1}, while the concentration of H_2 at the reactor outlet was monitored with a TCD detector.

Fourier transform infrared spectra were recorded on a JASCO FT/IR-4600 at room temperature from 400 to 4000 cm^{-1}. The sample was diluted 100 times with KBr and was pressed. Then the sample disk was set to the spectrometer under ambient conditions and the spectrum was recorded with 32 scans at 2.00 cm^{-1} resolution. KBr disk without sample was used for background measurement.

All $HAuCl_4$ solutions were characterized using a UV−vis spectrometer (V-670 spectrophotometer, JASCO) in the wavelength range from 200 to 800 nm with a resolution of 1 nm.

2-2-3 Catalytic decomposition of NO_3^- in M@AER(H_2) and Au@AER, and reusability test

M@AER(H_2) (0.1 g) was added to 100 mL of NO_3^- solution (C_0 = 1.62 mmol L^{-1}), and the mixture was stirred at 38 °C to take NO_3^- into M@AER(H_2). After 1 h, M@AER(H_2) was collected by filtration and the concentration of NO_3^- in the solution, which is referred to as C_{1h}, was determined using an ion-chromatograph (IC-8100, TOSOH) equipped with a column (TSKgel$^{@}$ Super IC-Anion HC). A solution of $NaHCO_3$ (7.5 mmol L^{-1}) and Na_2CO_3 (0.8 mmol L^{-1}) was used as eluent. The amount of NO_3^- taken in M@AER(H_2) (q_{taken}, mmol g^{-1}) was calculated by eq. 2-1,

$$q_{\text{taken}} = \frac{(C_0 - C_{1\text{h}})V}{m} \qquad \text{(eq. 2-1)}$$

where, V and m are the volume of the NO_3^- solution and the mass of M@AER(H_2), respectively.

Then, M@AER(H_2) with NO_3^- was fixed in a glass tube and N_2 (10 mL min^{-1}) was fed to the tube at room temperature for 30 min. After the gas was changed to H_2 (10 mL min^{-1}), the temperature was increased to 80 °C at a rate of 5 °C min^{-1} and was maintained for 2 h. Throughout this process, the gas at the outlet of the tube was blown into two trap bottles containing dilute sulfuric acid (20 mmol L^{-1}) to capture NH_3 as NH_4^+ if it formed. The trap solution was analyzed using a ion-chromatograph (IC-2001, TOSOH) equipped with a column (TSKgel SuperIC-AZ).

After that operation, the M@AER(H_2) was taken out from the tube and was added to 100 mL of NaCl solution (500 mmol L^{-1}), and the mixture was stirred at 38 °C for 1 h to exchange undecomposed NO_3^- in the resin with Cl^-. The resin was removed from the solution, and the solution was analyzed by an ion-chromatography to determine the

concentration of NO_3^-, which is referred to as $C_{undecomp}$. The amount of decomposed NO_3^- (q_{decomp}, mmol g^{-1}) was calculated by eqs. 2-2 and 2-3,

$$q_{undecomp} = \frac{C_{undecomp} V_{NaCl}}{m} \quad \text{(eq. 2-2)}$$

$$q_{decomp} = q_{taken} - q_{undecomp} \quad \text{(eq. 2-3)}$$

where V_{NaCl} and m are the volume of the NaCl solution and mass of M@AER(H_2), respectively.

Reusability of Au@AER was investigated by performing ion-exchange removal of NO_3^- and decomposition of NO_3^- in the resin repeatedly under the conditions mentioned above up to five times.

2-2-4 Ion-exchange isotherm for NO_3^- over AER and Au@AER

Au@AER (0.03 g) and 10 mL of NO_3^- solution with different concentrations (C_0 = 1, 2, 5, 10, 15, 20, 30, 40, 50 and 100 mmol L^{-1}) were added to a test tube. The mixture in the test tube was stirred at 38 °C for 8 h, and concentration of NO_3^- in the solution was analyzed using the ion-chromatograph. Amount of NO_3^- taken in Au@AER was calculated by eq. 2-4,

$$q = \frac{(C_0 - C_{eq})V}{m} \quad \text{(eq. 2-4)}$$

where C_{eq}, V, and m are the concentration of NO_3^- in the solution at 8 h, volume of the NO_3^- solution and the mass of Au@AER, respectively. The ion-exchange isotherm was also measured for AER in the same manner as that for Au@AER.

Kinetic analysis for the ion-exchange removal of NO_3^- was performed using the NO_3^- solution (C_0 = 1.62 mmol L^{-1}) in a process similar to that used for the ion-exchange isotherm, and small portions of the solution were collected at regular intervals.

2-2-5 Influence of dose of AER and Au@AER for ion-exchange removal of NO_3^-

To 10 mL of NO_3^- solution (C_0 = 1.62 mmol L^{-1}), different amount of Au@AER

(0.001 – 0.24 g) was added, and the mixture was stirred at 38 °C for 8 h. After Au@AER was removed by filtration, the concentration of NO_3^- in the filtrate was determined. A similar experiment was also performed with AER.

2-2-6 Ion-exchange rate of the introduction of $AuCl_4^-$ to AER

An aqueous solution of $HAuCl_4$ (C_0 = 7.5 mmol L^{-1}) was prepared by dissolving 0.1854 g of $HAuCl_4 \cdot 4H_2O$ to 60 mL of ultrapure water. To this solution, 1.5 g of AER was added, and this suspension was stirred at 38 °C up to 12 h. 1 mL of $HAuCl_4$ solution before AER addition was diluted 20 times by ultrapure water and 2 mL of the solution after AER addition was taken at different time. These solutions were analyzed by UV-vis spectroscopy.

2-2-7 Breakthrough test

A breakthrough test for the ion-exchange removal of NO_3^- was performed using a fixed-bed reactor at room temperature. One gram of Au@AER was fixed in a glass tube and NO_3^- solution (C_0 = 1.62 mmol L^{-1}) was continuously fed to the tube using a pump (LC-10AD, Shimadzu Co.) at a flow rate of 0.5 mL min^{-1}, while the concentration of NO_3^- at the outlet of the tube was determined every 30 min. A similar experiment was also performed with AER.

2-2-8 Treatment of AER with Dess-Martin periodinane

One gram of AER was heated in N_2 at 100 °C for 2 h to remove weakly adsorbed water. Separately, 0.5 g of Dess-Martin periodinane (Sigma-Aldrich, 97 %) was dissolved in 10 mL of dichloromethane (FUJIFILM Wako Pure Chemical Co.), and the treated AER was added to it. Then, the mixture was stirred at room temperature for 3 h and was filtered. The resulting resin is named AER-DMP. The treated resin was stored in ultrapure water not to be dried.

2-2-9 Introduction of $AuCl_4^-$ to AER-DMP

An aqueous solution of $HAuCl_4$ was prepared by dissolving 0.0247 g of $HAuCl_4 \cdot 4H_2O$ (FUJIFILM Wako Pure Chemical Co.) in 4 mL of ultrapure water. To the solution, 0.2 g of AER-DMP was added, and the suspension was stirred at room temperature for 12 h. The resin was collected by filtration and washed with ultrapure water. The content of Au was 0.3 mmol g^{-1}. The resulting resin is named Au@AER-DMP.

2-2-10 Treatment of Au@AER-DMP with $NaBH_4$

An aqueous solution of $NaBH_4$ was prepared by dissolving 0.011 g of $NaBH_4$ (Kanto Chemical Co., Inc.) in 10 mL of ultrapure water. To the solution, 0.1 g of Au@AER-DMP was added, and the mixture was stirred at room temperature for 1 h. The resin was collected by filtration and washed with ultrapure water.

2-2-11 Analysis of gaseous products formed by the decomposition of NO_3^- in Au@AER

Au@AER (0.2 g) was added to 200 mL of NO_3^- solution (C_0 = 1.62 mmol L^{-1}) and the mixture was stirred at 38 °C. After 1 h, Au@AER was collected by filtration. Au@AER with NO_3^- was fixed in a glass reactor and it was set to the reaction apparatus with a mass spectrometer (M-201QA-TDM, Canon ANELVA Co) shown in Fig. 2-1.

After N_2 (10 mL min^{-1}) was fed to the reactor at room temperature for 30 min, the temperature of the reactor was decreased to −50 °C by circulating refrigerant to the furnace. Then, the gas was changed to H_2 (10 mL min^{-1}). After 1 h, refrigerant circulation was stopped, and the temperature was allowed to naturally increase to 0 °C. During that process, no product was detected in the gas at the outlet of the reactor. Then, the temperature was increased to 80 °C at a rate of 5 °C min^{-1} and kept for 6 h. All the while, the gas at the outlet of the reactor was analyzed by the mass spectrometer.

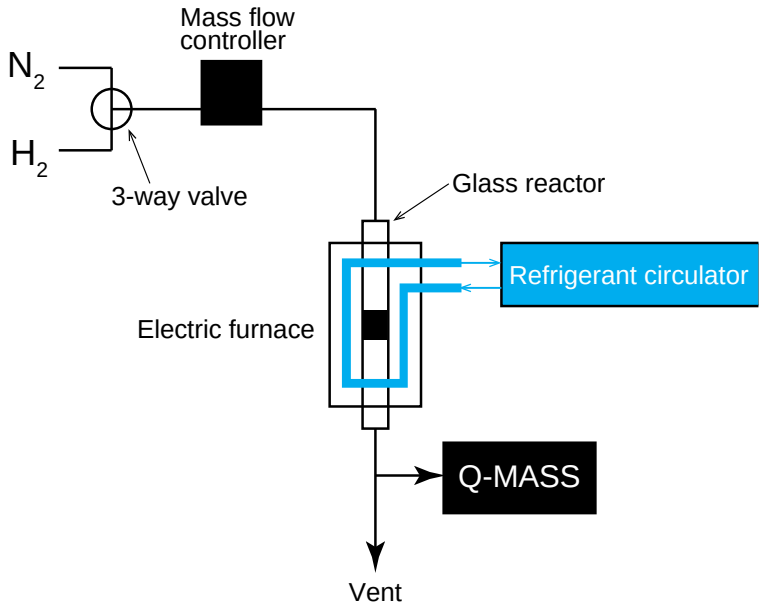

Fig. 2-1 Analysis of the gaseous products formed by the decomposition of NO_3^- in 0.3 mmol g^{-1} Au@AER. Conditions: mass of Au@AER, 0.2 g; concentration and volume of NO_3^- solution, 1.62 mmol L^{-1} and 200 mL; temperature range during NO_3^- decomposition process, -50 °C ~ 80 °C.

2-3 Results and discussion

2-3-1 Effect of metals on the performances of M@AER(H_2)

Fig. 2-2 shows the effect of metals in M@AER(H_2) on the performance for NO_3^- removal and decomposition, where M@AER(H_2) containing 0.2 mmol g^{-1} of metal was used and the NO_3^- decomposition was performed in H_2 at 80 °C for 2 h. Although 0.92 mmol g^{-1} of NO_3^- was taken in pristine AER without metal, no NO_3^- was decomposed. In contrast, NO_3^- was taken in M@AER(H_2) and was decomposed. While removal performance of M@AER(H_2) was almost the same as that of pristine AER, the catalytic activity for NO_3^- decomposition varied greatly depending on the metals. In the metals tested here, Ru, Au and Rh were particularly effective for NO_3^- decomposition. Among them, Ru@AER(H_2) showed the best catalytic activity and 0.20 mmol g^{-1} of NO_3^- was decomposed. This decomposed amount corresponded to 18 % relative to the amount of NO_3^- taken in it, namely 18 % NO_3^- conversion.

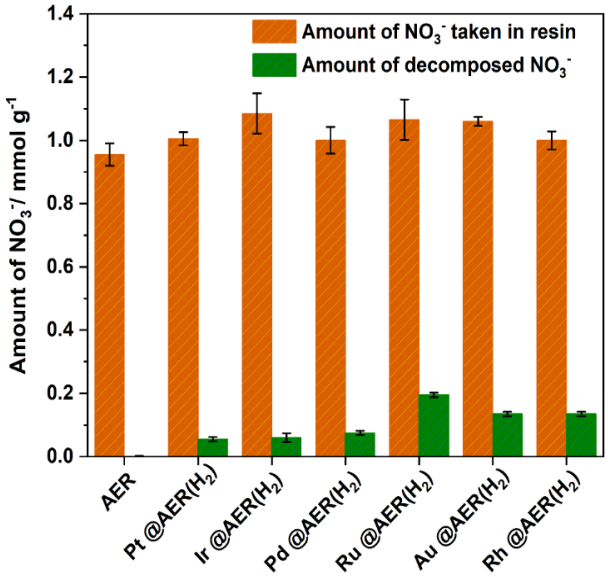

Fig. 2-2 Effect of metals on the performance of M@AER(H_2) for NO_3^- uptake and NO_3^- decomposition. The content of metal in M@AER(H_2) was 0.2 mmol g^{-1}. NO_3^- uptake measurement: $[NO_3^-]_0$ = 100 ppm (1.62 mmol L^{-1}); volume of solution, 100 mL; amount of M@AER(H_2), 0.1 g. NO_3^- decomposition was performed in H_2 flow at 80 °C for 2 h.

To form metal particles in AER, reduction of metal cation in the complex (MCl_x^{n-}) was necessary after the introduction of it into the resin. In fact, without the reduction treatment in H_2 at 80 ℃, Ru@AER and Rh@AER showed only very low catalytic activity for NO_3^- decomposition (Fig. 2-3). In contrast, Au@AER without the treatment showed almost the same catalytic activity as Au@AER(H_2) (Fig. 2-3), indicating that the reduction treatment in H_2 was unnecessary for Au@AER. This was because of occurrence of the spontaneous reduction of $AuCl_4^-$ in AER.

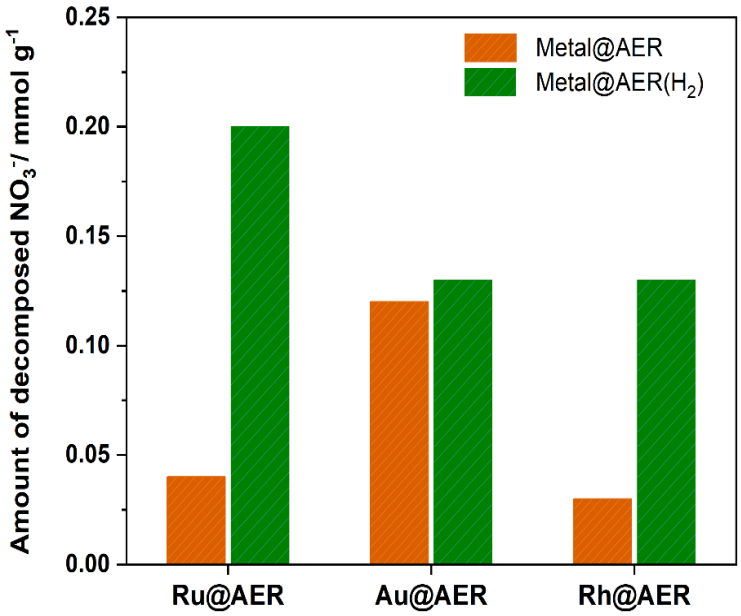

Fig. 2-3. Effect of H_2 treatment for M@AER (M=Ru, Au, and Rh) on NO_3^- decomposition. The content of the metal was 0.2 mmol g^{-1}. Conditions for H_2 treatment: in H_2 flow at 80 ℃ for 1 h. The conditions for NO_3^- uptake and NO_3^- decomposition was the same as those in Fig. 2-2.

Au@AER without H_2 treatment was also analyzed by H_2-TPR to confirm whether gold compounds in resin can be reduced by H_2, and the result is shown in Fig. 2-4. No H_2 consumption peak was observed on H_2-TPR profile for Au@AER up to 80 ℃.

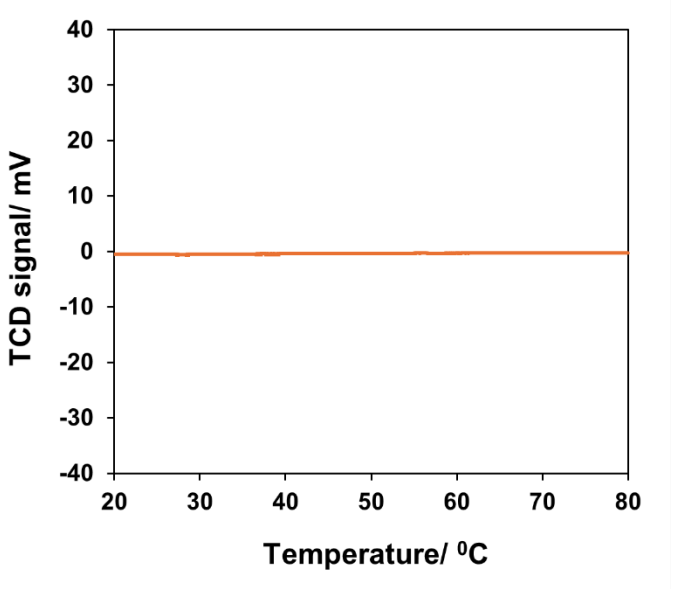

Fig. 2-4. H_2-TPR profile for Au@AER. In this experiment, Au@AER without NO_3^- was used. The content of Au in Au@AER was 0.3 mmol g^{-1}.

To confirm that $AuCl_4^-$ in AER was spontaneously reduced without H_2 treatment, the Au@AER and Au@AER(H_2) obtained by the treatment of Au@AER in H_2 flow at 80 ℃ for 1 h were analyzed by XRD, and the XRD patterns are shown in Fig. 2-5(g). As expected, there was obvious Au diffraction peaks in XRD pattern of Au@AER without H_2 treatment. It is noted that the treatment of Au@AER in H_2 at 80 ℃ to obtain Au@AER(H_2) did not change the XRD patterns. For comparison, other M@AER and M@AER(H_2) were also analyzed by XRD, and the results are also shown in Fig. 2-5. No diffraction peaks of other metals were observed in all the XRD patterns before and after H_2 treatment.

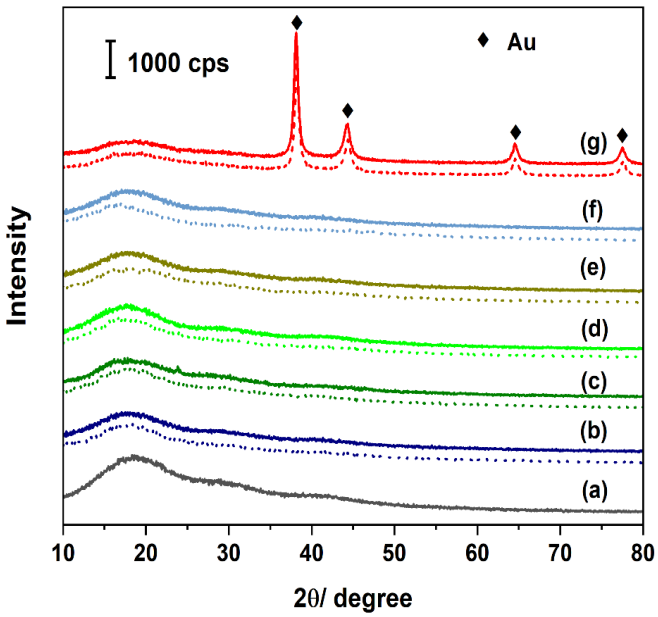

Fig. 2-5 XRD patterns of M@AER and M@AER(H_2). M@AER(H_2) were obtained by the treatment of M@AER in H_2 flow at 80 °C for 1 h. Dashed and solid lines are M@AER and M@AER(H_2), respectively. (a) Pristine AER, and M@AER and M@AER(H_2) with (b) Rh, (c) Ru, (d) Pd, (e) Ir, (f) Pt, and (g) Au.

Although there were no diffraction peaks of other metals in XRD patterns of M@AER(H_2) except for Au@AER(H_2), part of NO_3^- taken in M@AER(H_2) was decomposed by H_2, implying that these metals were already reduced to form metal particles in the resin. It was because the size of metals in M@AER(H_2) was too small to detect and the dispersion of that was high. To confirm this, M@AER(H_2) was analyzed by TEM, and Fig. 2-6 shows the TEM images of each M@AER(H_2). As expected, small size metal particles were present in each sample.

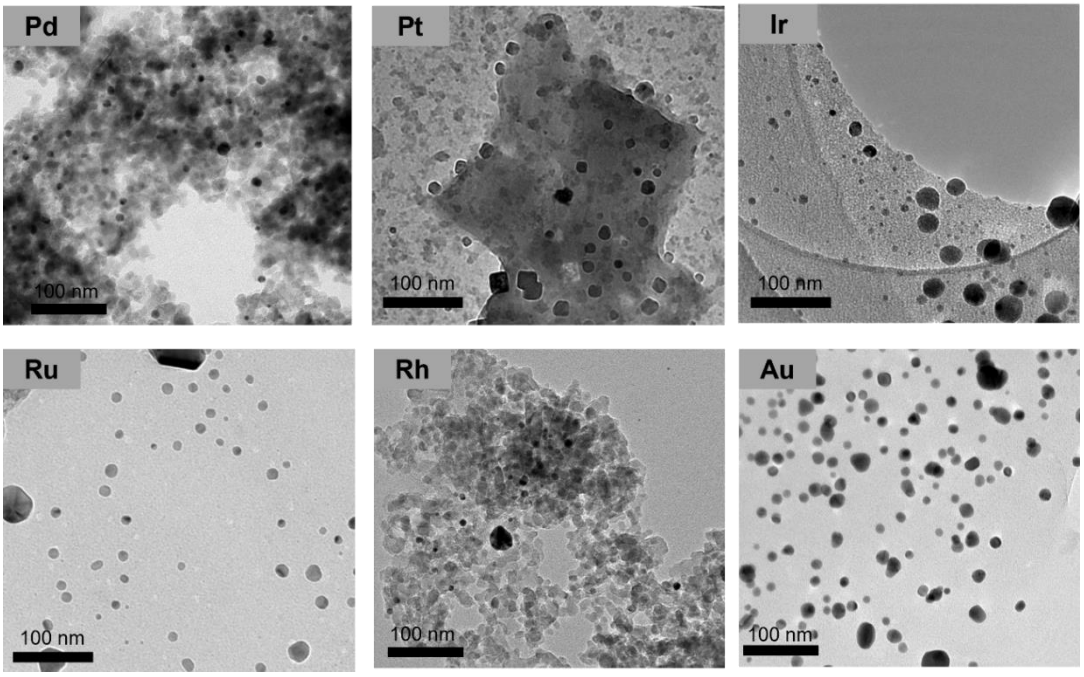

Fig. 2-6 TEM images of Pd@AER(H_2); Pt@AER (H_2); Ir@AER (H_2); Ru@AER (H_2); Rh@AER (H_2); Au@AER (H_2). M@AER(H_2) was treated in H_2 flow at 80 °C for 1 h. and the content of metals in AER are 0.2 mmol g^{-1}.

To investigate the effect of the reduction time of $AuCl_4^-$ in Au@AER in H_2 flow at 80 °C on the size of Au particles and the amount of decomposed NO_3^-, Au@AER was treated in H_2 for different treatment time. The prepared Au@AER(H_2) were analyzed by XRD, and the results are shown in Fig. 2-7. XRD pattern of Au@AER(H_2) was almost identical regardless of the treatment time. Fig. 2-8 shows the effect of H_2 treatment time on the amount of decomposed NO_3^-. The amount of decomposed NO_3^- was almost the same regardless of H_2 treatment time, suggesting that the reduction of $AuCl_4^-$ in AER was already completed even before the H_2 treatment. Among all M@AER(H_2), Au@AER shows high (but not the highest) catalytic activity for NO_3^- decomposition and it was unnecessary to reduce $AuCl_4^-$ in AER by additional reducing agents, which decreased the difficulty and cost of the catalyst preparation. Therefore, in the next and subsequent sections of this chapter, Au@AER was focused on the investigation.

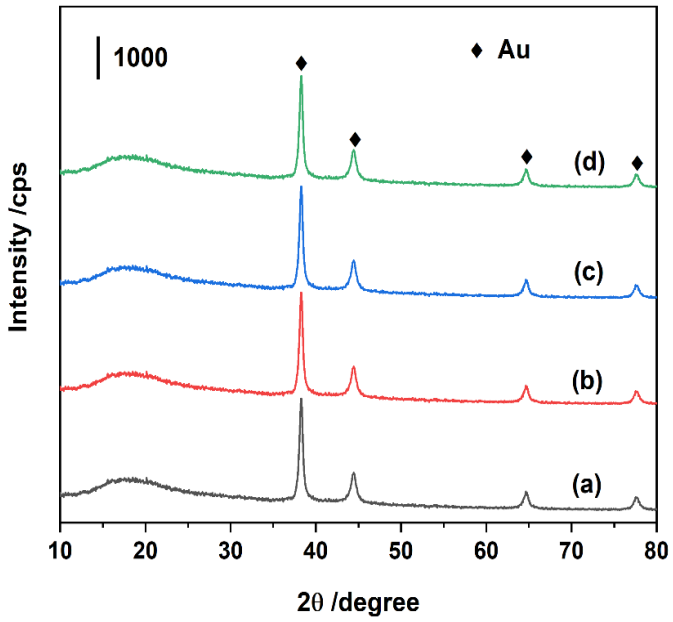

Fig. 2-7 XRD patterns of 0.2 mmol g^{-1} Au@AER that reduced by H_2 for different time. (a) without H_2 treatment; (b) 1 h; (c) 2 h; and (d) 3 h.

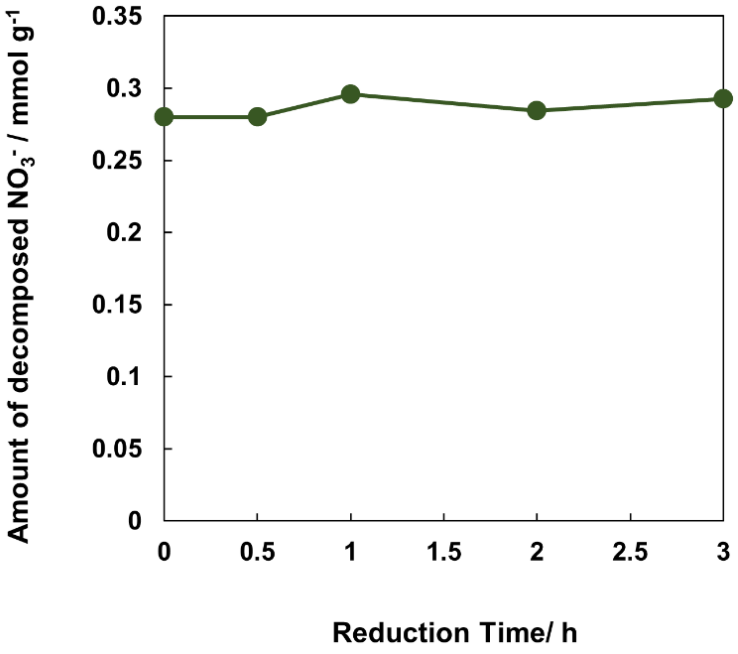

Fig. 2-8. Effect of H_2 treatment time for Au@AER on NO_3^- decomposition. The content of the metal was 0.2 mmol g^{-1}. Conditions for H_2 treatment: in H_2 flow at 80 °C for different time. The conditions for NO_3^- uptake and NO_3^- decomposition: NO_3^- uptake measurement: $[NO_3^-]_0$ = 100 ppm (1.62 mmol L^{-1}); volume of solution, 100 mL; amount of Au@AER(H_2), 0.1 g. NO_3^- decomposition was performed in H_2 flow at 80 °C for 5 h.

2-3-2 Introduction and reduction rate of $AuCl_4^-$ in AER

$AuCl_4^-$ was introduced in AER through ion-exchange process exchanging with Cl^- in AER. Therefore, in order to investigate the ion-exchange rate of $AuCl_4^-$, the concentration of $AuCl_4^-$ in $HAuCl_4$ solution was tracked with the ion-exchange time, and the UV-Vis absorption spectra and the calculated amount of $AuCl_4^-$ in AER are shown in Fig. 2-9 and Table 2-1. The $HAuCl_4$ solution shows an intense charge transfer band at 222 nm and a moderate D–d transition band at 290 nm and there is no obvious absorption in the range of 400–800 nm [4]. As shown in Fig. 2-9, after 1 h, the intense charge transfer band and moderate D-d transition band disappeared, indicating that almost all $AuCl_4^-$ in the solution was taken in resin. This concluded that the ion-exchange process between $AuCl_4^-$ in $HAuCl_4$ solution and Cl^- in AER was completed within one hour, meaning that it was a fast process.

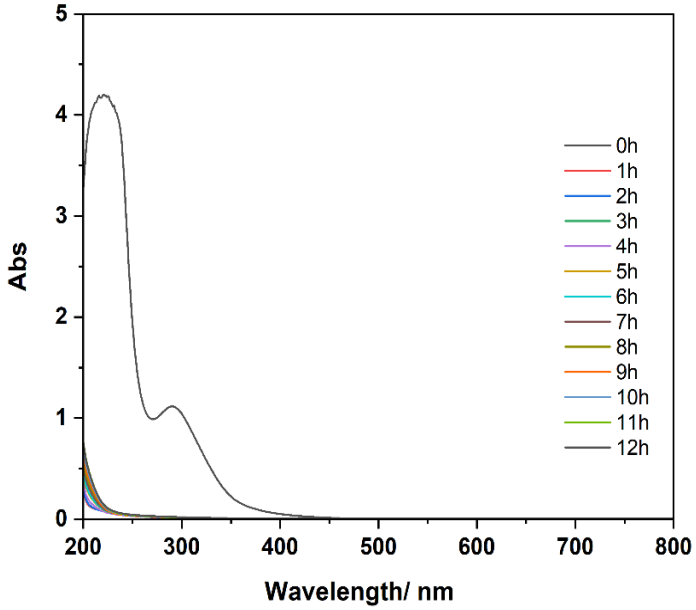

Fig. 2-9 UV-Vis spectra of $HAuCl_4$ solution at different time of the $AuCl_4^-$ introduction process. (Amount of AER, 1.0 g; volume and concentration of $HAuCl_4$ solution, 10 mL and 30 mmol L^{-1}; reaction temperature, 38 °C)

Table 2-1. The amount of $AuCl_4^-$ in AER calculated from the concentration difference of $HAuCl_4$ solution before and after ion-exchange process.

Time of ion-exchange/ h	Amount of $AuCl_4^-$ in AER[a]/ mmol g^{-1}
0	0
1	0.3
2	0.3
3	0.3
4	0.3
5	0.3
6	0.3
7	0.3
8	0.3
9	0.3
10	0.3
11	0.3
12	0.3

[a] Calculated from the maximum absorption value of UV-Vis spectrum.

According to the XRD patterns shown in Fig. 2-5 and Fig. 2-7, $AuCl_4^-$ in AER was spontaneously reduced before it was treated with H_2. Therefore, to investigate the spontaneous reduction rate of $AuCl_4^-$ in AER, the obtained Au@AER at different ion-exchange time were analyzed by XRD, and the results are shown in Fig. 2-10. As shown in Fig. 2-10, there were no diffraction peaks of Au in the XRD patterns of Au@AER with less than 2 h of the $AuCl_4^-$ introduction, while obvious Au diffraction peaks were observed in the XRD patterns of Au@AER with more than 3 h. Therefore, it can be concluded that the spontaneous reduction of $AuCl_4^-$ is a slow process compared to the introduction (ion-exchange) process of $AuCl_4^-$ into AER.

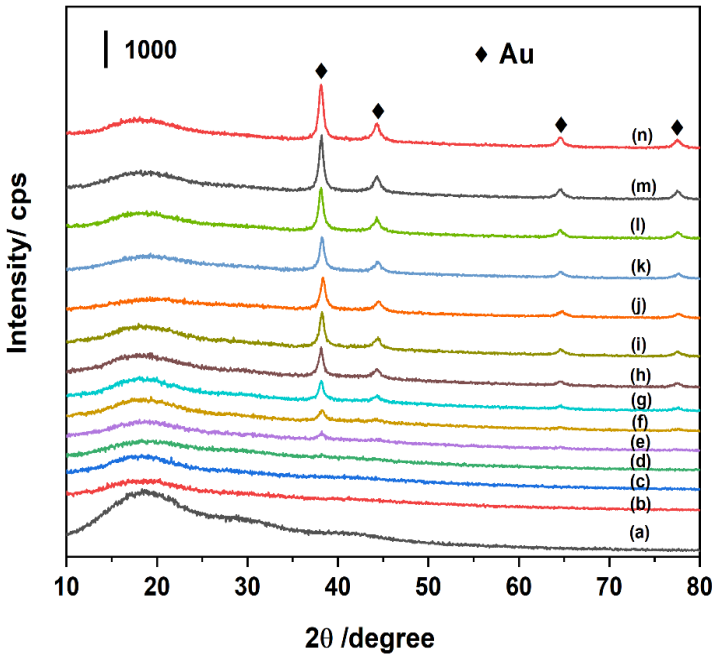

Fig. 2-10 XRD patterns of 0.3 mmol g^{-1} Au@AER that prepared with different time. (a) AER; (b) 0.5 h; (c) 1 h; (d) 2 h; (e) 3 h; (f) 4 h; (g) 5 h; (h) 6 h; (i) 7 h; (j) 8 h; (k) 9 h; (l) 10 h; (m) 11 h; (n) 12 h.

2-3-3 Spontaneous reduction of $AuCl_4^-$ in resin

Regarding to the spontaneous reduction of $AuCl_4^-$ in anion-exchange resin, Ishida et al. [5] reported that three anion-exchange resins which included two weak basic resins (Amberlite^{TM} IRA 743 and Amberlite^{TM} IRA 96SB) and one strong basic resin (DAIAION^{TM} HPA 25) were served not only as a support for Au particles but also acted as a reductant for $AuCl_4^-$ in the resins, in which $AuCl_4^-$ was reduced by the reaction with tertiary amino groups and quaternary ammonium one present in the resins to form Au^0 particles. The anion exchange resin used in this study was different to those used by Ishida et al. and had primary hydroxyl group at the anion-exchange site ($-[(CH_3)_2N(C_2H_4OH)]^+Cl^-$). Since generally alcohol acts as a reducing agent, the primary hydroxyl group in AER could act as a reductant for $AuCl_4^-$. Therefore, it was speculated that $AuCl_4^-$ introduced in AER was reduced by the reaction with primary hydroxyl group in AER to form Au^0 particles, and the hydroxyl group was also transformed to aldehyde group at the same time. In order to confirm this hypothesis, Au@AER and pristine AER were analyzed by FT-IR, and the results are shown in Fig. 2-11. It was found that as expected, a new IR band that was not present in pristine AER was observed at 1700 cm^{-1} in a spectrum of Au@AER, which is a characteristic band of C=O vibration in aldehyde group [6], which is consistent with the hypothesis.

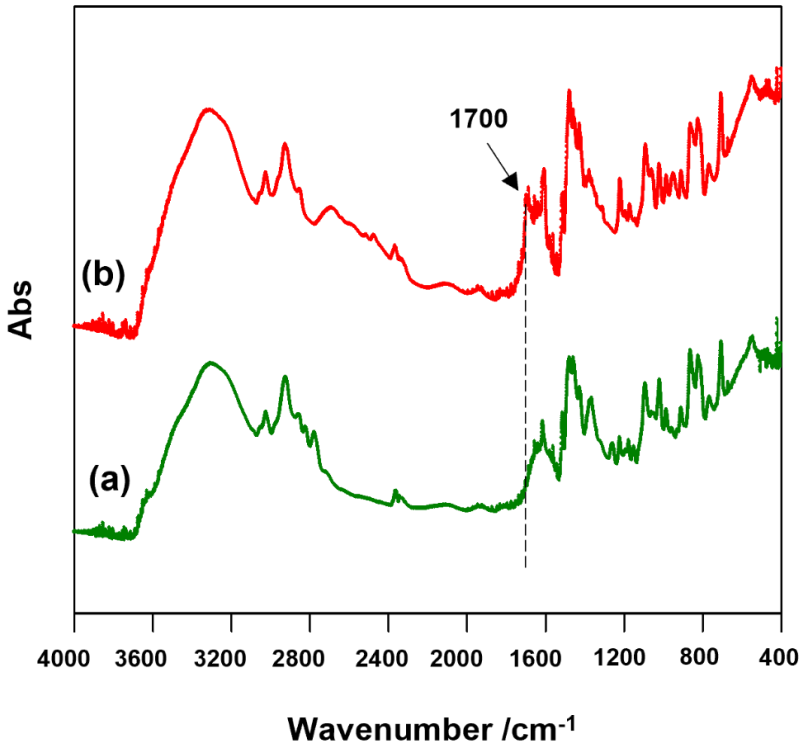

Fig. 2-11 FT-IR spectra of (a) AER and (b) 0.2 mmol g^{-1} Au@AER.

To further confirm the spontaneous reduction process of $AuCl_4^-$ by the reaction with primary hydroxyl group in AER, Dess-Martin periodinane (DMP), a common oxidizing agent to oxidize primary alcohol to aldehyde, was used to oxidize the primary hydroxyl groups in AER, and the pretreated AER was used to prepare Au@AER in the same procedure as that for previous Au@AER, where the obtained material is named Au@AER-DMP. The XRD pattern of Au@AER-DMP is shown in Fig. 2-12(c). No diffraction peaks of Au^0 particles that appeared in XRD pattern of Au@AER were observed, indicating that $AuCl_4^-$ was not spontaneously reduced in AER treated with DMP, which may be because the primary hydroxyl groups in AER was oxidized by DMP to aldehyde groups. In addition, the prepared Au@AER-DMP was treated with $NaBH_4$, and the XRD pattern of treated Au@AER-DMP is also shown in Fig. 2-12(d). The diffraction peaks of Au^0 particles appeared, indicating that $AuCl_4^-$ in AER-DMP was reduced by $NaBH_4$.

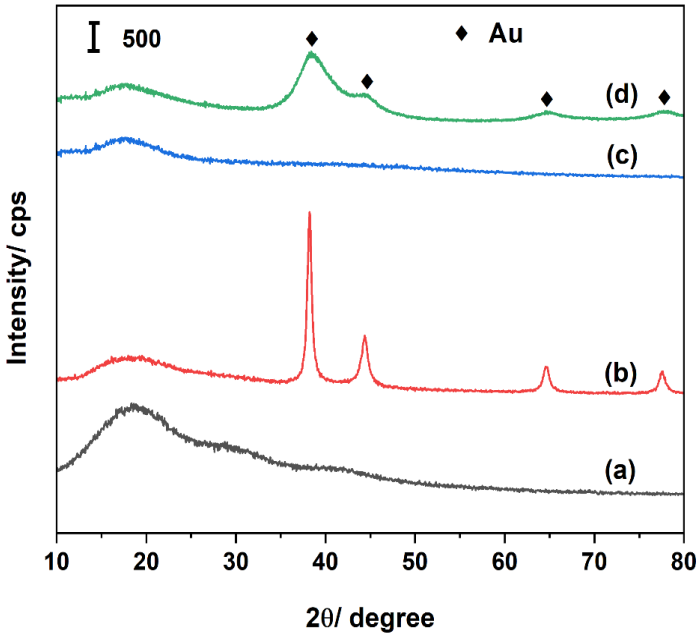

Fig. 2-12. XRD patterns of (a) pristine AER, (b) Au@AER, (c) Au@AER-DMP, and (d) Au@AER-DMP treated with $NaBH_4$. The content of Au was 0.3 mmol g^{-1}.

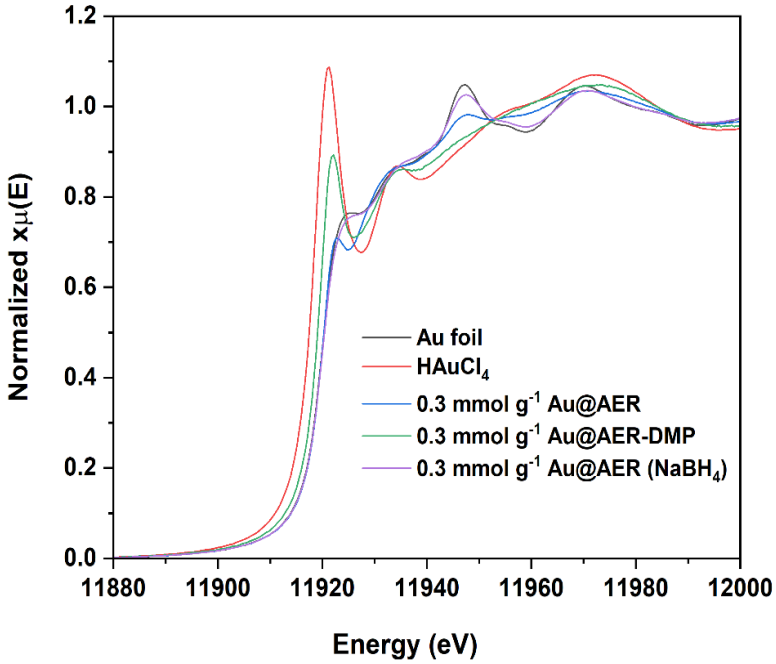

Fig. 2-13 XANES spectra for Au@AER with different treatments. All spectra are presented with phase shift correction.

Besides XRD, Au@AER and Au@AER-DMP were also analyzed by XAFS. Fig. 2-13 shows the Au-L_3 edge XANES spectra for Au@AER with different treatments and the compounds of $HAuCl_4$ and Au foil. In the spectrum of Au@AER, there are peaks at 11921 eV and 11945 eV, corresponding to Au^{3+} and Au^0 according to the spectra of $HAuCl_4$ and Au foil. The presence of the farmer peak (at 11921 eV) suggested that only part of $AuCl_4^-$ in AER was spontaneously reduced by the primary hydroxyl groups. For the spectrum of Au@AER-DMP, there was only a peak at 11921 eV, corresponding to Au^{3+}, indicating that $AuCl_4^-$ in Au@AER-DMP was not spontaneously reduced. The existence state of Au in the resin obtained based on the XANES results are consistent with the conclusion drawn based on the XRD analysis for Au@AER and Au@AER-DMP (Fig. 2-12). Therefore, it is concluded that $AuCl_4^-$ was reduced to Au^0 particles by the reaction with the primary hydroxyl group in AER. The spontaneous reduction process of $AuCl_4^-$ in AER is summarized as Scheme 2-1. $AuCl_4^-$ was introduced in AER by anion-exchange reaction. Then, it was reduced by primary hydroxyl in quaternary ammonium groups to form Au^0 particles and part of the generated Cl^- occupied the ion-exchange sites. At the same time, primary hydroxyl in quaternary ammonium groups was oxidized to aldehyde groups.

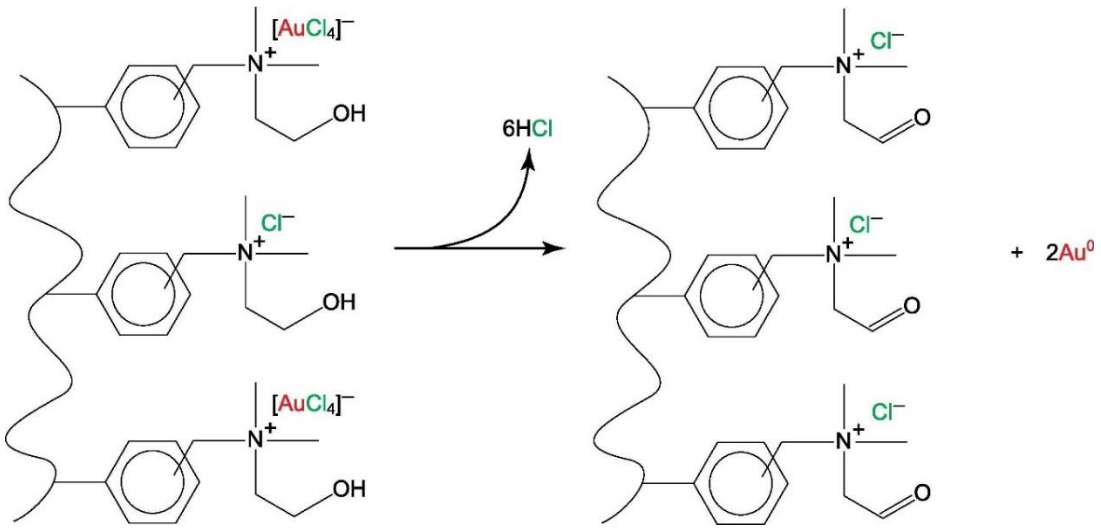

Scheme 2-1 Reaction scheme of the reduction of $AuCl_4^-$ occurring in AER.

2-3-4 Influence of the Au content in Au@AER on NO_3^- decomposition

In Fig. 2-14, the amount of NO_3^- taken in Au@AER and the amount of decomposed NO_3^- are plotted as a function of the Au content in Au@AER. It is noted that the amount of NO_3^- taken in Au@AER was increased with increase in the Au content up to 0.2 mmol g^{-1}, which was inconsistent with the theoretical ion-exchange process based only on the anion-exchange sites of AER. This fact suggested that ion exchange sites different from the originally present ones in AER were formed in Au@AER. It was speculated that those newly formed ion exchange sites originated from Cl^- that was formed during the reduction of $AuCl_4^-$ (Scheme 2-1) and were present on the surface of the Au^0 particles.

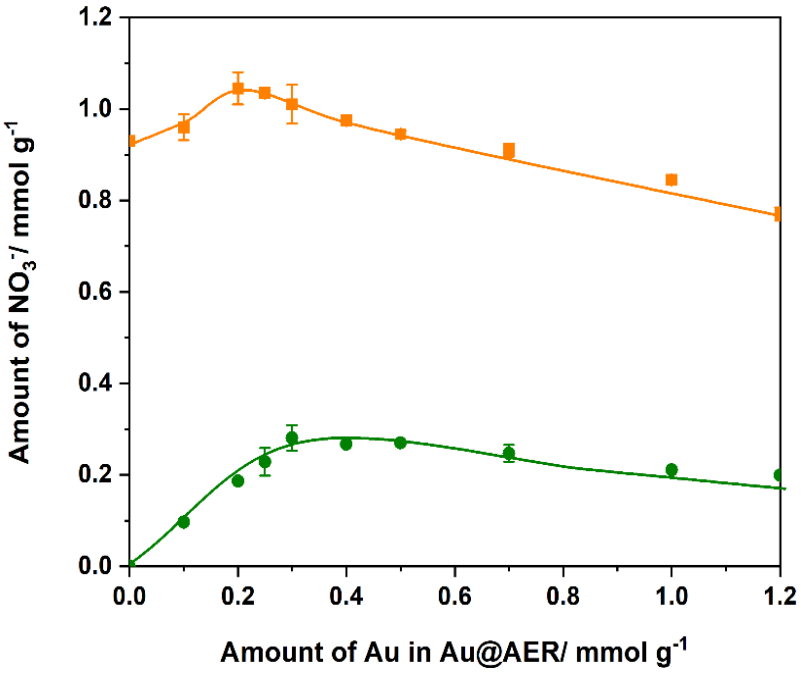

Fig. 2-14. Influence of Au content in Au@AER on the (■) amount of NO_3^- taken in the resin and (●) amount of decomposed NO_3^-. NO_3^- uptake measurement: $[NO_3^-]_0$ = 100 ppm (1.62 mmol L^{-1}); volume of solution, 100 mL; amount of Au@AER, 0.1 g. NO_3^- decomposition was performed in H_2 flow at 80 °C for 5 h.

To confirm this hypothesis, the amount of $AuCl_4^-$ and Cl^- in the solution before and after the $AuCl_4^-$ ion-exchange process was estimated, and Fig. 2-15 shows the relationship between the amount of Cl^- in the solution after ion-exchange process and the amount of $AuCl_4^-$ introduced into the resin. It was found that only a small amount of Cl^- was present in the solution after the ion-exchange process. According to Scheme 2-1, the theoretical amount of Cl^- released to solution is 3 times (molar ratio) that of the introduced $AuCl_4^-$, and the amount of Cl^- released from AER to the solution is the same as that of the $AuCl_4^-$ introduced to AER. Therefore, the theoretical amount of Cl^- in the solution is 4 times large amount of the introduced $AuCl_4^-$. But the actual amount of Cl^- in the solution was much smaller than the theoretical amount, which strongly supports the hypothesis that Cl^- was adsorbed on the Au^0 surface.

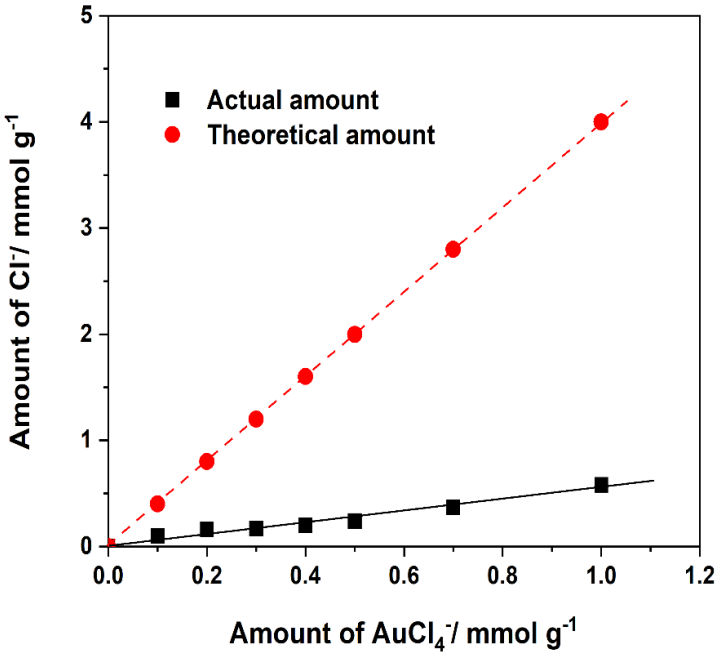

Fig. 2-15 Relationship between the amount of Cl^- released to the solution and the amount of $AuCl_4^-$ introduced into the resin.

Fig. 2-14 also shows the dependence of the amount of decomposed NO_3^- on the Au content in Au@AER. The amount of decomposed NO_3^- increased proportionally with the

Au content (up to 0.3 mmol g^{-1}) and reached a maximum value where 0.27 mmol g^{-1} of NO_3^- was decomposed. This amount corresponded to 25 % of NO_3^- conversion. This increase was simply due to the number of the Au sites available for the NO_3^- decomposition. However, the addition of excess Au, on the contrary, led to slight decrease of the amount of decomposed NO_3^-. The decrease of the amount of NO_3^- taken in Au@AER would be a primary reason for that of the decomposed NO_3^-. In addition, the formation of the large size Au particles in those Au@AER was another reason for it. Fig. 2-16 shows the TEM images of Au@AER. The large Au particles with an average diameter of 23 nm were formed in Au@AER with excess Au content (1.2 mmol g^{-1} of Au), while small and highly dispersed Au particles were present in Au@AER with low Au content (0.3 mmol g^{-1} of Au). The increase in the size of Au particles was also confirmed from the XRD patterns of Au@AER with different Au contents. The XRD patterns are shown in Fig. 2-17, and the crystallite size of Au calculated by Scherrer's equation is also shown in Fig. 2-18. The crystallite size of Au was increased from 12 to 24 nm as the Au content was increased from 0.1 to 1.2 mmol g^{-1}.

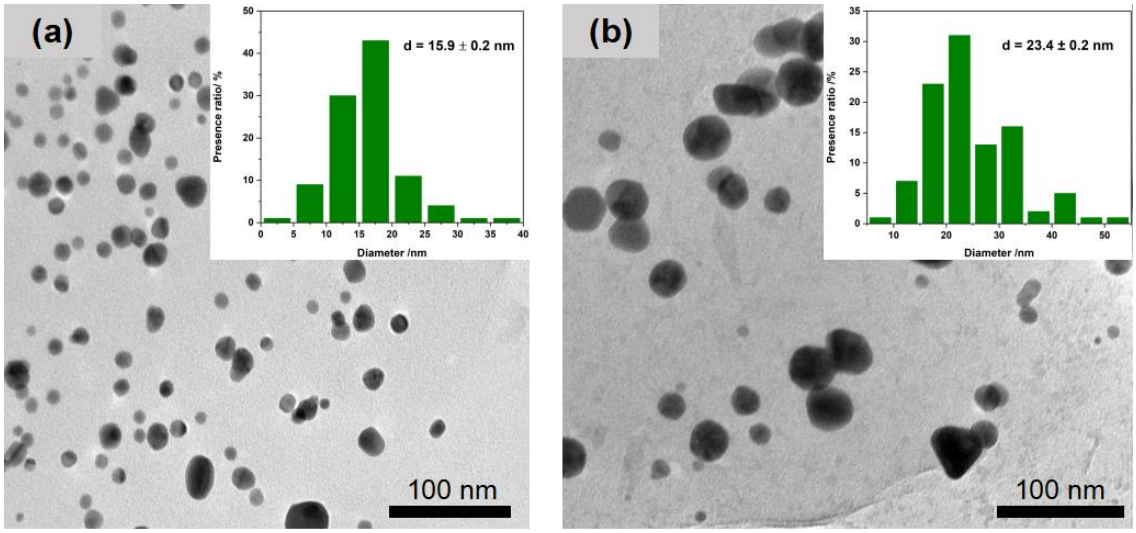

Fig. 2-16. TEM images and particle size distributions of Au particles for Au@AER with (a) 0.3 and (b) 1.2 mmol g^{-1} of Au.

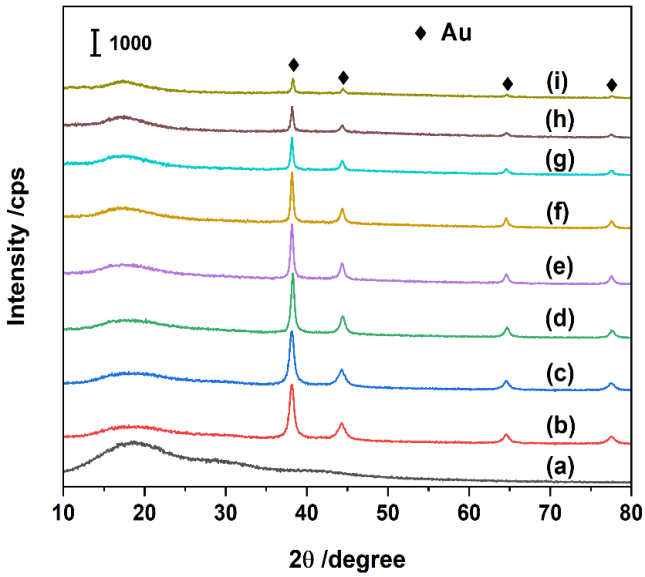

Fig. 2-17. XRD patterns of Au@AER with different Au contents. (a) Pristine AER and Au@AER with (b) 0.1 mmol g^{-1} Au, (c) 0.2 mmol g^{-1} Au, (d) 0.3 mmol g^{-1} Au, (e) 0.4 mmol g^{-1} Au (f) 0.5 mmol g^{-1} Au, (g) 0.7 mmol g^{-1} Au, (h) 1.0 mmol g^{-1} Au, and (i) 1.2 mmol g^{-1} Au. Those Au@AER were not treated with H_2 at 80 °C.

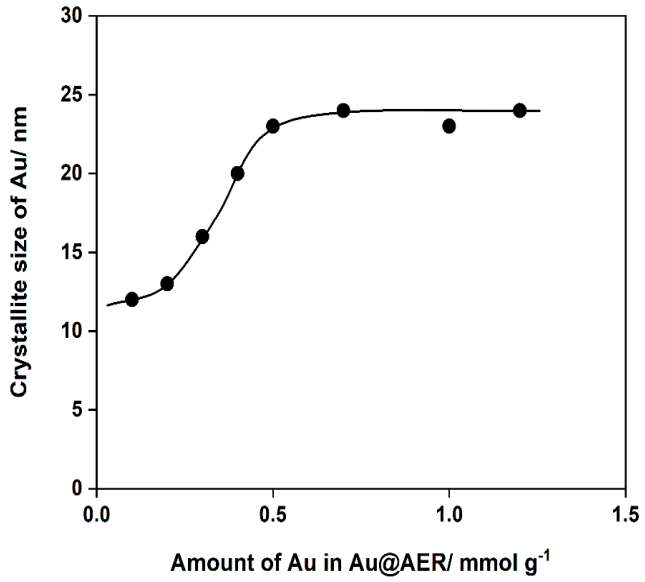

Fig. 2-18. Relationship between the amount of Au and crystallite size of Au particles in Au@AER. The crystallite size was calculated by Scherrer's equation applying to the strongest diffraction line.

There was another possible reason for the decrease of the NO_3^- decomposition and this is that the introduced $AuCl_4^-$ in AER was not completely reduced by primary hydroxyl groups when excess amount of $AuCl_4^-$ was introduced. Fig. 2-19 shows the Au-L_3 edge XANES spectra for Au@AER with different Au content and the compounds of $HAuCl_4$ and Au foil. In the spectrum of Au@AER (0.2 mmol g^{-1}), there is only one peak at 11945 eV, corresponding to Au^0. However, in the spectrum of Au@AER (0.3 mmol g^{-1}), peaks at 11921 eV and 11945 eV were observed, which means both Au^{3+} and Au^0 were present. As the amount of $AuCl_4^-$ was increased to 0.7 or 1.2 mmol g^{-1}, the peak at 11945 eV gradually disappeared while the peak at 11921 eV was gradually obvious, which may be because there was a large amount of unreduced $AuCl_4^-$ in AER. Therefore, it can be concluded that all $AuCl_4^-$ was reduced by primary hydroxyl when the amount of that was less than 0.2 mmol g^{-1} in AER, while only part of that was reduced when $AuCl_4^-$ was excess. Based on these results, it was concluded that Au@AER with 0.3 mmol g^{-1} of Au was the best material in terms of ion-exchange performance and catalytic activity for NO_3^- removal and decomposition, respectively.

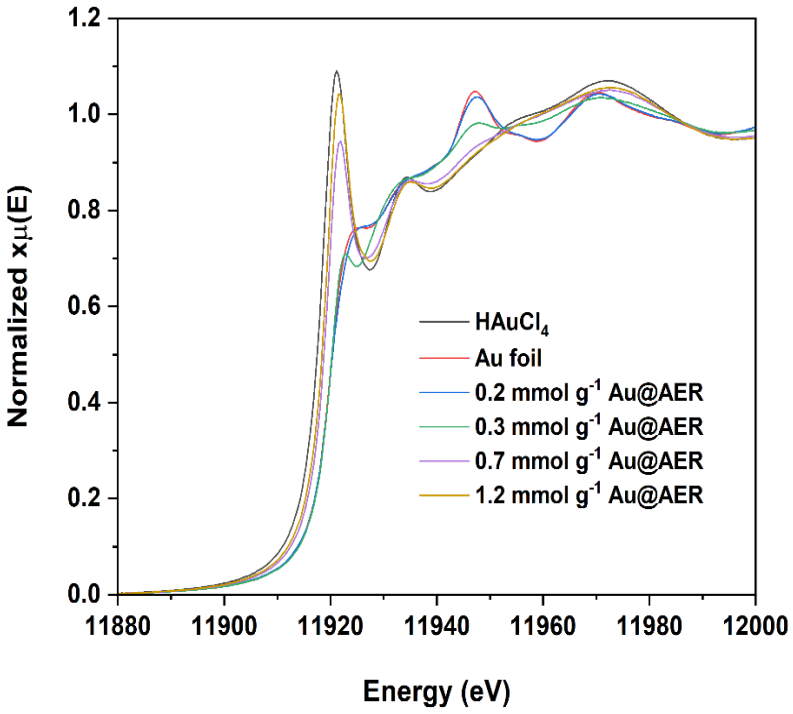

Fig. 2-19 XANES spectra for Au@AER with different loadings of Au.

2-3-5 Effect of the preparation method of Au@AER on NO_3^- decomposition

To improve the catalytic performance, the Au@AER treated with $NaBH_4$ and the Au@AER ground and treated with $NaBH_4$ were investigated. The results are shown in Fig. 2-20. As was discussed before, the treatment of Au@AER in H_2 at 80 °C, which gave Au@AER(H_2), had little impact on both NO_3^- uptake and NO_3^- decomposition performances. However, it should be noted that the treatment of Au@AER with $NaBH_4$, which is a strong reducing reagent, brought about a slight increase in the catalytic performance for NO_3^- decomposition, although the NO_3^- uptake was rather decreased (Fig. 2-20(C)). Consequently, the NO_3^- conversion was increased to 37 % by this treatment.

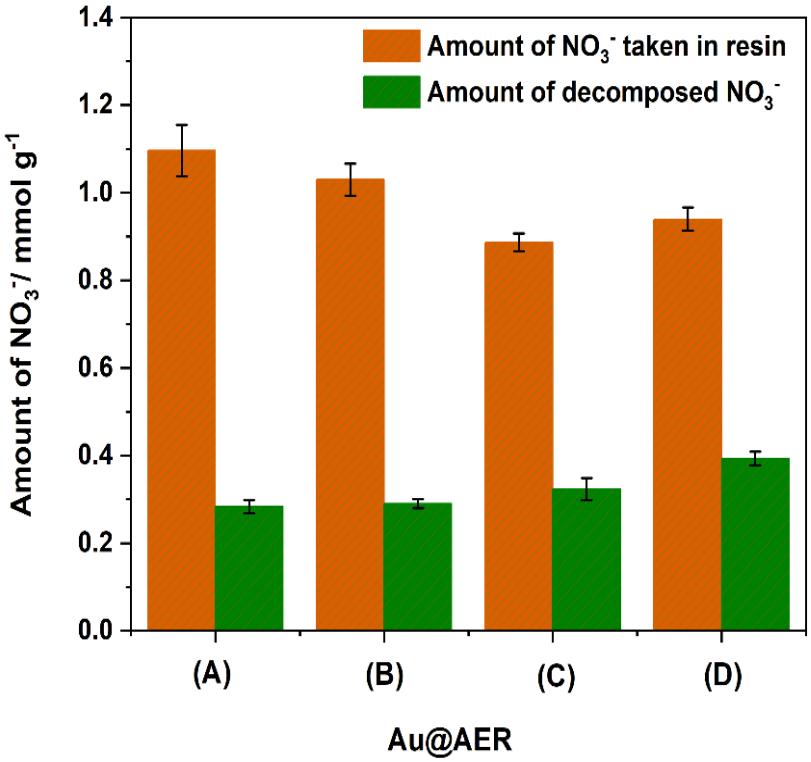

Fig. 2-20. Effects of the preparation procedure and treatment for Au@AER on NO_3^- uptake and NO_3^- decomposition. (A) Au@AER, (B) Au@AER(H_2), (C) Au@AER treated with $NaBH_4$, and (D) Au@AER ground and treated with $NaBH_4$.

The increase in the amount of decomposed NO_3^- was more significant when Au@AER was ground before treatment with $NaBH_4$ (Fig. 2-20(D)). Au@AER obtained using this procedure (grinding and then treatment with $NaBH_4$) decomposed 0.38 mmol g^{-1} of NO_3^-, which corresponded to 41 % of NO_3^- conversion. The improvement in the catalytic performance for NO_3^- decomposition caused by the grinding and treatment with $NaBH_4$ was probably because $AuCl_4^-$, which remained unreduced spontaneously with the primary hydroxyl groups in AER due to excess introduction of $AuCl_4^-$, was further reduced with $NaBH_4$ to produce additional Au^0 particles. The Au-L_3 edge XANES spectrum for Au@AER (0.3 mmol g^{-1}) treated with $NaBH_4$ also supported this conclusion (Fig. 2-13). In addition, as Fig. 2-21 shows, the crystallite size of Au in Au@AER

obtained with this procedure was 14 nm, which was smaller than those in Au@AER (17 nm). The formation of smaller Au particles (av. 13.5 nm) was also confirmed from the TEM image (Fig. 2-22). However, the grinding made small grains of the material, and it would make its handling difficult and thus somewhat impractical. The preparation method and conditions for obtaining Au@AER with high catalytic performance and ease of handling must be further investigated.

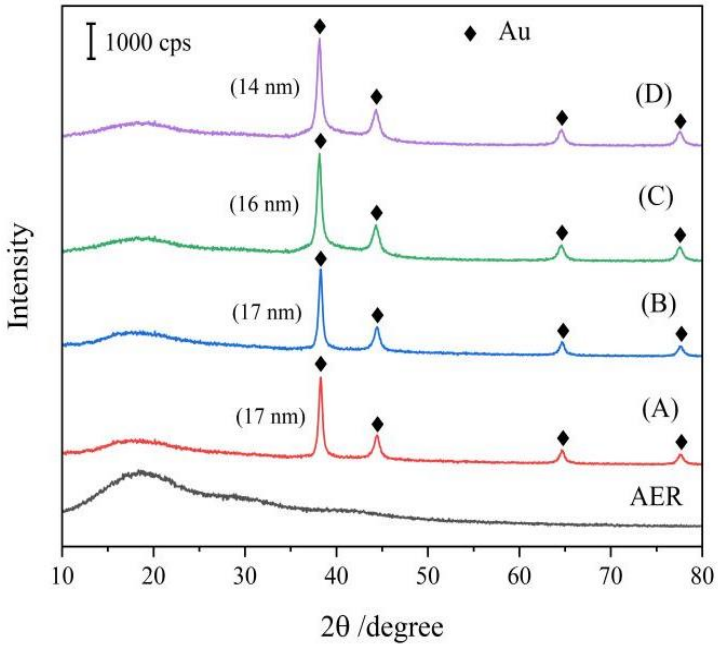

Fig. 2-21. XRD patterns of AER and Au@AER prepared by different preparation procedure and conditions. (A) Au@AER, (B) Au@AER(H_2), (C) Au@AER treated with $NaBH_4$, and (D) Au@AER ground and treated with $NaBH_4$. Figures in parenthesis are crystallite sizes of Au calculated by Scherrer's equation.

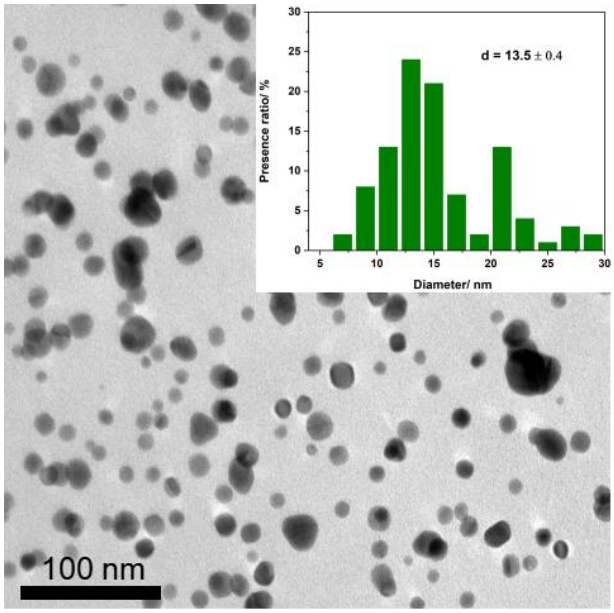

Fig. 2-22. TEM image and particle size distribution of Au particles for Au@AER ground and treated with $NaBH_4$.

2-3-6 Ion-exchange property of Au@AER and comparison with the pristine AER

As was demonstrated before (Fig. 2-14), the introduction of the optimal amount of Au (0.3 mmol g^{-1}) into AER increased the ion-exchange capacity. However, the ion-exchange sites in the material were changed with the introduction of Au particles due to the oxidation of the primary hydroxyl groups at the ion-exchange sites and the formation of new ion-exchange sites on the surface of Au particles, thereby altering the ion-exchange property of the material. Thus, the ion-exchange property of Au@AER was investigated in detail and compared with that of the pristine AER.

Fig. 2-23 exhibits the ion-exchange property of Au@AER and pristine AER. Fig. 2-23(a) shows the relationship between the dose of resin and concentration of NO_3^- in the solution at equilibrium. For both materials, the concentration of NO_3^- was decreased with the increase in the resin dose, and the difference between the two materials was minimal. Fig. 2-23(b) presents the kinetics for NO_3^- removal over the two materials. It is apparent that the kinetic behavior was nearly identical for both materials, and after 15 min almost all NO_3^- in the solution were removed under the conditions.

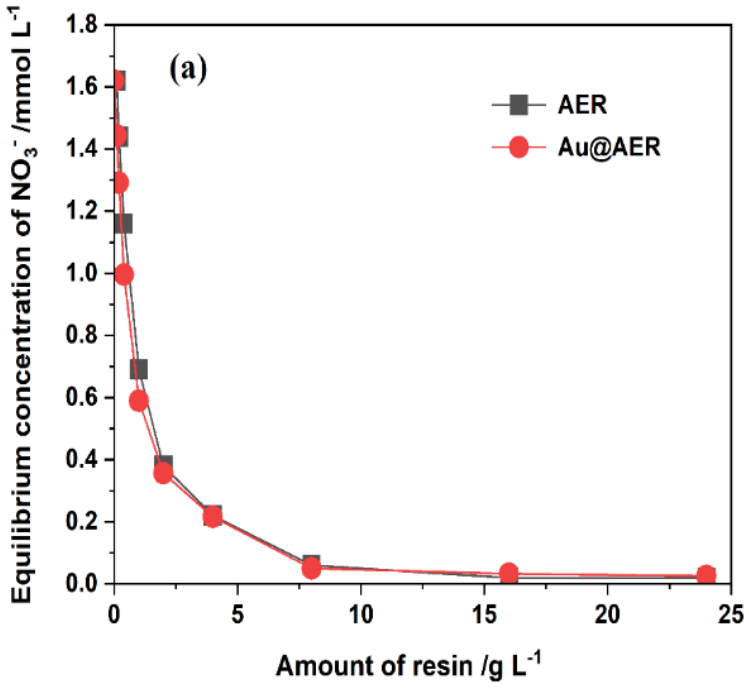
(a)
AER
Au@AER
Equilibrium concentration of NO_3^- /mmol L^{-1}
Amount of resin /g L^{-1}
0.0
0.2
0.4
0.6
0.8
1.0
1.2
1.4
1.6
1.8
0
5
10
15
20
25

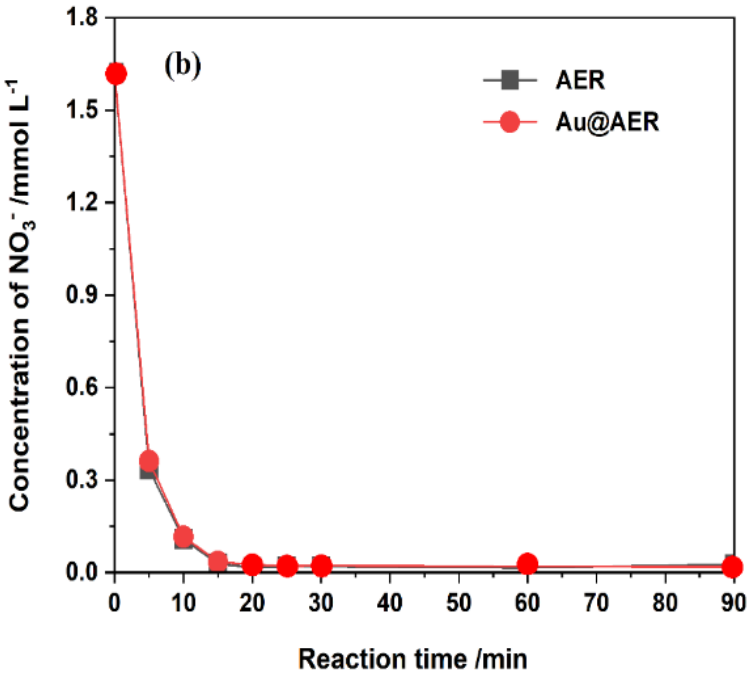
(b)
AER
Au@AER
Concentration of NO_3^- /mmol L^{-1}
Reaction time /min
0.0
0.3
0.6
0.9
1.2
1.5
1.8
0
10
20
30
40
50
60
70
80
90

Continued

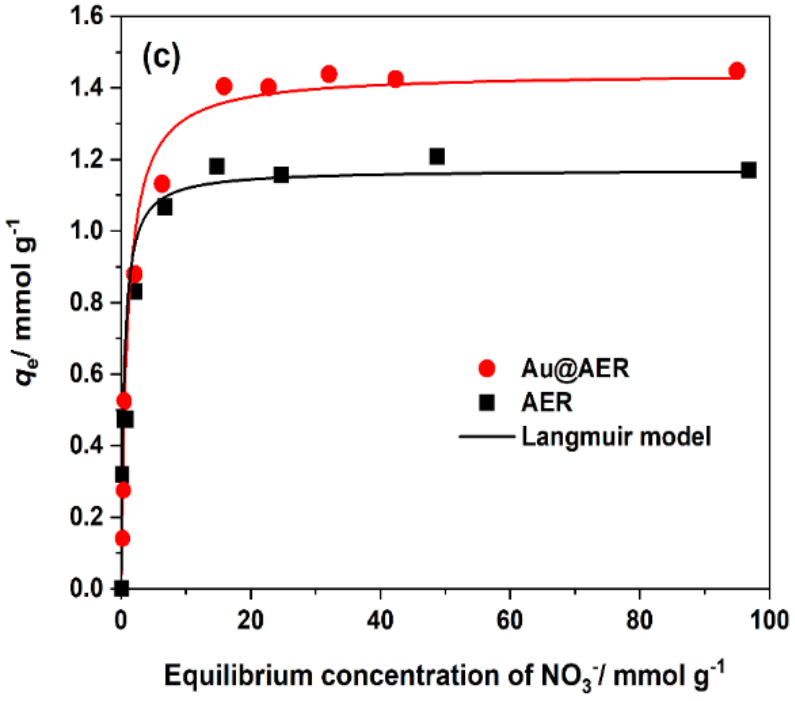

Fig. 2-23. (a) Influence of the dose of AER and Au@AER on equilibrium concentration of NO_3^- in the solution. Conditions: $[NO_3^-]_0$=100 ppm (1.62 mmol L^{-1}); volume of NO_3^- solution, 10 mL; time for ion-exchange, 8 h; and temperature, 38 ℃. (b) Kinetics for ion-exchange removal of NO_3^- over AER and Au@AER. Conditions; $[NO_3^-]_0$=100 ppm (1.62 mmol L^{-1}); volume of NO_3^- solution, 100 mL; amount of AER and Au@AER, 1.0 g; and temperature, 38 ℃. (c) Adsorption isotherm for NO_3^- over AER and Au@AER. The solid lines are drawn with Langmuir fitting parameters. Conditions: volume of NO_3^- solution, 10 mL; amount of AER and Au@AER, 0.1 g; and temperature, 38 ℃. The content of Au in Au@AER was 0.3 mmol g^{-1}. Langmuir fitting parameters for ion-exchange removal of NO_3^- on AER and Au@AER

Table. 2-2 Langmuir fitting parameters for ion-exchange removal of NO_3^- on AER and Au@AER.

Material	q_{max} (mmol g^{-1})	K (L mol^{-1})
AER	1.18	1.4
Au@AER[a]	1.46	0.83

[a]The content of Au in Au@AER was 0.3 mmol g^{-1}.

In contrast to these, a notable difference between the two materials was observed in the ion exchange isotherms for NO_3^- (Fig. 2-23(c)). Both isotherms had Langmuir-type shapes, and were analyzed using the Langmuir equation, yielding Langmuir fitting parameters including ion exchange equilibrium constant (K) and maximum ion exchange capacity (q_{max}) (Table 2-2). The introduction of Au particles to AER increased q_{max} from 1.18 (AER) to 1.46 mmol g^{-1} (Au@AER). However, the ion exchange equilibrium constant (K) decreased from 1.4 (AER) to 0.83 L mo1^{-1} (Au@AER) with the introduction of Au particles. A plausible reason for the decrease of K with the introduction of Au particles is the change in the structure of the ion exchange sites in the resin with the oxidation of the primary hydroxyl groups.

To confirm this, the primary hydroxyl groups at the ion exchange site in AER was oxidized to the corresponding aldehyde by the reaction with Dess-Martin periodinane, and the ion exchange isotherm for NO_3^- was measured using the obtained AER-DMP and the result is shown in Fig. 2-24. The result demonstrated that the change in the structure of the ion exchange sites decreased the ion exchange equilibrium constant (Table 2-3), which was almost the same as that for Au@AER, whereas the maximum ion exchange capacity remained unchanged. The hydrophobicity around the ion exchange sites may increase by changing the primary hydroxyl group to aldehyde, thereby weakening the interaction between NO_3^- and the ion exchange site.

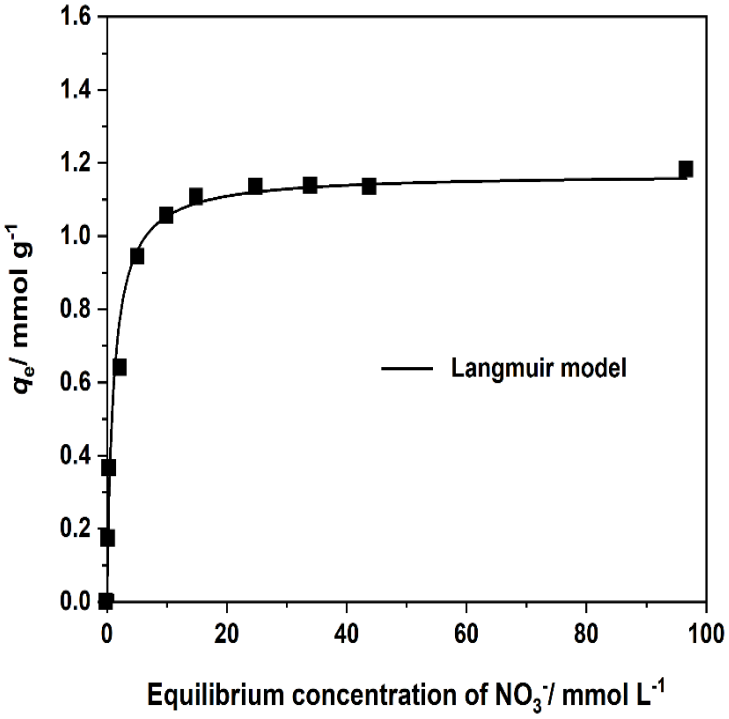

Fig. 2-24. Adsorption isotherm for NO_3^- over AER-DMP. The line is drawn with Langmuir fitting parameters. The conditions were the same as those shown in Fig. 2-23(c).

Table 2-3. Langmuir fitting parameters for ion-exchange removal of NO_3^- on AER-DMP.

q_{max} (mmol g^{-1})	K (L mol^{-1})
1.17 ± 0.04	1.1 ± 0.54

2-3-7 Optimization of the reaction conditions and product analysis for NO_3^- decomposition in Au@AER

To increase the amount of decomposed NO_3^-, reaction conditions for NO_3^- decomposition in Au@AER, including reaction temperature and time, were investigated using Au@AER containing 0.3 mmol g^{-1} of Au. The results are shown in Fig. 2-25. The amount of decomposed NO_3^- was increased with increase in the reaction temperature and the maximum decomposition amount of NO_3^- was 0.27 mmol g^{-1} at 80 °C. The reaction at higher temperature rather decreased the amount of decomposed NO_3^-, probably because the reduction of NO_3^- required the resin to swell with water, and the resin was dried out too quickly at the high temperatures.

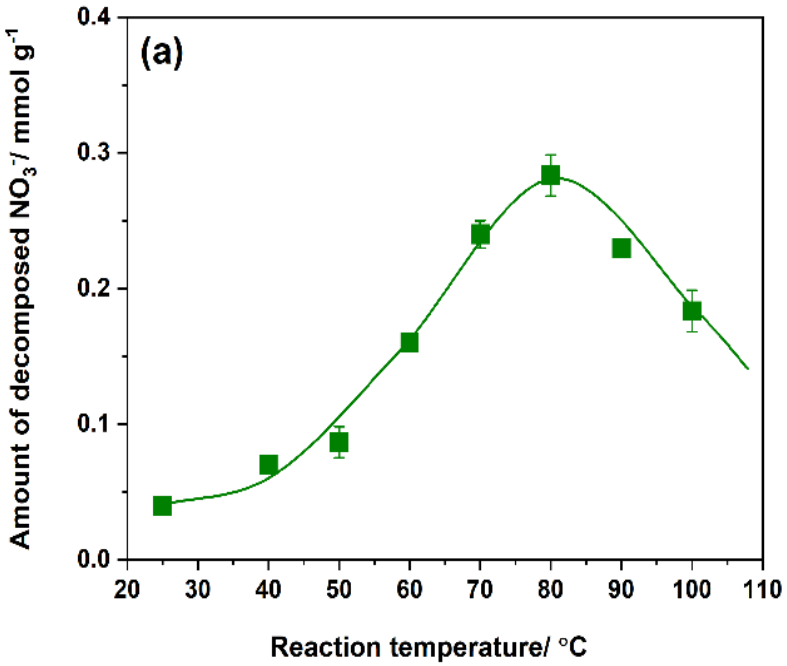

Continued

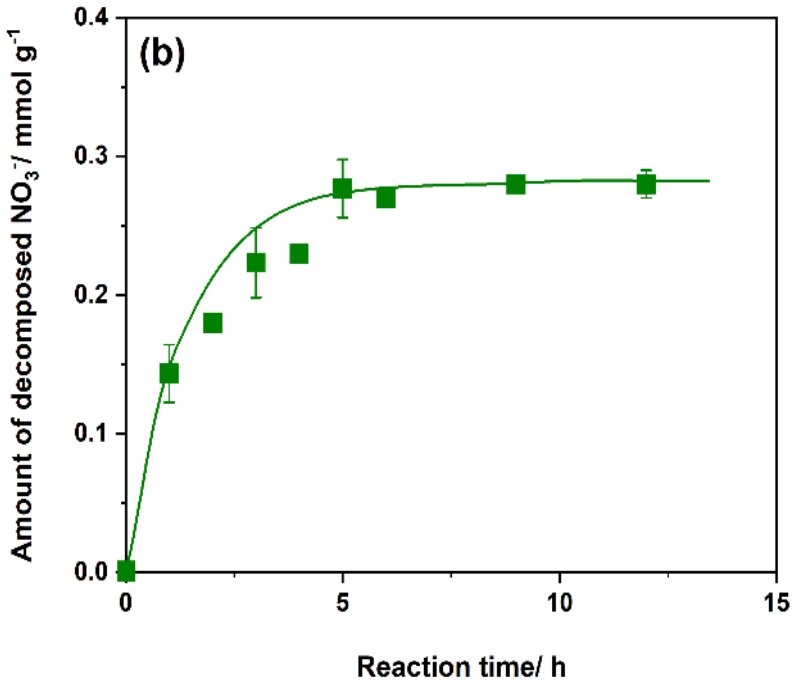

Fig. 2-25 Influence of (a) reaction temperature and (b) reaction time on the amount of decomposed NO_3^-. The content of Au in Au@AER was 0.3 mmol g^{-1}. Conditions for NO_3^- decomposition: (a) reaction time, 5 h and (b) reaction temperature, 80 °C.

The reaction time also had a significant impact on the amount of decomposed NO_3^-. The amount of decomposed NO_3^- gradually increased with the reaction time up to 5 h and reached an almost constant value of approximately 30 %, but in other words, approximately 70 % of NO_3^- remained undecomposed in Au@AER. NO_3^- was not decomposed further despite extending the reaction time, because only NO_3^- near Au particles could diffuse to the surface of the Au particle and be decomposed.

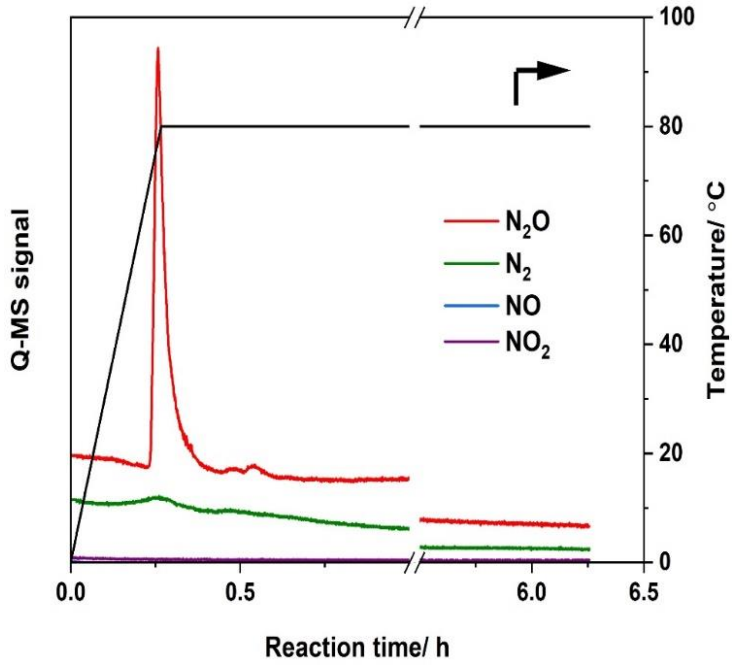

Fig. 2-26. Analysis of gaseous products formed by the decomposition of NO_3^- in H_2 flow using a mass spectrometer. The temperature was increased from 0 to 80 °C at 5 °C min^{-1} and was kept to 6.25 h, while H_2 was flown to the reactor in which 0.2 g of Au@AER with NO_3^- was fixed.

The products formed by the decomposition of NO_3^- in Au@AER were analyzed using a mass spectrometer. The reaction was performed using Au@AER with NO_3^- in H_2 flow from 0 to 80 °C. As Fig. 2-26 clearly shows, N_2O was the main product, and N_2 was a minor product, but NO and NO_2 were not detected. Ion chromatography analysis of the trap solution demonstrated that no ammonia was formed during the reaction. Moreover, NO_2^-, which is an intermediate product formed from NO_3^-, was not present in Au@AER after the reaction regardless of the reaction temperature and time. Therefore, it was concluded that NO_3^- in Au@AER was decomposed according to the following reactions.

Main reaction $\quad NO_3^- + 2H_2 \rightarrow 1/2N_2O + 3/2H_2O + OH^-$

Minor reaction $\quad NO_3^- + 5/2H_2 \rightarrow 1/2N_2 + 3/2H_2O + OH^-$

In addition, the products of NO_3^- decomposition were analyzed by Agilent 3000A Micro CG, and the generated amount of N_2O was calculated and the result is shown in Fig. 2-27. According to the theoretical amount of NO_3^- decomposition and the calculated amount of N_2O, it was concluded that N_2O and N_2 were the products formed by the NO_3^- decomposition in 0.3 mmol g^{-1} of Au@AER when it was treated by H_2 at 80 °C for 5 h and the selectivity was 86.4 and 13.6 %, respectively.

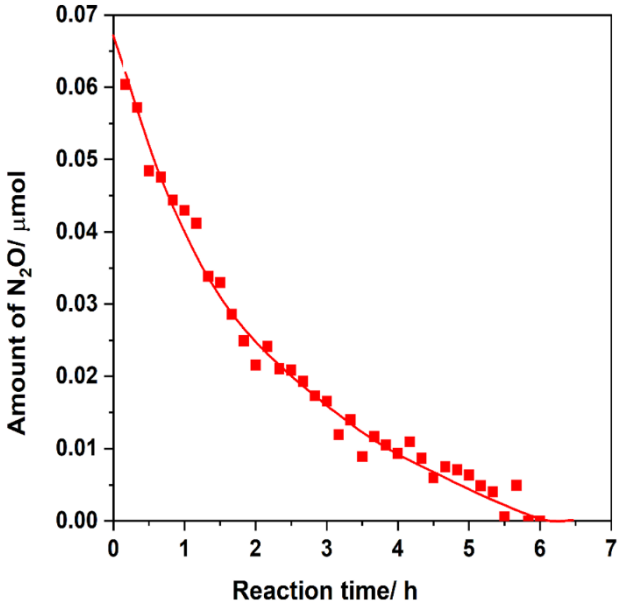

Fig. 2-27 Relationship of the amount of N_2O produced and the reaction time. The amount of Au in the resin was 0.3 mmol g^{-1}. Conditions for NO_3^- decomposition: reaction time, 6 h and reaction temperature, 80 °C.

Because N_2O is greenhouse gas with strong greenhouse effect [7], and thus its formation would be problematic. However, N_2O can be easily converted to N_2 by the reduction with H_2 in the presence of supported Ru or Rh catalyst [7, 8, 9, 10, 11]. Therefore, its formation is not a serious problem if the off gas is appropriately treated.

2-3-8 Breakthrough and reusability tests

When contaminated water is practically purified on a commercial scale, continuous treatment using a fixed-bed reactor is more suitable than intermittent treatment using a batch reactor. In addition, the material (Au@AER) must be reusable in the NO_3^- removal and NO_3^- decomposition cycle for the two-step process. Thus, breakthrough test for NO_3^- removal with Au@AER was performed, and the result was compared with that for the pristine AER. To a glass tube reactor containing 1.0 g of Au@AER, 1.62 mmol L^{-1} of NO_3^- solution was fed at a rate of 0.5 mL min^{-1} up to 60 h, which corresponded to 1800 mL of the feed volume. Fig. 2-28 shows the results of the breakthrough tests for AER and Au@AER. Initially, almost no NO_3^- was detected in the solution discharged from the reactor, and subsequently, the concentration of NO_3^- was gradually increased with increase in the amount of the feed volume and finally reached the same concentration as that in the feed solution. The total uptake-amount of NO_3^- for Au@AER was 1.34 mmol g^{-1}, which was larger than that for AER (1.09 mmol g^{-1}). This was indicated by the difference between the maximum ion exchange capacity of Au@AER (1.46 mmol g^{-1}) and AER (1.18 mmol g^{-1}). The increase in the concentration of NO_3^-, namely breakthrough, was slower for Au@AER than AER, because the ion exchange equilibrium constant of Au@AER (0.83 L mol^{-1}) was smaller than that of AER (1.4 L mol^{-1}), as demonstrated from ion exchange isotherm measurements.

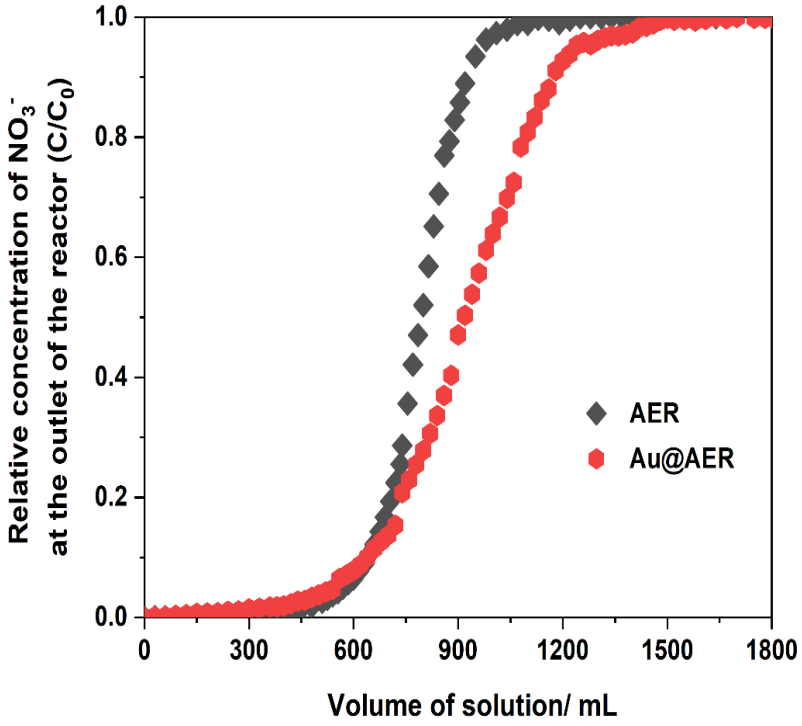

Fig. 2-28. Breakthrough curves for NO_3^- removal over AER and Au@AER. Conditions: $[NO_3^-]_0$=100 ppm (1.62 mmol L^{-1}); amount of AER and Au@AER, 1.0 g; flow rate of NO_3^- solution, 0.5 mL min^{-1}; and reaction temperature, room temperature. The content of Au in Au@AER was 0.3 mmol g^{-1}.

The reusability of Au@AER was investigated. Au@AER and Au@AER obtained by grinding and treatment with $NaBH_4$ were used as typical examples for the reusability test. The results are shown in Fig. 2-29. The results clearly shows that both materials did not show any noticeable decrease in the performances for NO_3^- uptake and NO_3^- decomposition up to five uses, demonstrating good stability in the repeated use in the ion-exchange removal and catalytic decomposition of NO_3^-. The spent Au@AER was analyzed by XRD (Fig. 2-30), TEM (Fig. 2-31) and XPS (Fig. 2-32), the crystallinity and crystallite size, particle size distribution, and the oxidation state of the surface of Au particles in Au@AER scarcely changed after five uses.

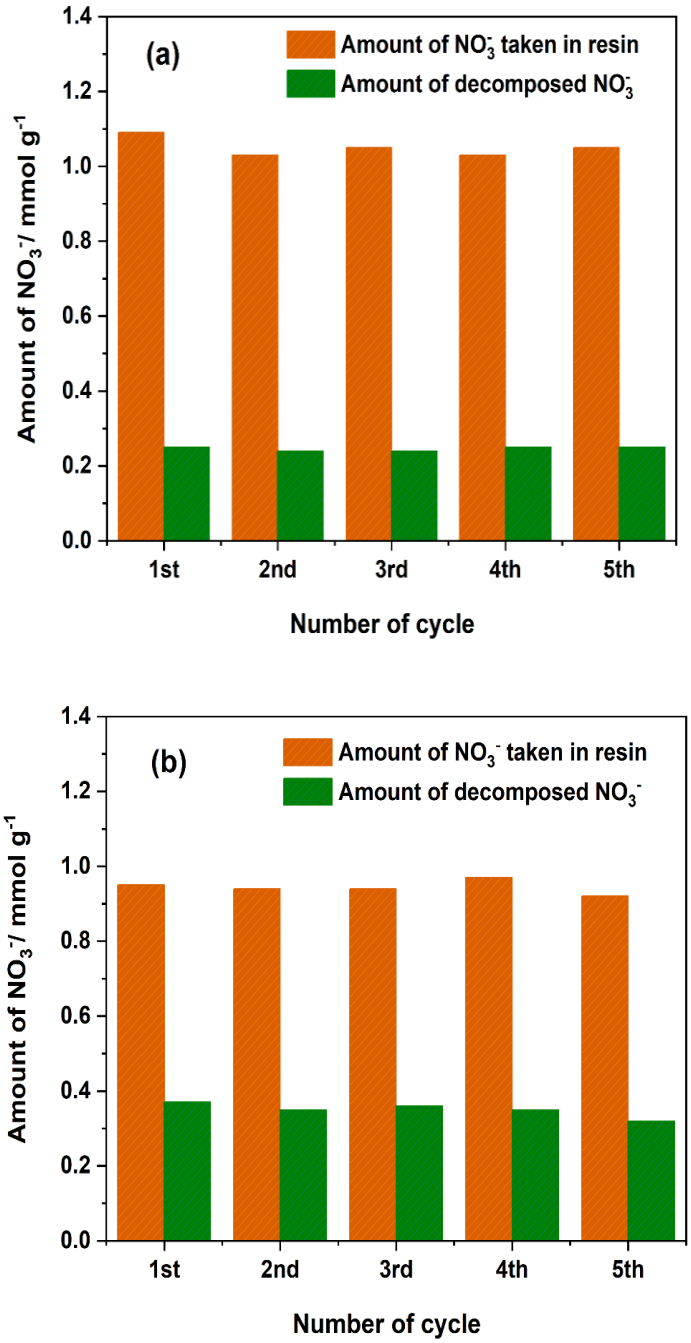

Fig. 2-29 Reusability test for ion-exchange removal and catalytic decomposition of NO_3^- in the two-step process. (a) Au@AER and (b) Au@AER ground and treated with $NaBH_4$.

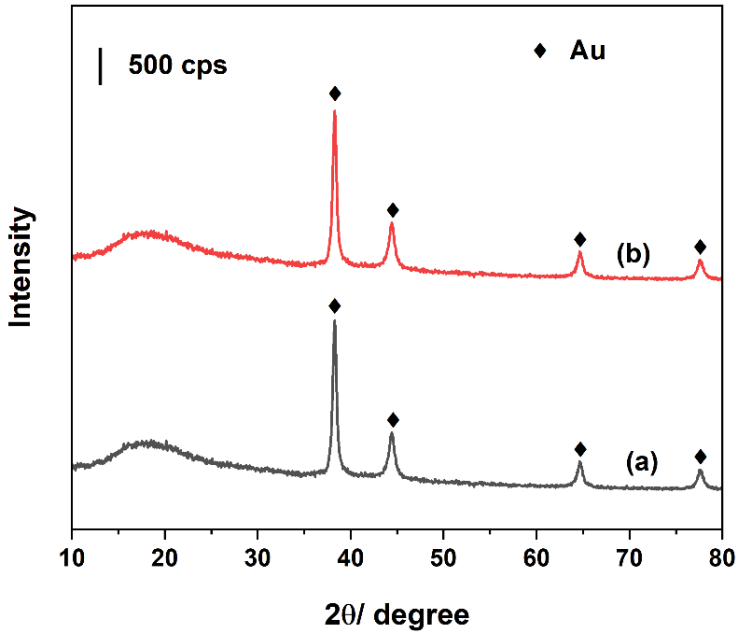

Fig. 2-30 XRD patterns of Au@AER (a) fresh and (b) spent.

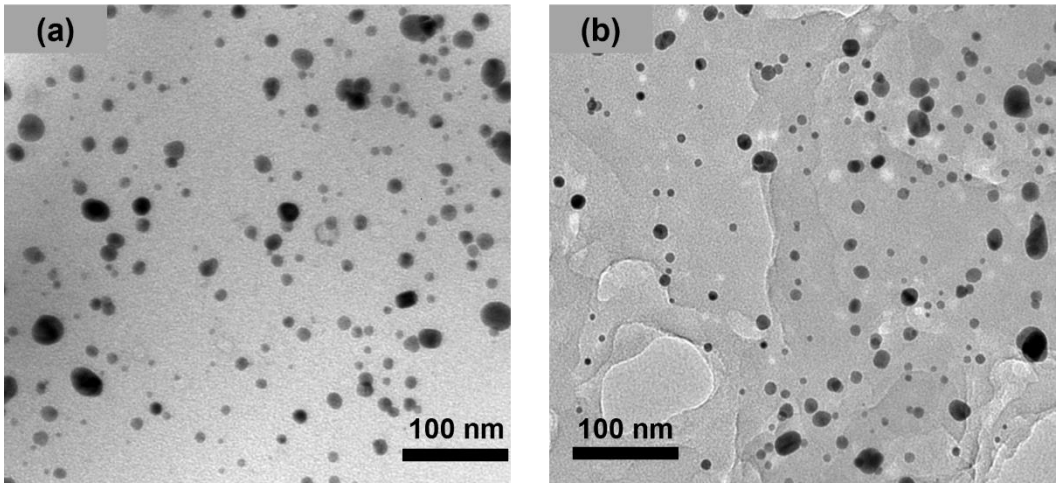

Fig. 2-31 TEM images of Au@AER (a) fresh and (b)spent.

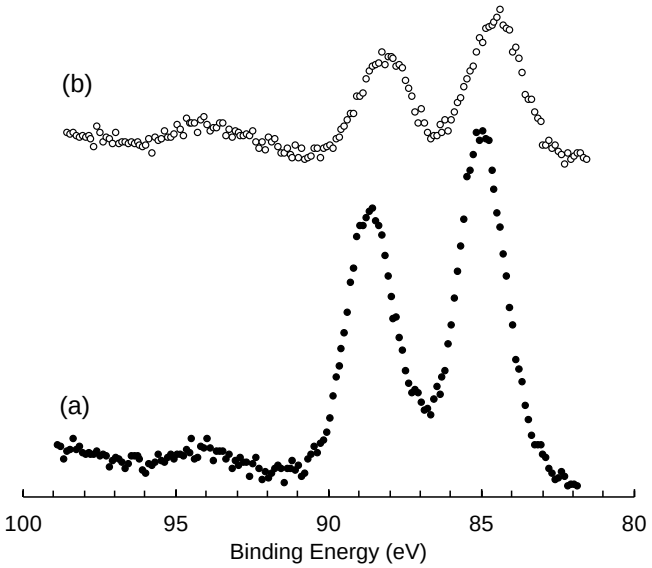

Fig. 2-32. Au 4f XPS spectra of Au@AER (a)fresh and (b) spent.

In addition, to confirm the long-term stability of Au in Au@AER under ambient conditions, Au@AER (0.2 mmol g^{-1}) was stored at room temperature in air (ambient conditions) for 6 months and they were analyzed by XAFS. Au-L_3 edge XANES spectra are shown in Fig. 2-33. There was only Au^0 peak in both spectra, indicating Au^0 particle in AER was not oxidized under ambient conditions for 6 months.

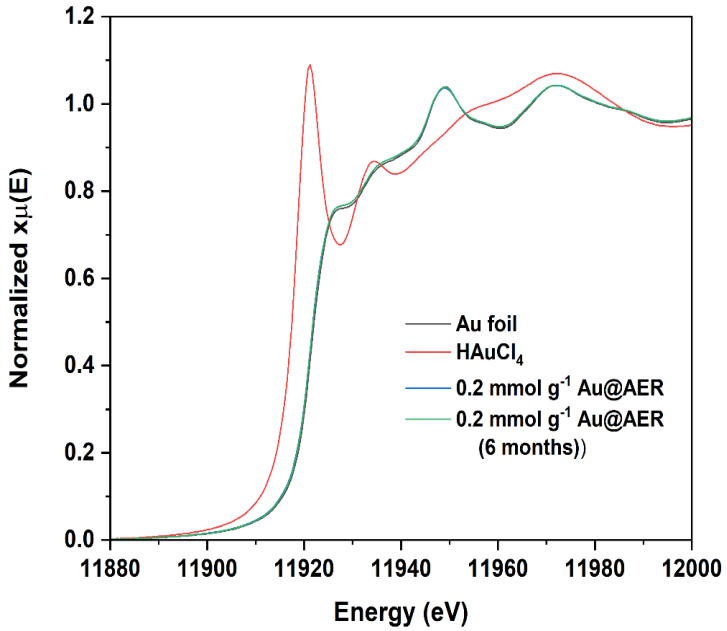

Fig. 2-33 XANES spectra for fresh Au@AER and Au@AER stored at room temperature in air for 6 months.

2-3-9 Comparison of the performance of Au@AER with those of previously reported catalysts

Finally, the catalytic performance of Au@AER for NO_3^- decomposition was compared with those of previously reported catalysts in the two-step process [1, 2, 3], which are summarized in Table 2-4. As mentioned in Chapter 2-1, all previously reported catalysts contained bimetallic Pd particles introduced into anion exchange resin. The catalytic activity of Au@AER is lower than that of previously reported materials, whereas the selectivity is comparable (Table 2-4). However, Au@AER is the first example to demonstrate that even a single-metal catalyst can exhibit activity for NO_3^- decomposition in the two-step process. This finding greatly advances optimal catalyst design and elucidates the reaction mechanism.

Table 2-4 Comparison of the catalytic performance of Au@AER with those previously reported.

Catalyst	Reductant[a]	Reaction conditions	Reaction time (h)	$X_{NO_3^-}$[b] (%)	S_{N_2,N_2O}[c] (%)	S_{NH_3}[d] (%)	Ref.
Pd(1%)Cu(1%)/resin	ethanol	6 bar H_2/CO_2 333 K	6	100	100	0	[1]
Pd(1%)Cu(1%)/resin	ethanol	6 bar H_2/CO_2 298 K	24	100	100	0	[1]
Pd(2%)Cu(0.5%)/WA30	hydrazine	1 bar H_2 r.t.	63	100	N/A[e]	N/A[e]	[2]
Pd(2%)Sn(0.5%)/WA30	hydrazine	1 bar H_2 r.t.	24	97.5	66.2	31.1	[3]
Au@AER	w/o reduction	1 bar H_2 353 K	5	41	100	0	This work

[a]Reductant used for making metal particles.

[b]Conversion of NO_3^-.

[c]Selectivity to N_2 and N_2O.

[d]Selectivity to NH_3.

[e]Products were not analyzed.

2-4 Conclusions

In this chapter, to demonstrate the hypothesis that the decomposition reaction of NO_3^- in anion exchange resin would proceed even with a single metal, it was investigated the anion exchange resin with various single metal particles for NO_3^- decomposition in the resin by the contact with 1 bar H_2 at 80 °C. NO_3^- decomposition reaction proceeded with various precious metals, while Ru, Au and Rh were particularly effective. Among them, only Au did not require the treatment in H_2 to reduce the metal complex in the resin to form metal particles, thus Au was the best metal introduced to the resin, although slightly less active than Ru. The resin with Au particles prepared under the optimal conditions and optimum Au contents decomposed 0.38 mmol g^{-1} of NO_3^-, which corresponded to 41 % conversion, mainly into N_2O in H_2 at 80 °C for 5 h. The introduction of Au particles in the resin increased the ion exchange capacity from 1.18 (pristine resin) to 1.46 mmol g^{-1} (with Au particles), while ion exchange equilibrium constant was decreased from 1.4 to 0.83 L mol^{-1}. The resin with Au was reusable for ion exchange removal of NO_3^- and its decomposition in H_2 at 80 °C up to five uses without any performance degradation. Based on the results, it was believed that the developed resin with Au particles will greatly contribute to improving the efficiency of the two-step process for purification of water contaminated with NO_3^-.

2-5 References

[1] Y.-N. Kim, M. Y. Kim and M. Choi. Synergistic integration of catalysis and ion-exchange for highly selective reduction of nitrate into N_2, Chemical Engineering Journal. 289 (2016) 423-432, https://doi.org/10.1016/j.cej.2016.01.002

[2] G. Mendow, A. Sánchez, C. Grosso and C. A. Querini. A novel process for nitrate reduction in water using bimetallic Pd-Cu catalysts supported on ion exchange resin, Journal of environmental chemical engineering. 5 (2017) 1404-1414, https://doi.org/10.1016/j.jece.2017.01.033

[3] B. S. Sanchez, C. A. Neyertz, M. S. Zanuttini, C. A. Querini and G. Mendow. Hybrid process for nitrates elimination in water, Catalysis Today. 394 (2022) 467-474, https://doi.org/10.1016/j.cattod.2021.06.031

[4] Y. Shang, C. Min, J. Hu, T. Wang, H. Liu and Y. Hu. Synthesis of gold nanoparticles by reduction of $HAuCl_4$ under UV irradiation, Solid State Sciences. 15 (2013) 17-23, https://doi.org/10.1016/j.solidstatesciences.2012.09.002.

[5] T. Ishida, S. Okamoto, R. Makiyama and M. Haruta. Aerobic oxidation of glucose and 1-phenylethanol over gold nanoparticles directly deposited on ion-exchange resins, Applied Catalysis A-General. 353 (2009) 243-248, https://doi.org/10.1016/j.apcata.2008.10.049.

[6] L. Zhang, P. Liu, Y. Wang and W. Gao. Study on physico-chemical properties of dialdehyde yam starch with different aldehyde group contents, Thermochim Acta. 512 (2011) 196-201, https://doi.org/10.1016/j.tca.2010.10.006

[7] S. Hinokuma, T. Iwasa, Y. Kon, T. Taketsugu and K. Sato. N_2O decomposition properties of Ru catalysts supported on various oxide materials and SnO_2, Scientific Reports. 10 (2020) 21605, https://doi.org/10.1038/s41598-020-78744-x

[8] C. Huang, Z. Ma, P. Xie, Y. Yue, W. Hua and Z. Gao. Hydroxyapatite-supported rhodium catalysts for N_2O decomposition, Journal of Molecular Catalysis A: Chemical. 400 (2015) 90-94, https://doi.org/10.1016/j.molcata.2015.02.011

[9] Y. Li, A. Sundermann, O. Gerlach, K.-B. Low, C. C. Zhang, X. Zheng, H. Zhu and S.

Axnanda. Catalytic decomposition of N_2O on supported Rh catalysts, Catalysis Today. 355 (2020) 608-619, https://doi.org/10.1016/j.cattod.2019.04.063

[10] I. Song, Y. Wang, J. Szanyi and K. Khivantsev. Co-existence of atomically dispersed Ru and Ce^{3+} sites is responsible for excellent low temperature N_2O reduction activity of Ru/CeO_2, Applied Catalysis B: Environmental. 343 (2024) 123487, https://doi.org/10.1016/j.apcatb.2023.123487

[11] Z. Zhuang, B. Guan, J. Chen, C. Zheng, J. Zhou, T. Su, Y. Chen, C. Zhu, X. Hu and S. Zhao. Review of nitrous oxide direct catalytic decomposition and selective catalytic reduction catalysts, Chemical Engineering Journal. (2024) 150374, https://doi.org/10.1016/j.cej.2024.150374

Chapter 3

Reaction mechanism of nitrate decomposition in anion-exchange resin containing gold nanoparticles

3-1 Introduction

In Chapter 2, it was demonstrated that Au@AER showed catalytic activity for NO_3^- decomposition in the resin, and the maximum amount of decomposed NO_3^- reached 0.38 mmol g^{-1}, corresponding to 41 % of NO_3^- taken in resin, but approximately 60 % of NO_3^- remained undecomposed in the resin even in the optimal reaction conditions. To improve the catalytic performance of Au@AER for NO_3^- decomposition, it is necessary to clarify how NO_3^- is decomposed in the resin.

Choi and co-workers proposed long-range diffusion of NO_3^- within resin is possible, and all of NO_3^- exchanged in the resin appeared to reach the surface of PdCu particles through consecutive ion-exchanges between the adjacent quaternary ammonium groups (ion-hopping) [1]. Mendow also proposed that NO_3^- present in the liquid reacted on the bimetal sites when H_2 was fed, forming OH^- by the reaction. These OH^- were then exchanged with the ions adsorbed in the resin, thus releasing NO_3^- that was reduced on the metal sites [2].

According to the conclusions by Choi et al. [1] and Mendow et al. [2], the free NO_3^- (NO_3^- in liquid swelling resin) in resin was first reduced, and OH^- was generated. Therefore, it was considered that water in resin plays an important role in the NO_3^- decomposition. Here, in Chapter 3, the effect of water in resin on NO_3^- decomposition was investigated in detail and the reaction mechanism of NO_3^- decomposition is proposed based on the obtained data.

3-2 Experimental

3-2-1 Catalytic decomposition of NO_3^- in Au@AER treated at 100 °C

The experimental procedure was the same as that in Chapter *2-2-3* but Au@AER containing NO_3^- was treated with N_2 (10 mL min^{-1}) at 100 °C for 1 h before it was contacted with H_2.

3-2-2 Continuous multiple decomposition of NO_3^- in Au@AER.

The experimental procedure was the same as that in Chapter *2-2-3* but Au@AER containing undecomposed NO_3^- (namely after NO_3^- decomposition) was soaked in 2 mL of ultrapure water at room temperature for 30 min and then contacted again with H_2 at 80 °C for 5 h.

3-2-3 Catalytic decomposition of NO_3^- in Au@AER in a high-pressure reactor

Au@AER (0.1 g) was added to 100 mL of NO_3^- solution (C_0 = 1.62 mmol L^{-1}), and the mixture was stirred at 38 °C to take NO_3^- into Au@AER, and the Au@AER containing NO_3^- was placed in a glass tube and 10 atm of H_2 was fed to the tube at room temperature, and then the temperature was increased to 80 °C and was maintained for 5 h. After that operation, Au@AER was taken out from the tube and was added to 100 mL of NaCl solution (500 mmol L^{-1}), and the mixture was stirred at 38 °C for 1 h to exchange undecomposed NO_3^- in the resin with Cl^-.

3-2-4 TG analysis of AER and Au@AER.

The weight change with heat was evaluated in the temperature range of 25-600 °C using a TG 8120 equipment (Rigaku Thermoplus). The heating was performed in a static air atmosphere with 10 mg sample at a rate of 10 °C min^{-1}.

3-3 Results and discussion

3-3-1 Water content in Au@AER

In Chapter 2, it was speculated that decomposition of only 40 % NO_3^- in Au@AER was because only NO_3^- near Au particles could diffuse to the surface of the Au^0 particles and decompose. The diffusion process of NO_3^- in resin may be affected by water in the resin. Therefore, to investigate the effect of water content in resin on the diffusion process and the decomposition of NO_3^-, the weight loss of Au@AER in 25~600 °C was evaluated by TG-DTA in a static air atmosphere. Fig. 3-1 shows the weight loss curves of AER and Au@AER. Three-stage weight losses were observed for both samples. In the first stage, the weight losses are up to 100 °C, corresponding to 41 and 47 % of the weights of AER and Au@AER, respectively. The weight loss between 100 to 420 °C (the second step) was caused by the decomposition of the quaternary amino group. Above 420 °C, the main backbone of the resin was completely decomposed.

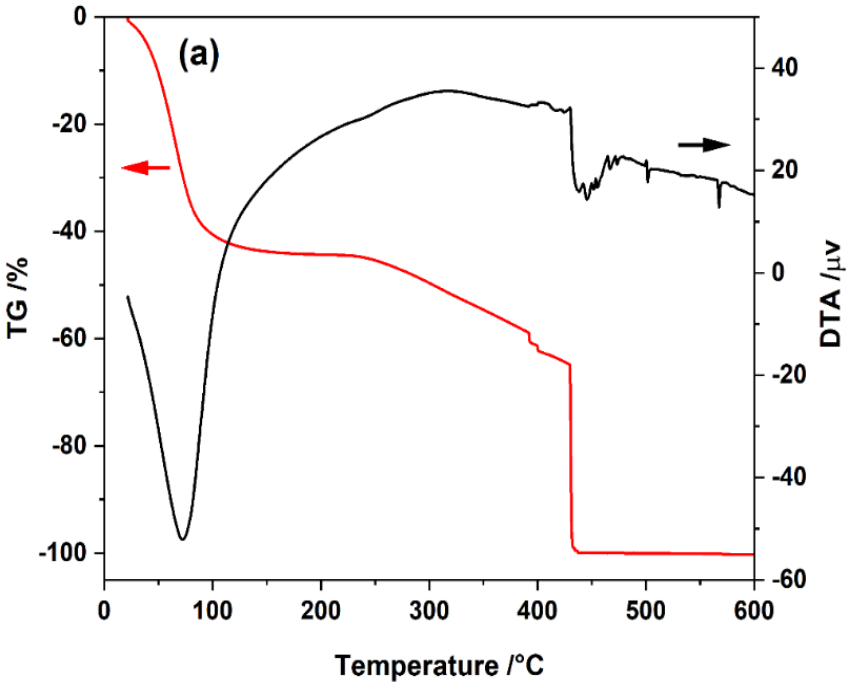

Continued

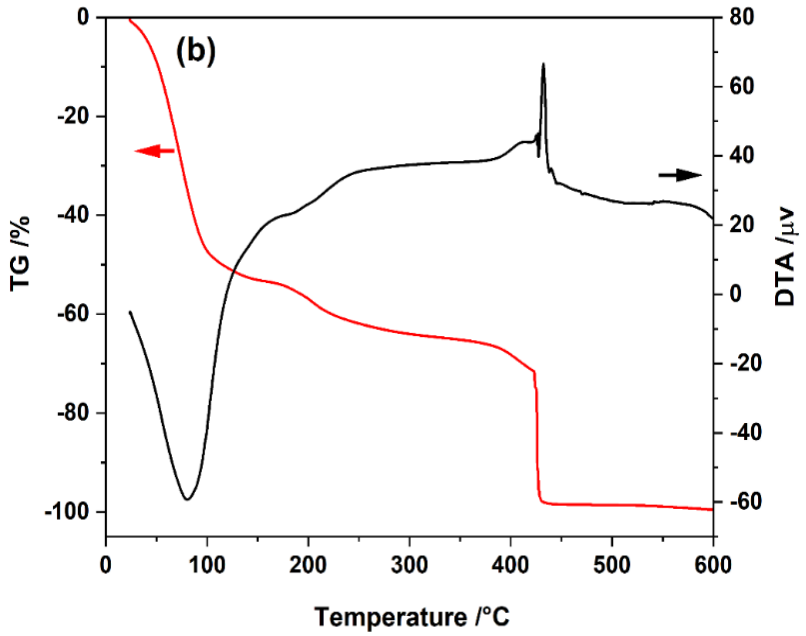

Fig. 3-1 TG-DTA curves of (a) AER and (b) Au@AER taken in static air.

In order to be closer to the actual conditions for NO_3^- decomposition, the weight loss of Au@AER was measured under the same temperature and time as those for the NO_3^- decomposition reaction except that the H_2 flow was replaced with static air. The result is shown in Fig. 3-2. It shows that most of water in the resin was removed before the temperature reached 80 °C in the first 12 min, giving 29 % of the weight loss, while the weight hardly changed after that. This TG analysis suggested that water corresponding to 18 % of the weight of Au@AER remained in Au@AER during the NO_3^- decomposition reaction. In addition, according to the results of Fig. 2-26 and Fig. 2-27, NO_3^- in Au@AER was rapidly decomposed in the first 30 min, and the decomposition rate of NO_3^- gradually slowed down as the reaction time was extended. Therefore, it was speculated that the amount of decomposed NO_3^- was related to the water content in the resin.

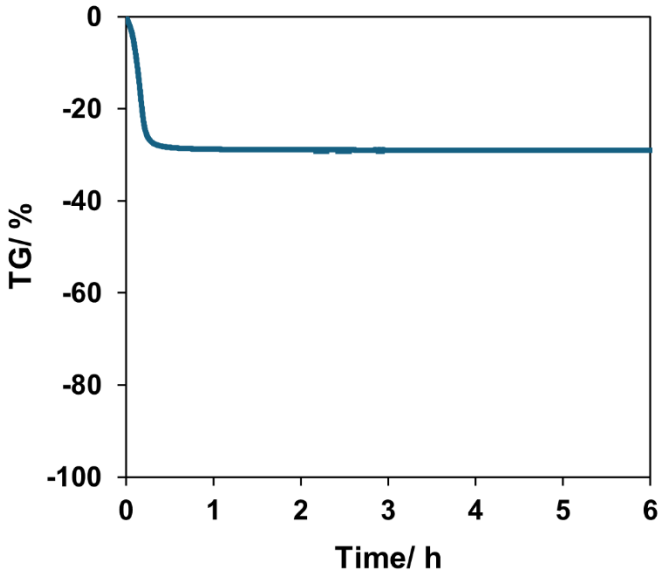

Fig. 3-2 TG curve of 0.3 mmol g^{-1} Au@AER. The temperature was increased from 20 to 80 °C at 5 °C min^{-1} and was kept to 6 h.

3-3-2 Decomposition of NO_3^- performed in different conditions

To investigate the effect of water in resin on the amount of decomposed NO_3^-, Au@AER containing NO_3^- was treated with N_2 at 100 °C for 1 h to remove water in the resin before NO_3^- decomposition with H_2. This state is defined as "Dry", and the amount of decomposed NO_3^- is shown in Fig. 3-3. Compared to the amount of decomposed NO_3^- with normal process, it was obviously decreased for "Dry", which were 0.3 and 0.18 mmol g^{-1} for "Normal" and "Dry", respectively. The amount of water in Au@AER containing NO_3^- treated in N_2 at 100 °C for 1 h (Dry) was analyzed by TG-DTA (Fig. 3-4), and it was found that only small amount of water (2.7 % of the weight of Au@AER) retained in the resin, while the water content of "Normal" was 47 % as mentioned before. Thus, it is speculated that the removal of water by the treatment at 100 °C hindered the diffusion of NO_3^- on the ion-exchange sites in the resin to the Au^0 surface and further speculated that only NO_3^- adsorbed on the newly formed ion-exchange sites on Au surface was decomposed in "Dry".

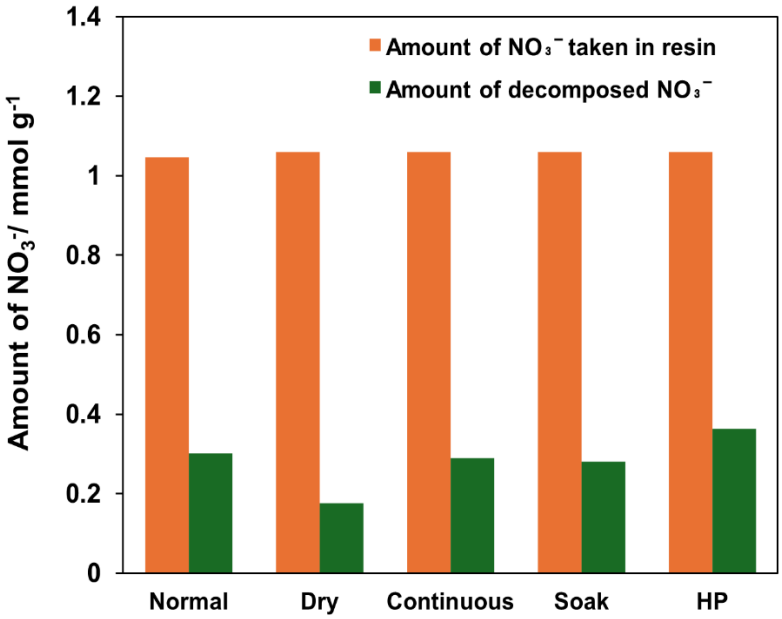

Fig. 3-3 Decomposition of NO_3^- in Au@AER in different treatment condition. The content of Au in Au@AER was 0.3 mmol g^{-1}. NO_3^- uptake measurement: $[NO_3^-]_0$ = 100 ppm (1.62 mmol L^{-1}); volume of solution, 100 mL; amount of Au@AER, 0.1 g. NO_3^- decomposition was performed in H_2 flow at 80 °C for 5 h. (Normal) Au@AER containing NO_3^- was contacted with H_2 at 80 °C for 5 h; (Dry) Au@AER containing NO_3^- was dried under N_2 atmosphere at 100 °C for 1h and then contacted with H_2 at 80 °C for 5 h; (Continuous) Au@AER containing NO_3^- was contacted with H_2 at 80 °C for 5 h, and it was socked in ultrapure water for 30 min and collected by filtration, then it was contacted with H_2 at 80 °C for 5 h again; (Soak) Au@AER containing NO_3^- was soaked in 1 mL of ultrapure water and simultaneously contacted with H_2 at 80 °C for 5 h; (HP) Au@AER containing NO_3^- was contacted with 10 atm of H_2 at 80 °C for 5 h.

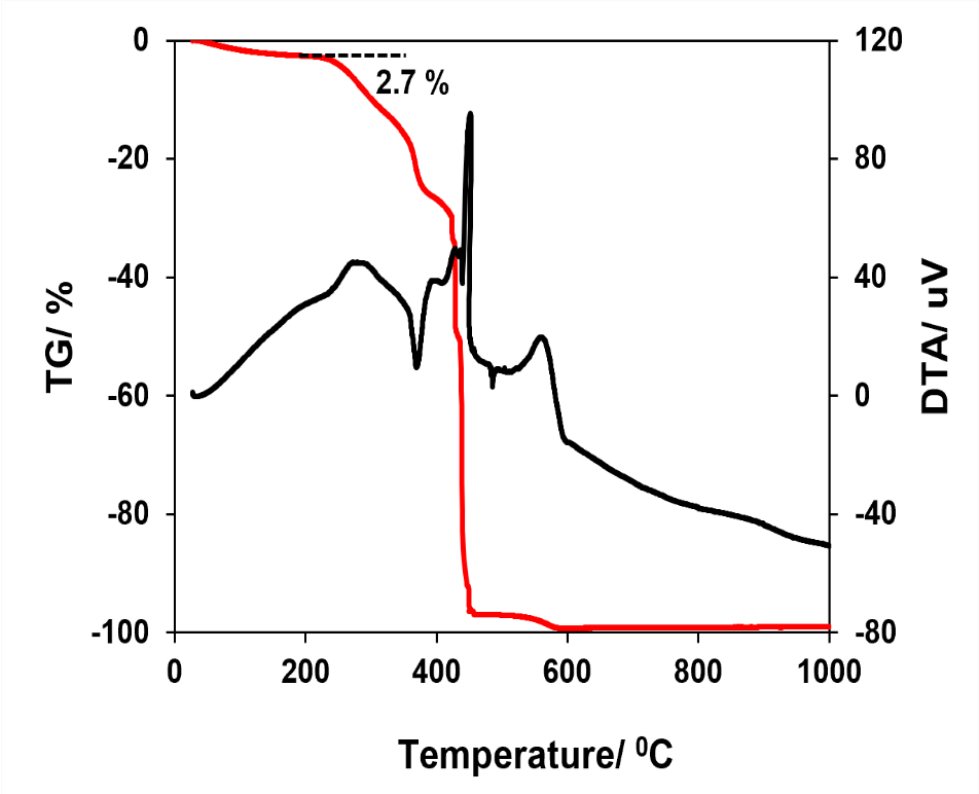

Fig. 3-4 TG-DTA curves of Au@AER treated in N_2 at 100 °C for 1 h.

In addition, the spent Au@AER that used for NO_3^- removal and decomposition in the two-step process was soaked in water to swell, and it was treated with H_2 at 80 °C for 5 h as a second decomposition process (this treatment is called "Continuous"), and the total amount of NO_3^- decomposed twice is also shown in Fig. 3-3 as "Continuous". The amount of decomposed NO_3^- for "Continuous" was almost the same as that for "Normal", indicating that no additional NO_3^- decomposition occurred with the swelling treatment. During the first NO_3^- decomposition, NO_3^- on Au surface, free NO_3^- in the resin and NO_3^- on ion-exchange sites of resin near to the Au^0 surface were decomposed, while NO_3^- on the ion-exchange sites of resin far away from Au^0 surface was not decomposed. In the second decomposition process, even though the resin swelled again, the NO_3^- on the ion-exchange sites of resin far away from the Au^0 surface could not diffuse to the Au^0 surface.

To Au@AER containing NO_3^-, 1 mL of ultrapure water was added to ensure the

presence of excess water to expect easy diffusion of NO_3^- in the resin and the Au@AER was contacted with H_2 at 80 °C for 5 h (this state is called “Soak”). The amount of decomposed NO_3^- under this state was investigated, and the result is shown in Fig. 3-3 (Soak). The amount of NO_3^- taken in resin and decomposed under this state was almost the same as those for “Normal”.

NO_3^- decomposition reaction also occurred under high-pressure (10 atm) H_2 atmosphere (this treatment is called “HP”) (Fig. 3-3 (HP)). There was a slight increase in the amount of decomposed NO_3^- from 0.3 (Normal) to 0.36 mmol g^{-1} (HP), and the decomposition amount was not further increased even extending the reaction time to 12 h (data not shown), which proved that NO_3^- on ion-exchange sites far away from the Au^0 surface did not diffuse to reach the Au^0 surface even under high-pressure H_2 atmosphere.

3-3-3 Reaction mechanism of NO_3^- decomposition

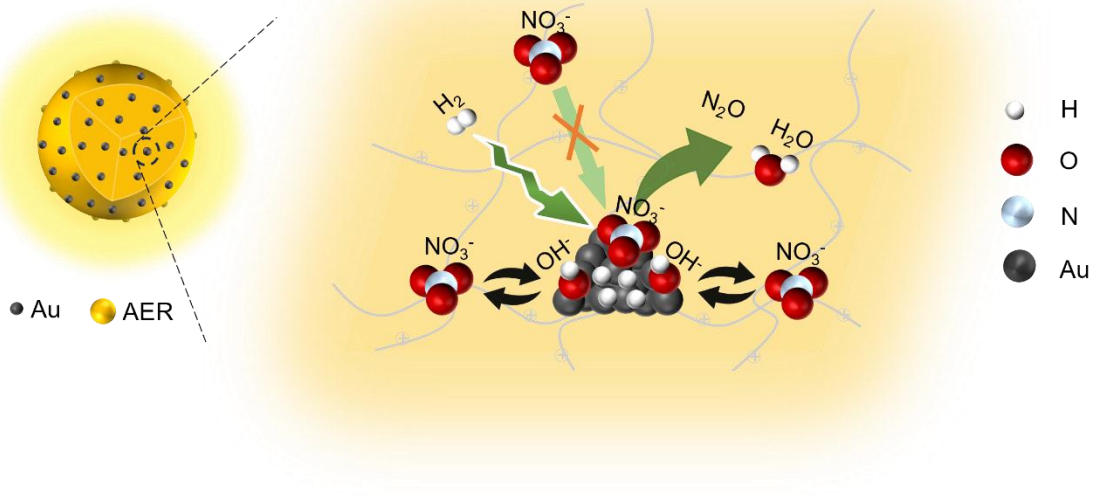

Fig. 3-5 Proposed reaction mechanism for NO_3^- decomposition in Au@AER.

According to the above results, the reaction mechanism for NO_3^- decomposition in the resin is proposed as Fig. 3-5. NO_3^- adsorbed on the Au^0 surface was firstly and instantly decomposed when the Au@AER containing NO_3^- was contacted with H_2, and the generated OH^- was adsorbed on the Au surface. And then, OH^- adsorbed on the Au^0 surface were ion-exchanged with the free NO_3^- in the resin or adjacent quaternary ammonium groups, and the NO_3^- that exchanged to the Au^0 surface was decomposed and the ion-exchange sites of the resin was occupied by OH^-. However, if the distance between OH^- on Au surface and NO_3^- on the ion-exchange sites of the quaternary ammonium groups exceeded a certain range, this ion-exchange process did not proceed and the NO_3^- was not decomposed any more. During the NO_3^- decomposition process, water promoted the diffusion of free NO_3^- and NO_3^- on the ion-exchange sites of the adjacent quaternary ammonium groups to the Au^0 surface.

3-4 Conclusions

It was demonstrated that water played an important role in the decomposition process of NO_3^- in resin. The decomposition of free NO_3^- and NO_3^- on ion-exchange sites of resin was hindered when the water was removed from the resin, while the decomposition of NO_3^- adsorbed on Au^0 surface proceeded in such conditions. During the NO_3^- decomposition process in the resin, NO_3^- adsorbed on Au surface was decomposed, and OH^- was generated and adsorbed on Au surface. Then, the generated OH^- exchanged with free NO_3^- in the resin or at adjacent quaternary ammonium groups, and water promoted the diffusion of free NO_3^- and NO_3^- on the ion-exchange sites to Au^0 surface. NO_3^- that exchanged to the Au^0 surface was decomposed and the ion-exchange sites of the resin were occupied by OH^-. However, NO_3^- on the ion-exchange sites of quaternary ammonium groups far from the Au^0 surface was not exchanged, thus was not decomposed.

3-5 References

[1] Y.-N. Kim, M. Y. Kim and M. Choi. Synergistic integration of catalysis and ion-exchange for highly selective reduction of nitrate into N_2, Chemical Engineering Journal. 289 (2016) 423-432, https://doi.org/10.1016/j.cej.2016.01.002

[2] G. Mendow, A. Sánchez, C. Grosso and C. A. Querini. A novel process for nitrate reduction in water using bimetallic Pd-Cu catalysts supported on ion exchange resin, Journal of environmental chemical engineering. 5 (2017) 1404-1414, https://doi.org/10.1016/j.jece.2017.01.033

Chapter 4

Rapid removal and catalytic decomposition of nitrate in anion-exchange resin containing Ru nanoparticles

4-1 Introduction

In Chapter 2, it was found that NO_3^- decomposition proceeded on various single-metal catalysts, and Ru, Au and Rh were particularly effective. Among the metals tested, only Au did not require additional treatment to reduce the metal complex in the resin to form metal (Au) particles because of spontaneous reduction. Therefore, the ion-exchange and catalytic performance of Au@AER for NO_3^- were investigated in that chapter. However, only 41 % of NO_3^- was decomposed when the resin with Au particles was prepared under optimal conditions and with optimum Au content, which was because the NO_3^- on ion-exchange sites far from the Au^0 surface could not diffuse to the Au^0 surface as clarified in Chapter 3.

In early catalyst screening studies, monometallic catalysts are practically inactive for the reduction of NO_3^-, and Ru shows only low activity [1, 2]. Therefore, Ru hydrogenation catalysts have been largely overlooked for such applications. However, Ru was considered again for nitrate reduction recently, because of the lower price than Pd and Pt, and it was also proved that Ru has high catalytic performance for NO_3^- decomposition [2, 3]. As the result in Chapter 2, among the metals tested, Ru showed the highest catalytic performance for NO_3^- decomposition. Therefore, the resin with Ru particles for the reduction of NO_3^- was taken in this chapter and was extensively investigated.

Strathmann [2] reported that 5wt% Ru/C showed high activity for NO_3^- decomposition when small amount of NO_3^- stock solution was introduced into an open semi-batch system containing ultrapure water and Ru/C under continuous H_2 sparging (1 atm, 40 mL min^{-1}) at constant temperature (25 ± 0.5 °C), but the Ru/C needed to be pretreated with H_2 at 350 °C for 2 h to reduce RuO_2 on Ru surface and the prepared Ru particles was easy to be oxidized to RuO_2 again. In addition, the selectivity of ammonia reached 90 %, and secondary pollution to the treated water was caused because the NO_3^- decomposition process was carried out in water.

In this chapter, Ru was chosen as a metal introduced into the resin and the

preparation conditions were systematically investigated to improve the catalytic performance for NO_3^- decomposition over the two-step process, and it was found that the temperature and pressure in the reduction of the Ru complex (precursor for Ru^0 particles) in the resin had a greatly impact on the generation of Ru^0 particles in resin. Optimization of the reaction conditions for NO_3^- decomposition was also investigated with Ru@AER, and it was found that water in resin greatly affected the amount of decomposed NO_3^-. Finally, the reusability of the resin with Ru was tested.

4-2 Experimental

4-2-1 Material preparation

Ru-incorporated AER was prepared as follows. A solution of $RuCl_3$ was prepared by dissolving a certain amount of $RuCl_3 \cdot nH_2O$ (FUJIFILM Wako Pure Chemical Co.) in 10 mL of HCl (20 %). To the solution, 0.5 g of AER was added, and the suspension was stirred at 38 °C for 12 h. The resin was collected by filtration and washed with ultrapure water. The obtained material is referred to as Ru@AER. Ru@AER with different Ru loadings were prepared by changing the amount of $RuCl_3 \cdot nH_2O$ in the solution.

Ru@AER(H_2) was prepared by treating Ru@AER with H_2 as that for Au@AER (H_2).

Ru@AER was treated with H_2 under high H_2 pressure atmosphere as follows. 0.1 g of Ru@AER was added to an autoclave, and the autoclave was pressurized to 10 atm of pure H_2 and heated at different temperatures for a certain time. The material after this treatment is referred to as Ru@AER(HP-H_2).

4-2-2 Characterization

The prepared Ru@AER, Ru@AER(H_2) and Ru@AER(HP-H_2) were analyzed by XRD, TEM and TG-DTA as Chapter *2-2-2*.

4-2-3 Catalytic decomposition of NO_3^- in Ru@AER(H_2) and reusability test

Procedure for the decomposition of NO_3^- in Ru@AER was the same as that in Chapter *2-2-3*.

4-2-4 Effect of reduction conditions of $RuCl_4^-$ in resin on NO_3^- decomposition

To an autoclave, 0.1 g of 0.1 mmol g^{-1} Ru@AER was added, and the autoclave was flushed with H_2 repeatedly and then pressurized to 10 atm of pure H_2. Reduction reactions of $RuCl_4^-$ were carried out at five different temperatures (80, 100, 110, 120 and 130 °C) for 3 h. To investigate the effect of reduction time of $RuCl_4^-$ on NO_3^- decomposition, the reduction reactions were also performed at 120 °C for different time (0.5, 1, 2 and 3 h). In addition, 0.1 mmol g^{-1} Ru@AER was also reduced under different pressure (1, 3, 5, 7.5 and 10 atm of pure H_2) at 120 °C for 3 h.

Then, the prepared 0.1 mmol g^{-1} Ru@AER(HP-H_2) was used to uptake NO_3^- as Chapter *2-2-3*. Ru@AER(HP-H_2) containing NO_3^- was added to an autoclave, and the autoclave was pressurized at 10 atm of pure H_2 and heated at 80 °C for 5 h to decompose NO_3^- in the resin. Finally, the Ru@AER(HP-H_2) was taken out from the autoclave and was added to 100 mL of NaCl solution (500 mmol L^{-1}) to exchange the undecomposed NO_3^- as Chapter *2-2-3*.

4-2-5 Influence of the amount of water in resin on NO_3^- decomposition

As Chapter *4-2-1*, Ru@AER(HP-H_2) was prepared by reducing Ru@AER under 10 atm H_2 atmosphere at 120 °C for 3 h, and it was used to ion-exchange with NO_3^- solution for 1 h. After that, Ru@AER(HP-H_2) containing NO_3^- was treated with three processes.

In the first process, Ru@AER(HP-H_2) containing NO_3^- was placed in a glass tube reactor, and N_2 was allowed to flow into the reactor and the temperature was increased to 100 °C and the reactor was maintained at this temperature for 1 h. The material obtained by this treatment is referred to as Ru@AER(Dry). The collected Ru@AER(Dry) containing NO_3^- was contacted with 10 atm H_2 at 80 °C for 5 h in an autoclave reactor.

In the second process, Ru@AER(HP-H_2) containing NO_3^- was placed in a glass tube, and 0.3 mL of ultrapure water was added to this tube, and the obtained material is referred to as Ru@AER(Wet) (all the NO_3^- decomposition process in this chapter, unless otherwise specified, were carried out under this condition). The collected Ru@AER(Wet) containing NO_3^- was contacted with 10 atm H_2 at 80 °C for 5 h in an autoclave reactor.

In the third process, 3 mL of ultrapure water was added into the glass tube with Ru@AER (HP-H_2) containing NO_3^- to make sure the resin was soaked in water, and the obtained material is referred to as Ru@AER(Soak). The collected Ru@AER(Soak) containing NO_3^- was contacted with 10 atm H_2 at 80 °C for 5 h in an autoclave reactor.

4-2-6 Influence of reaction conditions on NO_3^- decomposition

Ru@AER(HP-H_2) was prepared by treating 0.1 mmol g^{-1} Ru@AER under 10 atm of pure H_2 atmosphere at 120 °C for 3 h. Then, the prepared Ru@AER(HP-H_2) was used to uptake NO_3^- as Chapter *2-2-3*. Ru@AER(HP-H_2) containing NO_3^- was added to an autoclave, and the autoclave was pressurized to different pressures (1, 3, 5, 6, 7.5 and 10 atm) of pure H_2 and then heated at 80 °C for 5 h to decompose NO_3^- in resin. In addition, Ru@AER(HP-H_2) containing NO_3^- was also treated under 10 atm H_2 at 80 °C for different time (1-5 h) to investigate the effect of reaction time on NO_3^- decomposition. Finally, the Ru@AER(HP-H_2) was taken out from autoclave and was added to 100 mL of NaCl solution (500 mmol L^{-1}) to exchange the undecomposed NO_3^- as Chapter *2-2-3*.

4-3 Results and discussion

4-3-1 Effect of reduction conditions of $RuCl_4^-$ on the performance of Ru@AER(H_2)

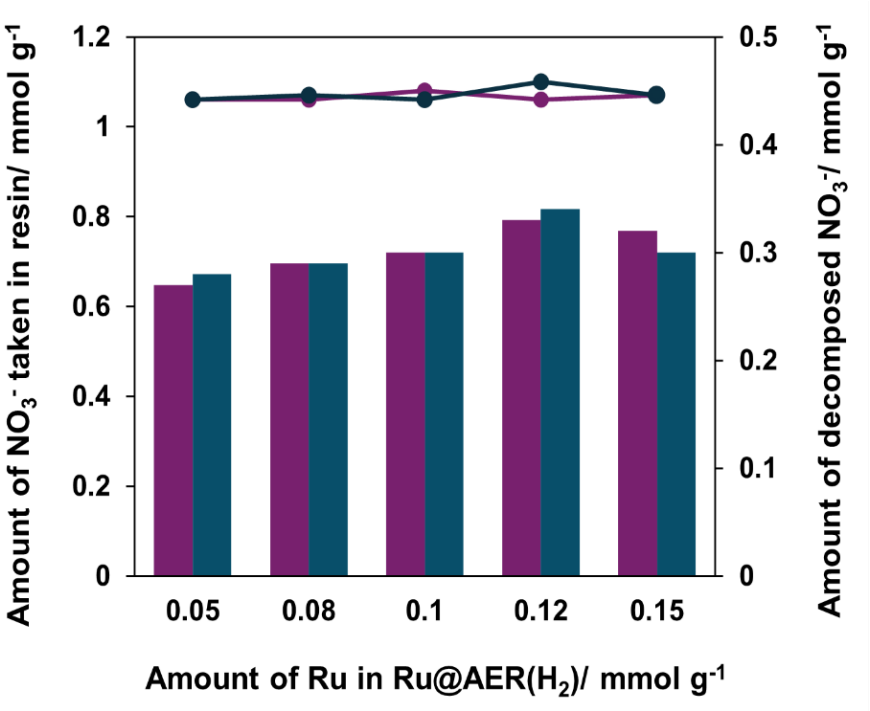

Fig. 4-1 Influence of the reduction time of $RuCl_4^-$ on the performance of Ru@AER(H_2) for NO_3^- decomposition. The line chart represents the amount of NO_3^- taken in resin and bar chart represents the amount of decomposed NO_3^-. Purple represents the $RuCl_4^-$ was reduced by H_2 for 1 h and blue represents 3 h. Conditions: reduction temperature and pressure, 80 °C and 1 atm; amount of Ru@AER(H_2), 0.1 g; volume and concentration of NO_3^- solution, 100 mL and 1.62 mmol L^{-1}. NO_3^- decomposition was performed under 1 atm H_2 atmosphere at 80 °C for 5 h.

Fig. 4-1 shows the influence of the reduction time of $RuCl_4^-$ (1 h or 3 h) in the resin and Ru content in Ru@AER(H_2) on the performance of NO_3^- decomposition. For these experiments, NO_3^- decomposition was performed under 1 atm H_2 atmosphere at 80 °C for 5 h, but the $RuCl_4^-$ in each Ru@AER(H_2) was reduced with 1 atm H_2 at 80 °C. About

1.06 mmol g^{-1} of NO_3^- was taken in each Ru@AER(H_2) regardless the Ru content. In addition, the decomposition performance of these Ru@AER(H_2) was also almost the same and was not increased with increase of the Ru content. Moreover, the performance did not improve even though the reduction time was extended from 1 h to 3 h. It was speculated that only a small amount of $RuCl_4^-$ in resin was reduced to Ru^0 particles in the conditions.

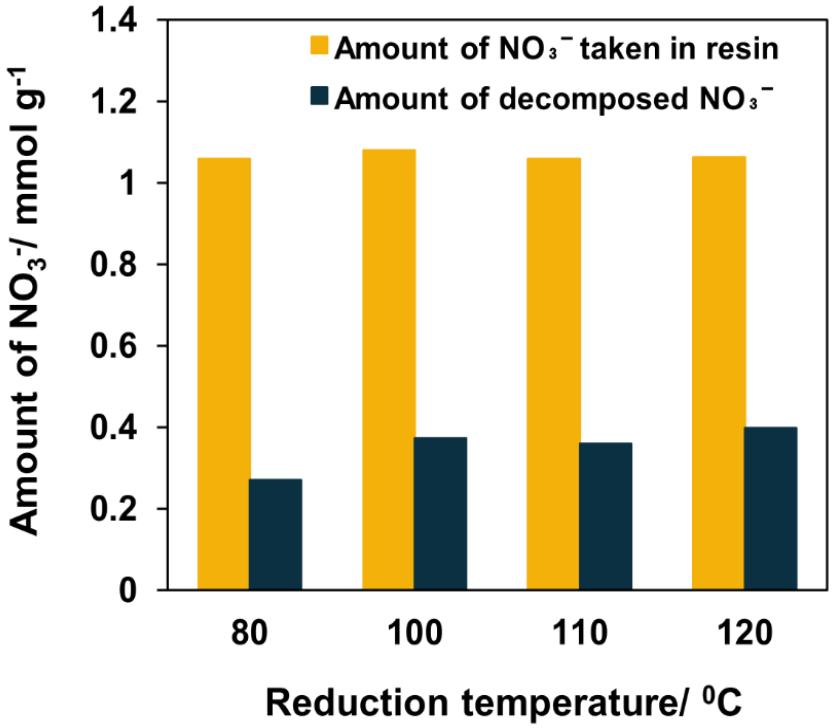

Fig. 4-2 Influence of the reduction temperature of $RuCl_4^-$ on the performance of Ru@AER(H_2) for NO_3^- decomposition. Conditions: reduction time and pressure, 3 h and 1 atm; amount of Ru@AER(H_2), 0.1 g; volume and concentration of NO_3^- solution, 100 mL and 1.62 mmol L^{-1}. NO_3^- decomposition was performed under 1 atm H_2 atmosphere at 80 °C for 5 h.

To improve the catalytic performance of Ru@AER for NO_3^- decomposition, the reduction temperature of $RuCl_4^-$ in Ru@AER(H_2) was increased up to 120 °C (Fig. 4-2).

The ion-exchange performance of each Ru@AER(H_2) for NO_3^- was almost unchanged, meaning that the structure of the resin was not changed up to 120 °C. However, the amount of decomposed NO_3^- was increased from 0.28 mmol g^{-1} (25 % NO_3^- conversion) to 0.37 mmol g^{-1} (35 % NO_3^- conversion) when the reduction temperature was increased to 100 °C and kept it the same even when the temperature was further increased. According to the result in Fig. 3-3, the amount of decomposed NO_3^- increased when the NO_3^- in Au@AER was decomposed by 10 atm of H_2, indicating that H_2 pressure also affected the amount of decomposed NO_3^-, and it will be discussed in detail in the next section.

4-3-2 Effect of the Ru content in Ru@AER(HP-H_2) and the reduction temperature of $RuCl_4^-$ on NO_3^- decomposition

Fig. 4-3 shows the effect of reduction temperature of $RuCl_4^-$ in Ru@AER under 10 atm H_2 atmosphere on NO_3^- decomposition. For all Ru@AER(HP-H_2), the amount of decomposed NO_3^- at each temperature was higher than that for Ru@AER(H_2). It was proved that H_2 pressure had a great impact on the reduction of $RuCl_4^-$ in the resin. In addition, the amount of decomposed NO_3^- was also affected by the Ru content in Ru@AER (Fig. 4-3). For 0.05 and 0.08 mmol g^{-1} Ru@AER(HP-H_2), the amount of decomposed NO_3^- was increased with increase of the reduction temperature and reached a maximum where 0.75 and 1.04 mmol g^{-1} of NO_3^- were decomposed when the temperature was 120 °C, corresponding to 70 and 96 % of NO_3^- conversion, respectively. This increase was attributed to the increased number of Ru sites available for NO_3^- decomposition. However, when the temperature was further increased to 130 °C, the amount of decomposed NO_3^- decreased, which may be because of the formation of large size Ru particles. In comparison, for other Ru@AER(HP-H_2) that Ru loading was more than 0.1 mmol g^{-1}, the amount of decomposed NO_3^- was increased with increase of the reduction temperature to 120 °C and reached the highest value of about 1.06 mmol g^{-1},

corresponding to 100 % NO_3^- conversion, and it was maintained at the value until 130 °C. For 0.15 mmol g^{-1} Ru@AER (HP-H_2), the maximum amount of decomposed NO_3^- was obtained at 110 °C, which may be because enough Ru sites available for NO_3^- decomposition were generated even though not all $RuCl_4^-$ in the resin was reduced to Ru particles.

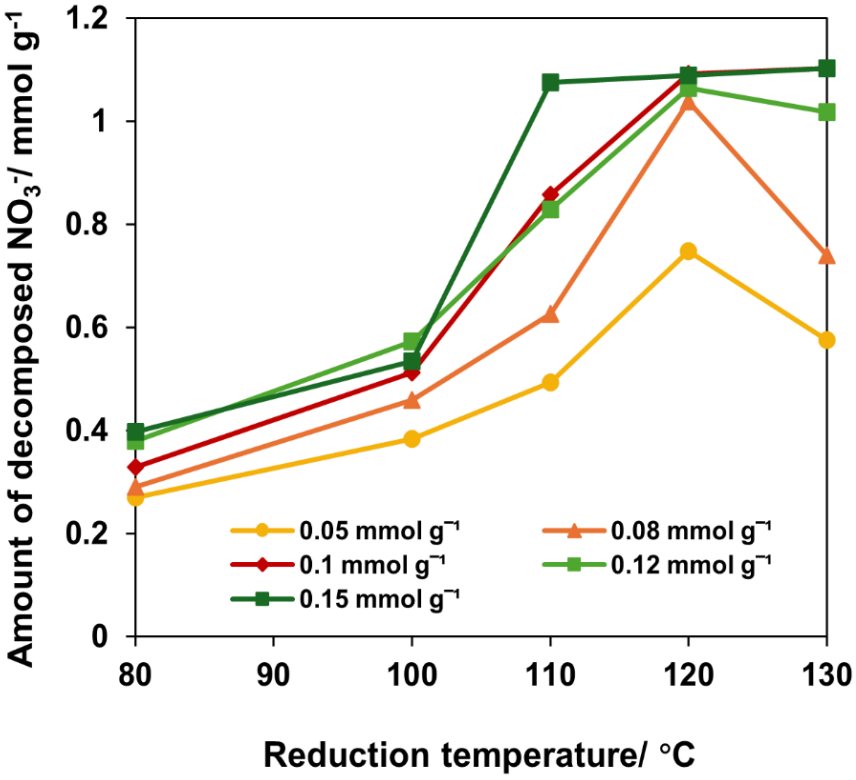

Fig. 4-3. Influence of Ru content in Ru@AER(HP-H_2) and the reduction temperature of $RuCl_4^-$ on the amount of decomposed NO_3^-. $RuCl_4^-$ reduction was performed under 10 atm H_2 atmosphere for 3 h. NO_3^- uptake measurement: $[NO_3^-]_0$ = 100 ppm (1.62 mmol L^{-1}); volume of solution, 100 mL; amount of Ru@AER(HP-H_2), 0.1 g. NO_3^- decomposition was performed under 10 atm H_2 atmosphere at 80 °C for 5 h.

Size of Ru particles in Ru@AER(HP-H_2) with different Ru loading obtained by the treatment of Ru@AER under 10 atm H_2 atmosphere at 120 °C for 3 h were analyzed by XRD, and the XRD patterns are shown in Fig. 4-4. No diffraction peaks due to Ru^0 was

observed in all XRD patterns, which may be because the size of Ru was too small to be detected and the dispersion of Ru in resin was high.

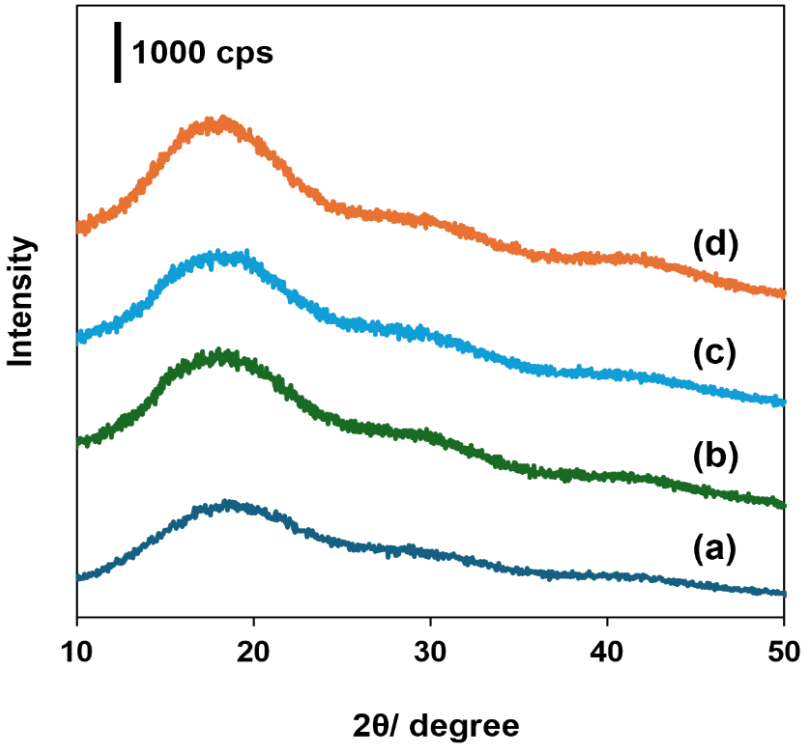

Fig. 4-4. XRD patterns of Ru@AER(HP-H_2) with different Ru contents. (a) Pristine AER and Ru@AER(HP-H_2) with (b) 0.05 mmol g^{-1} Ru, (c) 0.08 mmol g^{-1} Ru, (d) 0.1 mmol g^{-1} Ru. Those Ru@AER(HP-H_2) were treated with 10 atm of H_2 at 120 ℃ for 3 h.

Fig. 4-5(a) shows the TEM image of Ru@AER(HP-H_2) that AER with $RuCl_4^-$ was treated with 10 atm H_2 at 80 ℃ for 3 h. There was no obvious Ru particle generated. Therefore, the reason why only 40 % of NO_3^- taken in resin was decomposed may be because only a part of $RuCl_4^-$ was reduced by H_2 at 80 ℃. In contrast, highly dispersed Ru particles in the resin were detected when the reduction temperature was increased to 120 ℃ (Fig. 4-5(b)), and the size of the Ru particle was about 3 nm. When the temperature was increased to 120 ℃, more $RuCl_4^-$ in resin was reduced to form small size Ru^0 particles, thus enough Ru sites were generated for NO_3^- decomposition.

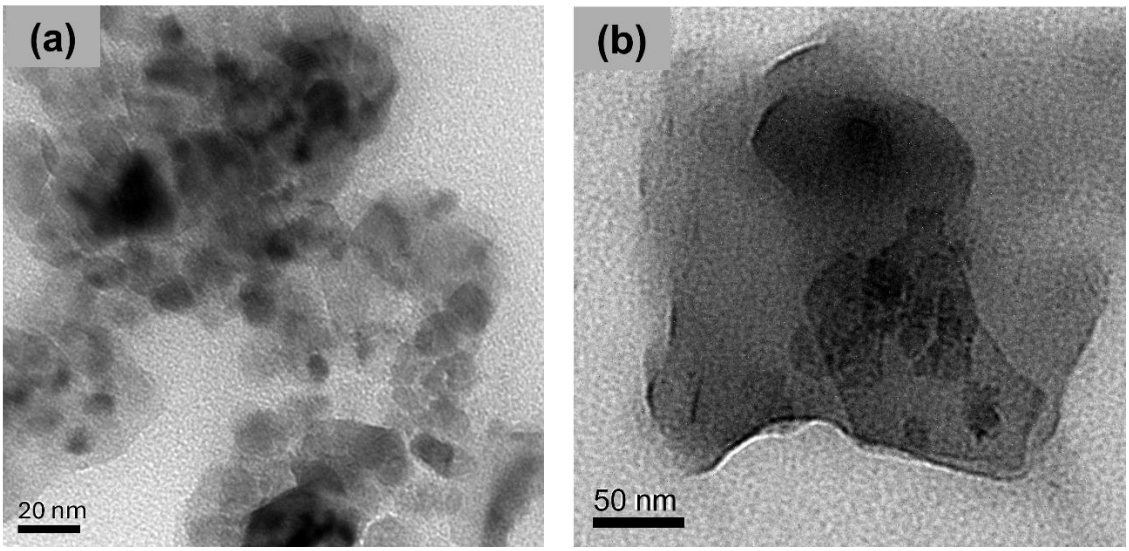

Fig. 4-5. TEM images of 0.1 mmol g^{-1} Ru@AER(HP-H_2) that $RuCl_4^-$ in Ru@AER was treated with 10 atm of H_2 for 3 h at (a) 80 ℃ and (b) 120 ℃.

4-3-3 Effects of the reduction time and H_2 pressure of $RuCl_4^-$ on the performance for NO_3^- decomposition

Fig. 4-6 shows the effect of reduction time of $RuCl_4^-$ on the amount of NO_3^- taken in resin and decomposed NO_3^-. The ion-exchange performance of these samples was almost the same regardless of the reduction time of $RuCl_4^-$. However, the amount of decomposed NO_3^- was greatly affected by the reduction time, and it gradually increased with increase of the reduction time, reaching 95 % of NO_3^- conversion at 2 h. And 100 % of NO_3^- taken in resin was decomposed when the reduction time was further extended to 3 h.

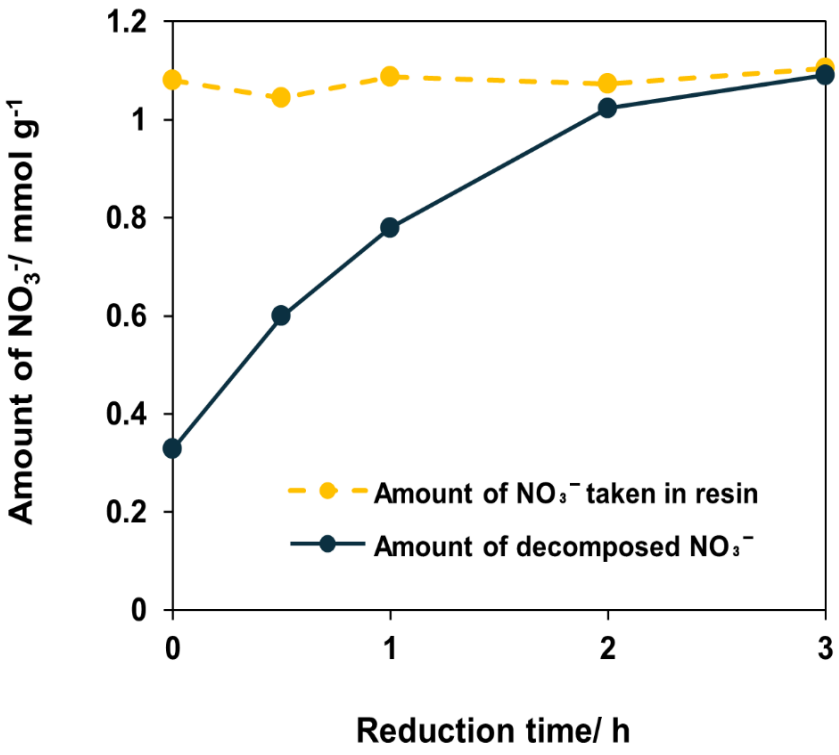

Fig. 4-6 Influence of reduction time of $RuCl_4^-$ on the amount of decomposed NO_3^-. The content of Ru in Ru@AER(HP-H_2) was 0.1 mmol g^{-1}. Mass of Ru@AER(HP-H_2), 0.1 g; $RuCl_4^-$ was reduced under 10 atm H_2 atmosphere at 120 °C. Conditions for NO_3^- decomposition: reaction temperature and pressure, 80 °C and 10 atm; reaction time, 5 h.

The H_2 pressure of the reduction of $RuCl_4^-$ in the resin also had a significant impact on the amount of decomposed NO_3^- (Fig. 4-7). The amount of decomposed NO_3^- gradually increased with the increase of the H_2 pressure to 5 atm and reached about 100 % of NO_3^- conversion.

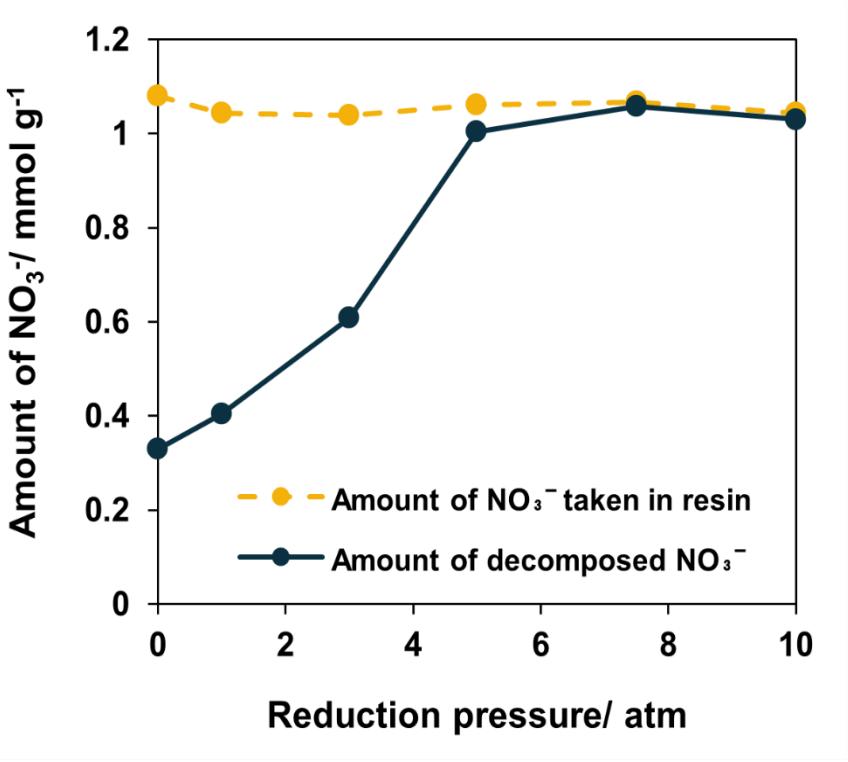

Fig. 4-7 Influence of reduction pressure of $RuCl_4^-$ on the amount of decomposed NO_3^-. The content of Ru in Ru@AER(HP-H_2) was 0.1 mmol g^{-1}. Mass of Ru@AER(HP-H_2), 0.1 g; $RuCl_4^-$ was reduced at 120 °C for 3 h. Conditions for NO_3^- decomposition: reaction temperature and pressure, 80 °C and 10 atm; reaction time, 5 h.

4-3-4 Optimization of the reaction conditions for NO_3^- decomposition in Ru@AER(HP-H_2)

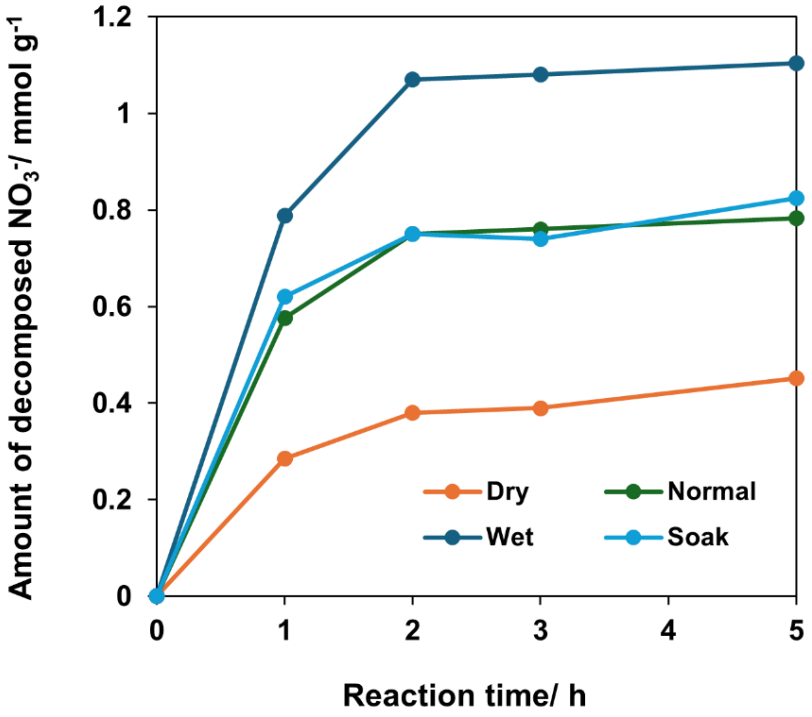

Fig. 4-8 Influence of reaction time for NO_3^- decomposition on the amount of decomposed NO_3^-. The content of Ru in Ru@AER(HP-H_2) was 0.1 mmol g^{-1}. Ru@AER(HP-H_2) was treated under 10 atm H_2 atmosphere at 120 °C for 3 h. Conditions for NO_3^- decomposition: reaction pressure, 10 atm and reaction temperature, 80 °C.

Fig. 4-8 shows the change of the amount of decomposed NO_3^- with the reaction time for NO_3^- decomposition. Ru@AER(HP-H_2) containing NO_3^- was treated with four different processes to change the amount of water in the resin, and the catalytic performance of Ru@AER(HP-H_2) treated with different processes were also investigated. Regardless of the processes, the amount of decomposed NO_3^- was increased with increase of the reaction time to 2 h and then became constant even extending the reaction time. However, the water content in the resin had a great impact on the amount of decomposed NO_3^-, which was consistent with the results in Chapter 3. To more intuitively reflect the

water content in the resin, TG analysis was performed on the three samples (except the sample soaked in water), and the weight loss curves are shown in Fig. 4-9. Only 0.45 mmol g^{-1} of NO_3^-, corresponding to 41 % of NO_3^- taken in resin, was decomposed when the resin was dried at 100 °C for 1 h before NO_3^- decomposition, and the water content in the resin was only 2 % of the weight of this sample. As mentioned in Chapter 3, NO_3^- was decomposed through the diffusion of NO_3^- from ion-exchange sites of resin to metal surface, so the water in the resin promoted the diffusion of NO_3^-. Therefore, the low catalytic performance of Ru@AER(Dry) may be because the small amount of water hindered the diffusion of NO_3^- in the resin and only NO_3^- near to Ru particles was decomposed. For Ru@AER(Normal), the amount of water in resin was 27 %, and the amount of decomposed NO_3^- (0.78 mmol g^{-1}), which corresponds 71 % of NO_3^- conversion, was higher than that of Ru@AER(Dry). Ru@AER(Wet) was prepared by adding 0.3 mL of ultrapure water to Ru@AER(Normal) to make sure the resin was in a wet state, and the amount of water was 48 %. Accordingly, the amount of decomposed NO_3^- was also increased to 1.10 mmol g^{-1}, corresponding to 100 % of NO_3^- conversion. Therefore, it can be concluded that about 48 % of water content is enough to promote the decomposition of all NO_3^- in resin. However, NO_3^- decomposition performance was decreased when the resin was soaked in water, which may be because the excess water hindered the diffusion of H_2 to deep-inside the resin.

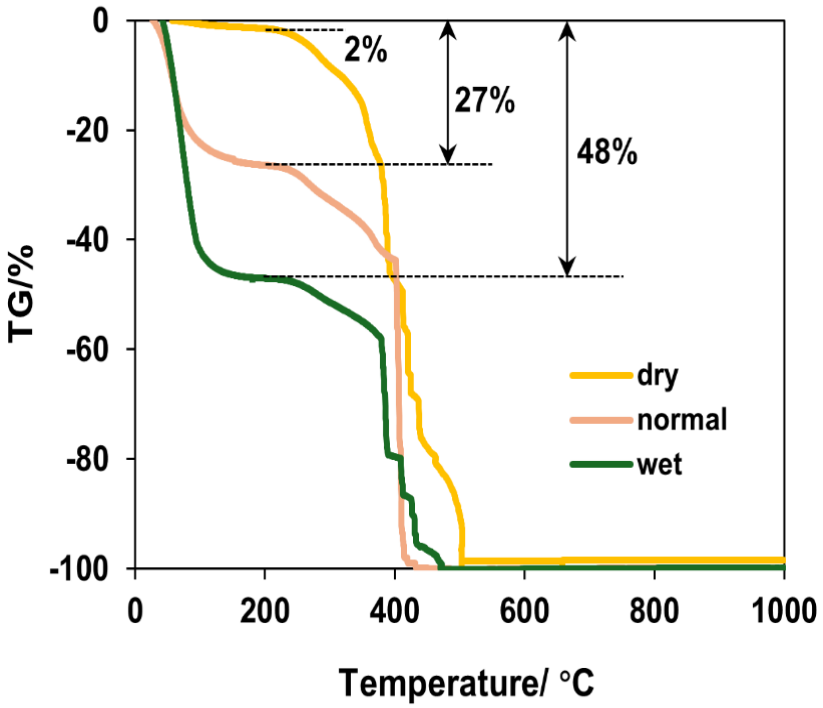

Fig. 4-9 TG curves of Ru@AER(HP-H_2) that treated with different processes.

Besides the water content, H_2 pressure for NO_3^- decomposition also affected the amount of decomposed NO_3^- (Fig. 4-10). The amount of decomposed NO_3^- increased until the pressure was increased to 7.5 atm, and then reached the maximum value (1.1 mmol g^{-1}). The increase of the decomposed amount may be because the high pressure promotes the diffusion of H_2 to deep-inside of resin, increasing the contact probability between H_2 and NO_3^- in resin, which is also consistent with the results in Chapter 3.

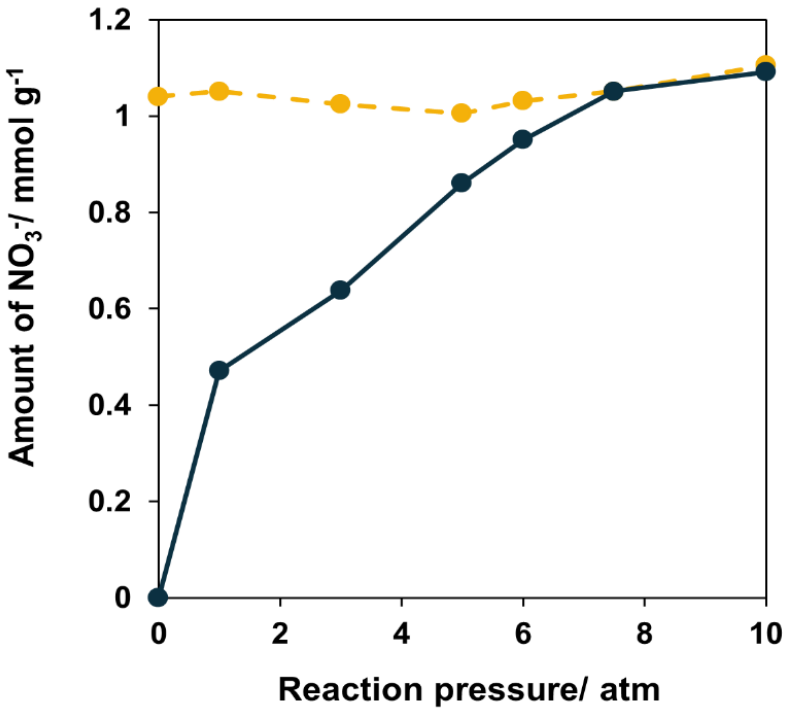

Fig. 4-10 Influence of reaction pressure on the amount of decomposed NO_3^-. The content of Ru in Ru@AER(HP-H_2) was 0.1 mmol g^{-1}. Ru@AER(HP-H_2) was reduced under 10 atm H_2 atmosphere at 120 °C for 3 h. Conditions for NO_3^- decomposition: reaction time, 3 h and reaction temperature, 80 °C.

4-3-5 Reusability tests

Finally, reusability of Ru@AER(HP-H_2) was investigated. 0.1 mmol g^{-1} Ru@AER(HP-H_2) was used as a typical sample for the five-cycle reusability test (Fig. 4-11), and the result shows slight decrease of the uptake and decomposition performance for NO_3^- before the second cycles, which may be because the Ru@AER was treated at 120 °C for 3 h during the preparation process of Ru@AER(HP-H_2), the water in resin was removed. Therefore, in the first ion-exchange process, part of NO_3^- solution was adsorbed into resin to replenish the water of resin, thus more NO_3^- was taken in resin than the subsequent four times. Totally, according to the results of five cycles, it was proved that Ru@AER(HP-H_2) had good stability for NO_3^- removal and decomposition.

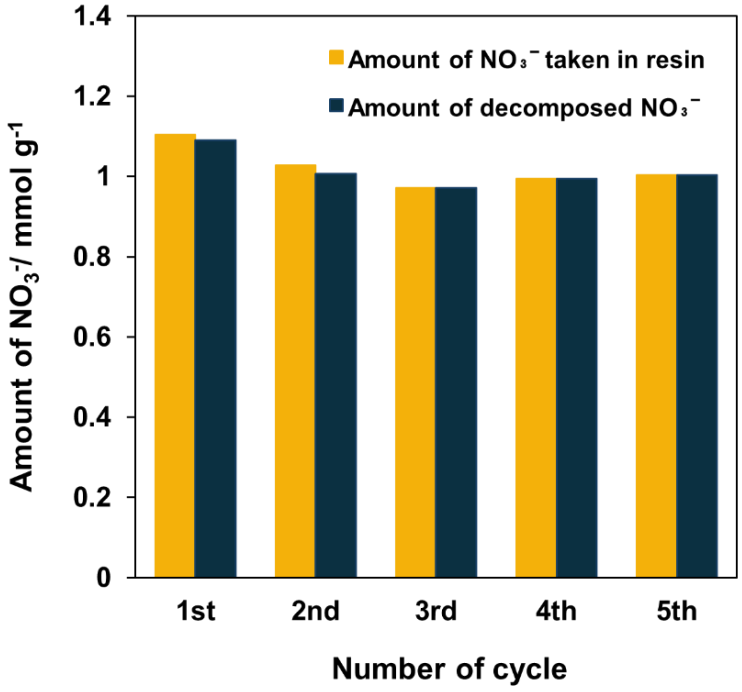

Fig. 4-11 Reusability test for ion-exchange removal and catalytic decomposition of NO_3^- in the two-step process. Five cycles of 0.1 mmol g^{-1} Ru@AER(HP-H_2). Ru@AER(HP-H_2) obtained by the treatment of 10 atm H_2 at 120 °C for 3 h. Conditions for NO_3^- decomposition: reaction time and pressure, 5 h and 10 atm; reaction temperature, 80 °C.

4-4 Conclusions

In this chapter, it was demonstrated that Ru had high catalytic performance for NO_3^- decomposition. At atmospheric pressure of H_2, the maximum amount of decomposed NO_3^- was only 0.4 mmol g^{-1}, corresponding to 37 % of NO_3^- conversion, even when the Ru content and reduction temperature of $RuCl_4^-$ in resin were increased, which was because most of $RuCl_4^-$ in resin was not reduced. Highly dispersed and small size (3 nm) Ru particles were generated when the temperature and H_2 pressure for the reduction of $RuCl_4^-$ was increased to 120 °C and 10 atm, respectively. The increase of temperature or pressure alone could not promote the reduction of $RuCl_4^-$. 100 % of NO_3^- taken in resin was decomposed at 80 °C for 5 h when the resin with Ru particles prepared under optimal conditions. Moreover, water in resin affected the diffusion process of free NO_3^- and the exchange process of NO_3^- on ion-exchange sites to Ru surface, and 48 % of water in resin was enough to promote all NO_3^- taken in resin was decomposed. The resin with Ru particles was reusable for the ion-exchange removal of NO_3^- and NO_3^- decomposition for up to five reuses without performance degradation.

4-5 References

[1] O. S. G. Soares, J. J. Órfão and M. F. R. Pereira. Activated carbon supported metal catalysts for nitrate and nitrite reduction in water, Catalysis letters. 126 (2008) 253-260, DOI 10.1007/s10562-008-9612-4

[2] X. Huo, D. J. Van Hoomissen, J. Liu, S. Vyas and T. J. Strathmann. Hydrogenation of aqueous nitrate and nitrite with ruthenium catalysts, Applied Catalysis B: Environmental. 211 (2017) 188-198, https://doi.org/10.1016/j.apcatb.2017.04.045

[3] J. P. Troutman, J. S. P. Mantha, H. Li, G. Henkelman, S. M. Humphrey and C. J. Werth. Tuning the selectivity of nitrate reduction via fine composition control of RuPdNP catalysts, Small. (2024) 2308593, https://doi.org/10.1002/smll.202308593

Chapter 5

Conclusions

In this study, two single metal catalysts (Au@AER and Ru@AER) were developed and both of them are active for NO_3^- decomposition in the two-step process, indicating that the decomposition reaction of NO_3^- proceeded even with a single metal, demonstrating my hypothesis stated in Chapter 1.

Firstly, Au@AER was developed for NO_3^- decomposition because it did not require the treatment in H_2 to reduce the metal complex ($AuCl_4^-$) in the resin to form metal particles. 0.38 mmol g^{-1} of NO_3^-, corresponding to 41 % conversion, was decomposed at 80 °C for 5 h when the resin with Au particles prepared under optimal conditions and Au content. The maximum ion-exchange capacity was increased from 1.18 to 1.46 mmol g^{-1} due to the formation of new ion-exchange sites on Au surface. N_2O was produced when Au@AER containing NO_3^- was contacted with H_2, which was because the NO_3^- adsorbed on Au surface and free NO_3^- in resin were decomposed, and thus the NO_3^- on ion-exchange sites of quaternary ammonium group diffused to Au surface through exchanging with OH^- generated from NO_3^- decomposition and was decomposed in the resin. However, the amount of decomposed NO_3^- was not increased even extending the reaction time because the diffusion of NO_3^- on ion-exchange sites to Au surface was hindered by the long-distance between ion-exchange sites and Au surface.

Then, to improve the catalytic performance of single metal catalyst for NO_3^- decomposition, Ru replaced Au was introduced into anion exchange resin because it showed higher activity than Au. The amount of decomposed NO_3^- reached the maximum value 1.06 mmol g^{-1} of NO_3^-, corresponding to 100 % conversion, when $RuCl_4^-$ in resin was reduced by H_2 under 10 atm atmosphere at 120 °C for 3 h and the NO_3^- decomposition reaction was carried out under 10 atm H_2 atmosphere at 80 °C for 5 h.

It was also proved that water in resin greatly affected the amount of decomposed NO_3^-, which was because the presence of water in resin promoted the diffusion of NO_3^- on ion-exchange sites of resin to metal surface. And the catalytic performance of the developed two single metal catalysts for NO_3^- decomposition hardly degradation when both of them were reused five times.

This study broke the common sense that had been believed, which was that single metal catalysts had low activity for NO_3^- decomposition. It was proposed that anion exchange resin containing single metal particles showed high activity for NO_3^- reduction in the two-step process, and the prepared single metal catalysts were stable in resin. Easily preparation method and highly catalytic performance of this single metal catalysts promoted the large-scale application in industry. Moreover, single metal catalysts for NO_3^- reduction were hardly reported previously, and the development of the single metal catalysts in this study provided a direction for the widespread use of that in the field of NO_3^- decomposition.

Research accomplishments

1. Research papers (related to dissertation)

(1) Bobo Yan, Koki Kato, Shuhei Shimoda, Ryoichi Otomo, Yuichi Kamiya. "Rapid removal and catalytic decomposition of nitrate in anion-exchange resin containing gold nanoparticles toward purification of groundwater." *Chemical Engineering Journal* 498 (2024): 155721.

2. Presentations (related to dissertation)

(1) Bobo Yan, Koki Kato, Shuhei Shimoda, Ryoichi Otomo, Yuichi Kamiya: "Rapid removal and catalytic decomposition of nitrate in anion-exchange resin containing gold nanoparticles toward purification of groundwater." 12th International Conference on Environmental Catalysis (ICEC 2022) (2022.08)

(2) Bobo Yan, Koki Kato, Shuhei Shimoda, Ryoichi Otomo, Yuichi Kamiya. "Rapid removal and catalytic decomposition of nitrate in anion-exchange resin containing gold nanoparticles toward purification of groundwater." The 19th Korea-Japan Symposium on Catalysis (19th KJSC) (2023.05)

(3) Bobo Yan, Koki Kato, Shuhei Shimoda, Ryoichi Otomo, Yuichi Kamiya. "Rapid removal and catalytic decomposition of nitrate in anion-exchange resin containing gold nanoparticles toward purification of groundwater." Aurora seminar (2023.08)

(4) Bobo Yan, Koki Kato, Shuhei Shimoda, Ryoichi Otomo, Yuichi Kamiya. "Rapid removal and catalytic decomposition of nitrate in anion-exchange resin containing gold nanoparticles toward purification of groundwater." 2nd China-Japan Symposium on Catalysis (2ndCJSC) (2024.11)